(1)

DEPARTMENT OF THE AIR FORCE
AIR UNIVERSITY

AIR FORCE INSTITUTE OF TECHNOLOGY

Wright-Patterson Air Force Base, Ohio

TRACKING A HYPERSONIC AIRCRAFT FROM A SPACE PLATFORM

David W. Ziegler
Captain, USAF

AFIT/GA/ENY/89D-7

AFIT/GA/ENY/89D-7

TRACKING A HYPERSONIC AIRCRAFT FROM A SPACE PLATFORM

THESIS

Presented to the Faculty of the School of Engineering

of the Air Force Institute of Technology

Air University

In Partial Fulfillment of the

Requirements for the Degree of

Master of Science in Astronautical Engineering

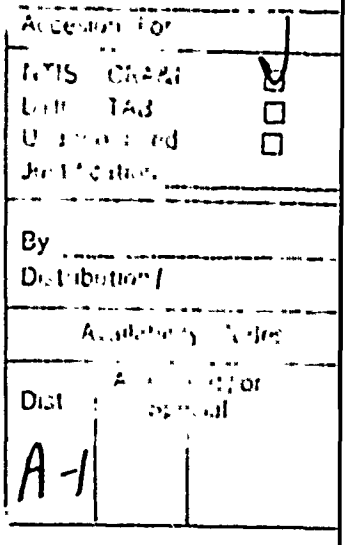

David W. Ziegler, B.S.

Captain, USAF

December 1989

Approved for public release; distribution unlimited

Acknowledgements

I am profoundly grateful to the many people whose guidance, patience and support made this finished product a reality. Many thanks to my faculty advisor, Dr. W. E. Wiesel, for his expertise, interest, and continuing involvement amidst trying circumstances. A great big, special thanks to my new bride and best friend, Jan. The memories of academic rigors and challenges will soon fade, but your sacrifices and the delight of our first year of marriage will never be forgotten. Finally, praise and thanksgiving to the Lord Jesus, creator of Kalman filters and computers, author of many a textbook, and giver of life. He endures forever.

Table of Contents

List of Figures

List of Tables

Abstract

This study developed a data processing algorithm for a space-based platform engaged in tracking a hypersonic transatmospheric vehicle. The geosynchronous platform was assumed to possess passive sensors measuring target position from data angles. The hypersonic vehicle was assumed to be operating in the outer fringes of the atmosphere.

Four element state and six element state Kalman filters were developed, coded, and tested against typical transatmospheric flight profiles. Accuracy of the filters in estimating position, velocity, heading, and acceleration was determined for 1, 5 and 10 second data intervals.

From this test data, it was concluded that the six element state Kalman filter posed a viable option for tracking and estimating performance parameters of hypersonic aircraft.

TRACKING A HYPERSONIC AIRCRAFT FROM A SPACE PLATFORM

I. Introduction

Transatmospheric vehicle (TAV) technology synthesizes the advantages of airbreathing aircraft and platforms in orbit. Airbreathing aircraft have long enjoyed the advantage of operating from a variety of bases, many remote and outside the effective range of hostile detection networks. The maneuverable nature of aircraft allows frequent inflight changes to course and destination, much to the chagrin of those attempting to predict the when and where of a possible hostile flight. It is no surprise that airbreathing aircraft are the weapon system of choice when it comes to the invaluable tactic of operational surprise. Unlike airbreathing aircraft, platforms in orbit do not enjoy the advantage of operating outside the range of detection networks. Indeed, they are continuously in full view of a host of tracking networks. These platforms are handicapped in their ability to frequently maneuver, as well, being constrained by fuel requirements and the dynamics of space operations. What platforms in orbit lack relative to their airbreathing counterparts, however, they possess in the way of range, speed and endurance. Operating in the ultimate "high ground", on-orbit platforms can reach worldwide targets in a matter of minutes and do so at a time unpredictable to observers.

A TAV, possessing the advantages of both airbreathing aircraft and on-orbit platforms, would be a formidable opponent. Central to efforts

to defend against such a system is the ability to accurately detect, observe, and predict any given TAV flight. Success in this task is made possible, in large part, by a distinct disadvantage of the TAV concept: the TAV is second only to the sun as an infrared source. The TAV's hot and powerful engines are easy prey for currently available infrared sensor technology. Even in the absence of engine operation, the TAV's proposed Mach 20 operation in the outer fringes of the atmosphere, will result in exceedingly hot airfoil surfaces. These surfaces again provide a strong infrared signature to any observing sensor.

Objective

This thesis capitalizes on the TAV's infrared visibility and investigates details of the associated tracking problem. The specific objective is to develop a capability to process data from a tracking node into information that exposes as much of a TAV's capabilities and intentions as possible. The product of this thesis will be validated software algorithms designed to receive data from a specific tracking sensor and estimate position, direction, speed, and acceleration of a TAV under observation.

Approach

The approach to achieving this objective can be subdivided into five areas. First, an assessment of the system, in a general sense, must be completed. Where is the tracking sensor? Where is the TAV? Are there any underlying assumptions to be stated? Second, the dynamics of the TAV must be modelled accurately by equations of motion permitting propagation of typical flight profiles over time. Third, the nature of the sensor data itself must be expressly defined and related to the

TAV's motion. Fourth, an algorithm to process this sensor data and estimate the TAV's position, heading, speed and acceleration must be generated. In this thesis, a Kalman type estimation algorithm will be employed to this end. Finally, the estimation algorithm must be tested against typical TAV flight profiles (truth models) to determine how accurately the algorithm estimated true position, heading, speed, and acceleration. The next section addresses the first of these five steps.

System Overview

The tracking sensor platform will be located in a geosynchronous orbit. This orbit affords uninterrupted coverage of a large geographical region where TAV activity might be expected. Realizing that a TAV at hypersonic transatmospheric flight will almost certainly produce a strong thermal signature from exhaust products and high speed flow over airfoil surfaces, the platform will carry a passive infrared sensor package. For this study, sensor error introduced by platform pointing and position uncertainties will not be considered. Vibration of the sensor will be assumed to be negligible.

The TAV will be modelled as a hot, isotropically radiating point source operating in the outer fringes of an atmosphere surrounding a perfectly spherical and rotating earth. The residual atmosphere between the TAV and sensor should introduce negligible atmospheric jitter and distortion into sensor position estimates. In addition, the ratio of the geosynchronous range to the maximum height of the atmosphere is very large, allowing the assumption of negligible TAV motion in the vertical (increasing/decreasing altitude) direction.

II. Transatmospheric Vehicle Dynamics Model

As stated, one of the primary objectives of this thesis is to produce an algorithm that estimates TAV position, direction, speed, and acceleration. The evaluation of this algorithm requires knowledge of the *true* position, direction, speed, and acceleration thus allowing a direct comparison to assess the estimator's accuracy. The TAV dynamics model is the algorithm that constructs this true trajectory.

Definition of Dynamic Parameters

TAV dynamics will be specifically represented by six dynamic parameters: longitude, latitude, heading, speed, intrack acceleration, and transverse acceleration. As previously noted, TAV altitude relative to the surface of the earth is assumed to be a constant zero and hence does not represent a meaningful dynamic parameter. This assumption is the result of the atmosphere's maximum height being much smaller than the great range involved with a geosynchronous sensor.

The dynamics algorithm and the estimation algorithm express TAV position in terms of earth longitude (λ) and earth latitude (δ). In these algorithms, longitudes east of the Greenwich Meridian are taken as positive numbers, while longitudes west of the Greenwich Meridian are taken as negative. North latitudes are taken as positive and south latitudes as negative numbers, zero latitude, of course, being the equator.

TAV direction of travel is expressed in terms of heading (h). Heading is the angle measured positive, in the clockwise direction, from the line connecting the TAV's position with the north pole. The

convention for heading is illustrated in Figure 2.1:

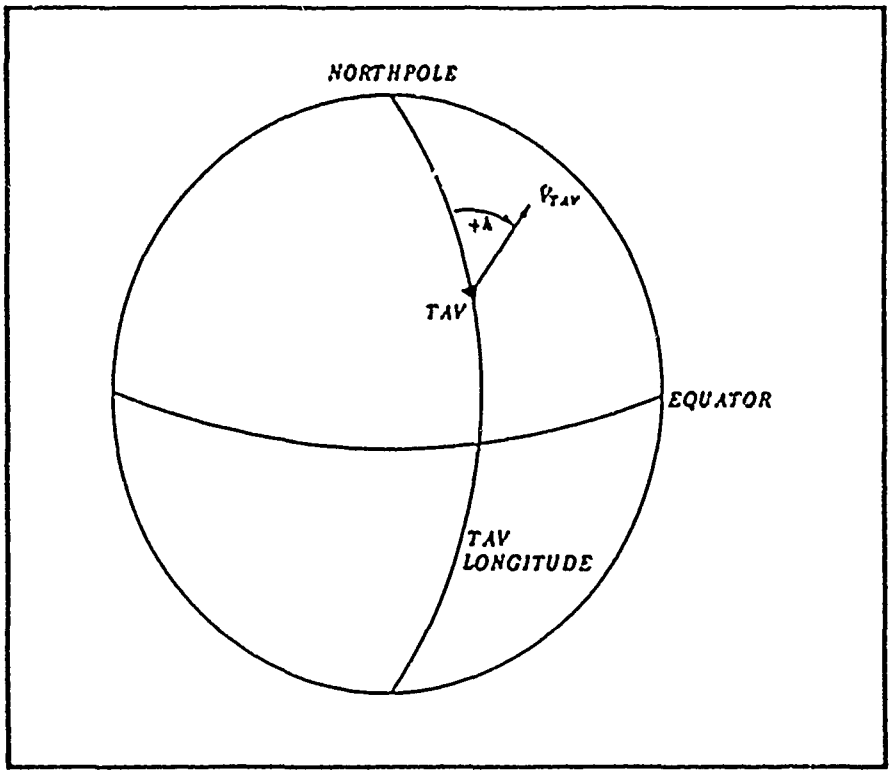

Figure 2.1. Convention for TAV Heading

TAV velocity (V) will always be defined as the rate of change of position along the direction of heading.

The acceleration of the TAV is decomposed into two distinct components, intrack acceleration (a_I) and transverse acceleration (a_T). a_I is the measured rate of change of speed along the direction of the heading. Accelerations are considered positive, decelerations negative. a_T is the acceleration normal to the direction of heading with accelerations out the left wing considered positive.

Equations of Motion

The TAV equations of motion can be expressed in terms of the six

parameters in the previous section. Consider Figure 2.2:

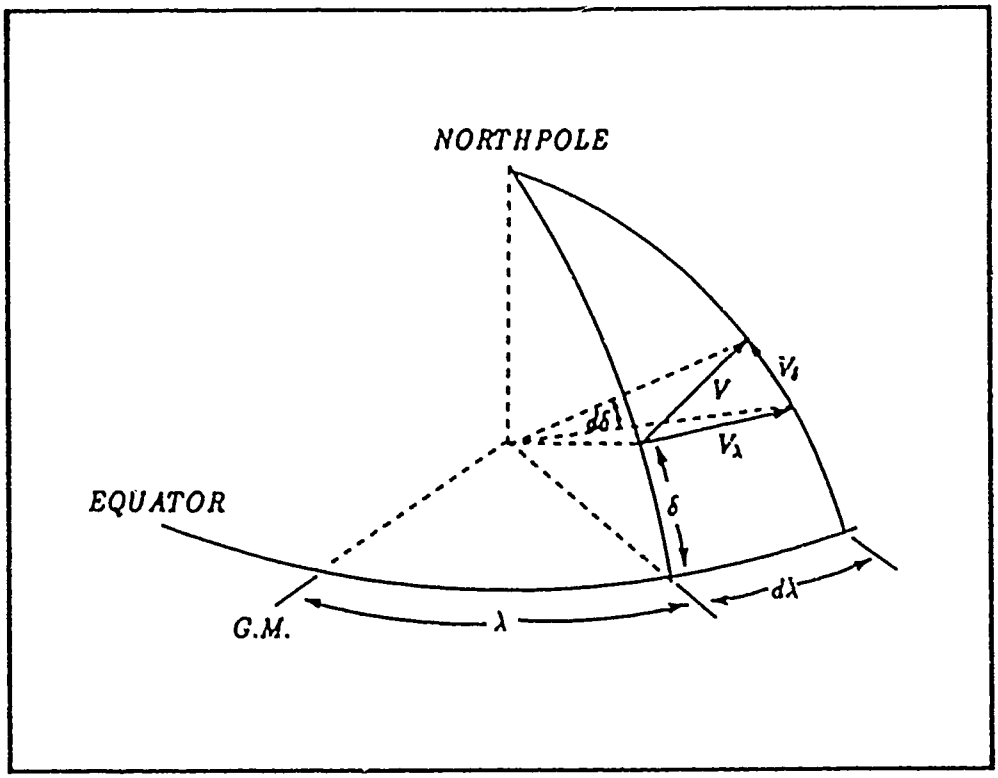

Figure 2.2. TAV Dynamics Over a Small Time Interval

Over time interval, dt, the TAV travels angular distance $d\lambda$ and $d\delta$ from some starting longitude/latitude of λ and δ. The velocity of the TAV can be broken into velocity components across lines of latitude (V_δ) and across lines of longitude (V_λ). Assuming the effect of the earth's curvature on the TAV trajectory is negligible over time interval dt, the planar geometry of this motion is represented by the planar triangle in Figure 2.3.

From basic dynamics, velocity = angular velocity x radial distance. In the direction of changing latitude

$$V_\delta = \omega_\delta \cdot R_e \qquad (2.1)$$

where

V_δ is the TAV velocity across lines of latitude

ω_δ is the TAV angular rate of change in latitude

R_e is the radius of the earth

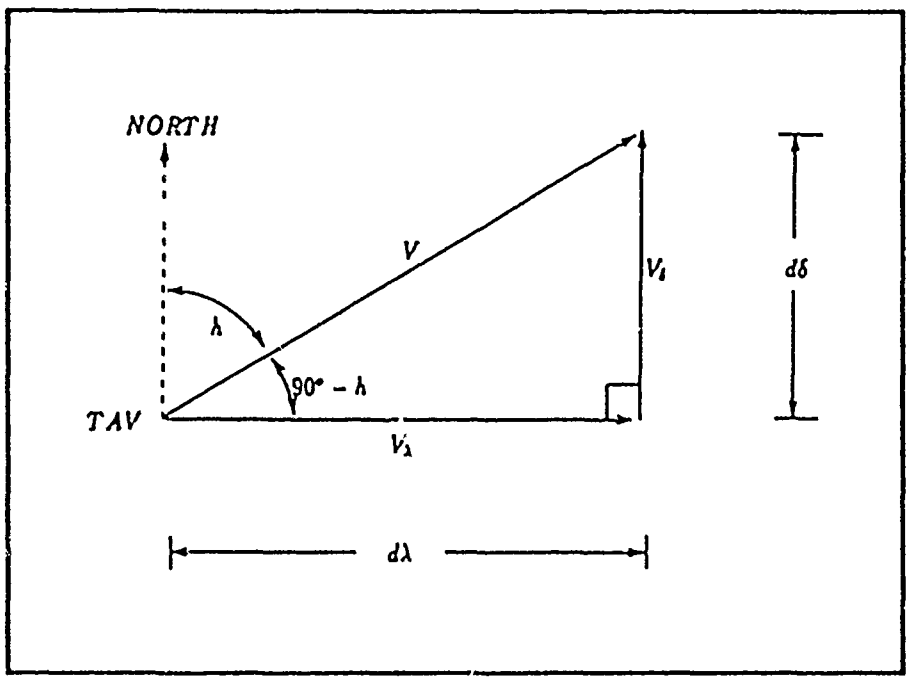

Figure 2.3. Planar Approximation of TAV Trajectory Over Time dt

Eq (2.1) can be rewritten

$$V \cdot \cos h = \frac{d\delta}{dt} \cdot R_e \qquad (2.2)$$

where from Figure 2.3, $V_\delta = V \cdot \sin(90^\circ - h)$, or by trigonometric identity $V_\delta = V \cdot \cos h$. Rearranging, produces the first equation of motion

$$\dot{\delta} = \frac{V \cdot \cos h}{R_e} \qquad (2.3)$$

The equation of motion for $\dot{\lambda}$ is derived in similar fashion. Across lines of longitude

$$V_\lambda = \omega_\lambda \cdot R_e \cdot \sin \delta \qquad (2.4)$$

where

V_λ is the TAV velocity across lines of longitude

ω_λ is the TAV angular rate of change in longitude

$R_e \cdot \sin \delta$ is the radial moment arm as a function of latitude

From Figure 2.3, $V_\lambda = V \cdot \cos(90^\circ - h)$ or $V_\lambda = V \cdot \sin h$. Eq (2.4) can now be rewritten

$$V \cdot \sin h = \frac{d\lambda}{dt} \cdot R_e \cdot \sin \delta \qquad (2.5)$$

Rearranging produces the equation of motion for a non-rotating earth

$$\dot{\lambda} = \frac{V \cdot \sin h}{R_e \cdot \sin \delta} \qquad (2.6)$$

Correcting for the contribution of the earth's rotation to the TAV trajectory results in the second equation of motion

$$\dot{\lambda} = \frac{V \cdot \sin h}{R_e \cdot \sin \delta} - \omega_e \qquad (2.7)$$

To derive the equations of motion for $\dot{h}$ and $\dot{V}$, two additional reference frames must be introduced. First, consider the ENZ frame with origin at the TAV (Figure 2.4):

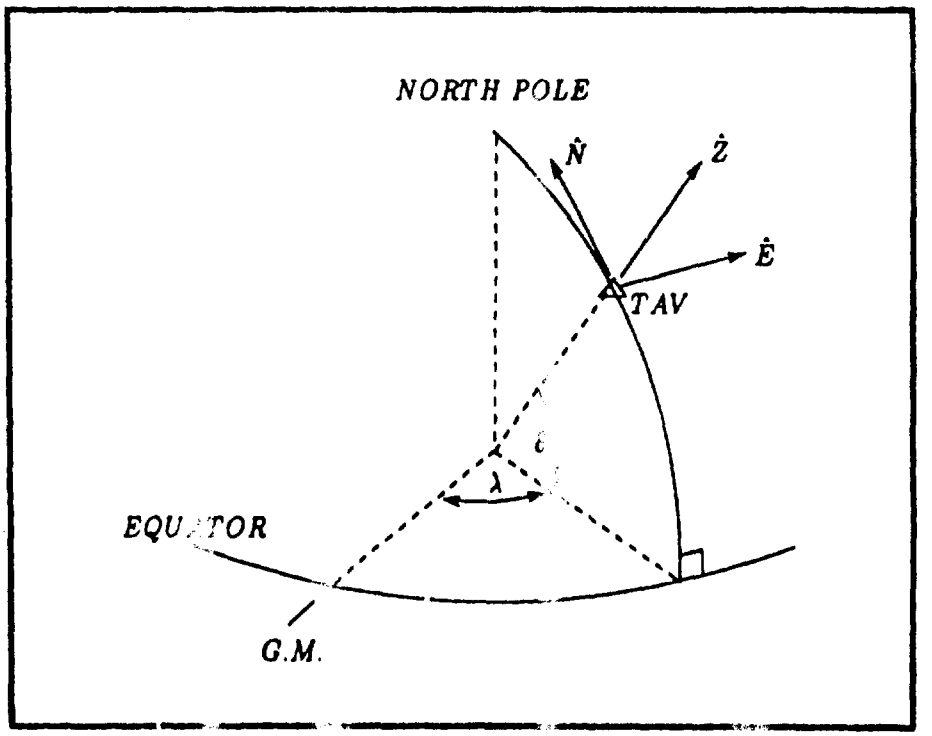

Figure 2.4. ENZ Reference Frame

The $\hat{E}$ axis always points due east, while the $\hat{N}$ axis points continuously to the north. The final axis, $\hat{Z}$, rounds out this right handed orthogonal set and points directly to the zenith.

The second reference frame, the body reference frame B, will also be attached to the TAV. In this frame of reference, $\hat{B}_1$ points out the TAV nose, $\hat{B}_2$ out the TAV left wing, and $\hat{B}_3$ rounds out the right handed, orthogonal system. If small bank angles are assumed for any TAV flight profile then the ENZ frame and B frame are related as in Figure 2.5. Note the coincidence of the $\hat{B}_3$ and the $\hat{Z}$ axes.

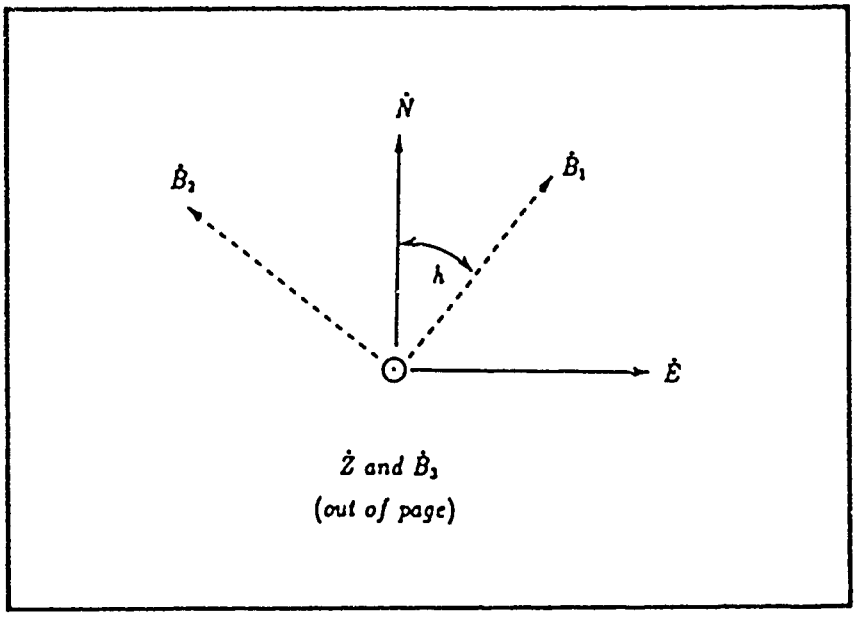

Figure 2.5. ENZ and B Frame Relationships

From the geometry of Figure 2.5, the coordinate transformation from the ENZ frame coordinates to B frame coordinates are

$$\hat{E} = \sin h\, \hat{B}_1 - \cos h\, \hat{B}_2 \qquad (2.8a)$$

$$\hat{N} = \cos h\, \hat{B}_1 + \sin h\, \hat{B}_2 \qquad (2.8b)$$

$$\hat{Z} = \hat{B}_3 \qquad (2.8c)$$

With these reference frames and the above transformation established, the equations of motion for $\dot{h}$ and $\dot{V}$ will now be derived.

The inertial velocity of the TAV, expressed in the body frame is

$$\bar{V}^b = V \hat{B}_1 \tag{2.9}$$

The inertial acceleration of the TAV is

$$\bar{A} = \frac{d^b}{dt}(\bar{V}) + \bar{\omega}^{bI} \times \bar{V}^b \tag{2.10}$$

$$= \frac{d^b}{dt}(V \hat{B}_1) + \bar{\omega}^{bI} \times V \hat{B}_1 \tag{2.11}$$

$$= \dot{V} \hat{B}_1 + \bar{\omega}^{bI} \times V \hat{B}_1 \tag{2.12}$$

Now, expanding the $\bar{\omega}^{bI}$ term in Eq (2.12)

$$\bar{\omega}^{bI} = \bar{\omega}^{b\ ENZ} + \bar{\omega}^{ENZ\ I} \tag{2.13}$$

where

$\bar{\omega}^{bI}$ is the angular velocity of the B frame with respect to the inertial reference frame

$\bar{\omega}^{b\ ENZ}$ is the angular velocity of the B frame with respect to the ENZ reference frame

$\bar{\omega}^{ENZ\ I}$ is the angular velocity of the ENZ frame with respect to the inertial reference frame.

From Figure 2.5

$$\bar{\omega}^{b\ ENZ} = -\dot{h} \hat{B}_3 \tag{2.14}$$

and realizing that rotation of the ENZ frame with respect to the inertial frame consists of contributions from the earth's rotation ($\bar{\omega}_e$) and the TAV angular velocities

$$\bar{\omega}^{ENZ\ I} = \bar{\omega}_e + \bar{\omega}_{TAV\ MOTION} \tag{2.15}$$

$$= \bar{\omega}_e + \dot{\lambda}_{TAV} + \dot{\delta}_{TAV} \tag{2.16}$$

$$= \bar{\omega}_e + \dot{\lambda} \cdot \cos\delta\, \hat{N} + \dot{\lambda} \cdot \sin\delta\, \hat{Z} - \dot{\delta}\, \hat{E} \tag{2.17}$$

In the ENZ frame

$$\bar{\omega}_e = \omega_e \cdot \cos\delta\, \hat{N} + \omega_e \cdot \sin\delta\, \hat{Z} \tag{2.18}$$

and substituting this result into Eq (2.17) produces

$$\bar{\omega}^{ENZ\,i} = -\dot{\delta}\,\hat{E} + (\dot{\lambda} + \omega_e)\cdot\cos\delta\,\hat{N} + (\dot{\lambda} + \omega_e)\cdot\sin\delta\,\hat{z} \qquad (2.19)$$

Transforming Eq (2.19) from ENZ coordinates to the body frame coordinates with the transformations of Eq (2.8) results in

$$\begin{aligned}\bar{\omega}^{ENZ\,i} = {} & (\dot{\lambda}\cdot\cos\delta\cdot\cos h - \dot{\delta}\cdot\sin h + \omega_e\cdot\cos\delta\cdot\cos h)\,\hat{B}_1 \\ & + (\dot{\lambda}\cdot\cos\delta\cdot\sin h + \dot{\delta}\cdot\cos h + \omega_e\cdot\cos\delta\cdot\sin h)\,\hat{B}_2 \\ & + (\dot{\lambda}\cdot\sin\delta + \omega_e\cdot\sin\delta)\,\hat{B}_3 \qquad (2.20)\end{aligned}$$

Substituting Eq (2.14) and Eq (2.20) into Eq (2.13) results in the expanded form of $\bar{\omega}^{bi}$:

$$\bar{\omega}^{bi} = \omega_1\,\hat{B}_1 + \omega_2\,\hat{B}_2 + \omega_3\,\hat{B}_3 \qquad (2.21)$$

where

$$\omega_1 = (\dot{\lambda}\cdot\cos\delta\cdot\cos h - \dot{\delta}\cdot\sin h + \omega_e\cdot\cos\delta\cdot\cos h)\,\hat{B}_1 \qquad (2.22)$$

$$\omega_2 = (\dot{\lambda}\cdot\cos\delta\cdot\sin h + \dot{\delta}\cdot\cos h + \omega_e\cdot\cos\delta\cdot\sin h)\,\hat{B}_2 \qquad (2.23)$$

$$\omega_3 = (\dot{\lambda}\cdot\sin\delta + \omega_e\cdot\sin\delta - \dot{h})\,\hat{B}_3 \qquad (2.24)$$

With $\bar{\omega}^{bi}$ now expressed in body frame coordinates, Eq (2.12) can be written

$$\bar{A} = \dot{V}\,\hat{B}_1 + \begin{vmatrix} \hat{B}_1 & \hat{B}_2 & \hat{B}_3 \\ \omega_1 & \omega_2 & \omega_3 \\ V & 0 & 0 \end{vmatrix} \qquad (2.25)$$

where the notation inside the brackets represents a cross product. Since motion in the vertical ($\hat{B}_3$) direction is being neglected due to assumptions of Chapter I, the acceleration in the $\hat{B}_3$ direction will be zero, so Eq (2.25) reduces to

$$\bar{A} = \dot{V}\,\hat{B}_1 + (V\cdot\dot{\lambda}\cdot\sin\delta + V\cdot\omega_e\cdot\sin\delta - V\cdot\dot{h})\,\hat{B}_2 \qquad (2.26)$$

Substituting Eq (2.7) for $\dot{\lambda}$ in Eq (2.26) produces the result

$$\bar{A} = \dot{V}\,\hat{B}_1 + \left[\frac{V^2\cdot\sin h\cdot\sin\delta}{R_e\cdot\cos\delta} - V\cdot\dot{h}\right]\hat{B}_2 \qquad (2.27)$$

From the definitions of the acceleration parameters in the previous section

$$\text{intrack acceleration} \equiv a_I = A \cdot B_1 \tag{2.28}$$

and

$$\text{transverse acceleration} \equiv a_T = A \cdot B_2 \tag{2.29}$$

or

$$a_I = \dot{V} \tag{2.30}$$

$$a_T = \left[\frac{V^2 \cdot \sin h \cdot \sin \delta}{R_e \cdot \cos \delta} - V \cdot \dot{h} \right] \tag{2.31}$$

From these two equations come the equations of motion for $\dot{V}$ and $\dot{h}$:

$$\dot{V} = a_I \tag{2.32}$$

$$\dot{h} = \frac{-a_T}{V} + \frac{V \cdot \sin h \cdot \sin \delta}{R_e \cdot \cos \delta} \tag{2.33}$$

To complete the set of six equations of motion in the six dynamic parameters λ, δ, h, V, a_I, and a_T, assume for the TAV system constant jerk. That is

$$\dot{a}_I = 0 \tag{2.34}$$

$$\dot{a}_T = 0 \tag{2.35}$$

Eqs (2.3), (2.7), (2.32), (2.33), (2.34) and (2.35) define six equations of motion, in the six dynamic parameters, for TAV motion over a rotating earth. Summarizing

$$\dot{\delta} = \frac{V \cdot \cos h}{R_e} \tag{2.3}$$

$$\dot{\lambda} = \frac{V \cdot \sin h}{R_e \cdot \sin \delta} - \omega_e \tag{2.7}$$

$$\dot{V} = a_I \tag{2.32}$$

$$\dot{h} = \frac{-a_T}{V} + \frac{V \cdot \sin h \cdot \sin \delta}{R_e \cdot \cos \delta} \tag{2.33}$$

$$\dot{a}_I = 0 \tag{2.34}$$

$$\dot{a}_T = 0 \qquad (2.35)$$

Propagation of the Equations of Motion

The dynamics of the TAV have been reduced to a system of six first order equations of form $\dot{\bar{x}} = f(\bar{x},t)$ where $\bar{x}$ is the vector consisting of the six TAV dynamic parameters. By varying the values assigned $\bar{x}$ over time, the data for any TAV profile can be generated by integrating the six equations of motion in parallel.

In this thesis, a predictor-corrector method developed by Hamming was used to propagate the equations of motion over time. Given initial conditions for $\bar{x}$, the time step size, and the right hand side of the equations of motion, the Haming algorithm produced detailed time histories for λ, δ, h, V, a_I, and a_T. To prevent numerical difficulties during the integration, care was taken in selecting the units associated with each one of these parameters. This involved expressing each parameter in units that make it equivalent in magnitude to the other parameters during the integration. For this thesis, λ, δ, and h were expressed in radians, V was expressed in DU/TU, and the accelerations (a_I and a_T) were expressed in DU/TU^2 (Gs). These units were successfully implemented in all algorithms.

III. Sensor Data Model

In this chapter, the process of data collection at the geosynchronous sensor is developed. The definitions of the data elements are enumerated, followed by discussion of preprocessing of this data before its input to the Kalman estimation algorithm. This preprocessing allows simplification of the Kalman algorithm code.

Definition of Data Elements

As stated earlier, the platform carrying the sensors is located in a geosynchronous orbit. The sensors themselves are assumed to be of the passive infrared type, collecting data on the position of the TAV's thermal signature. This position data consists of two measured angles, azimuth (Az) and elevation (El), both represented in Figure 3.1.

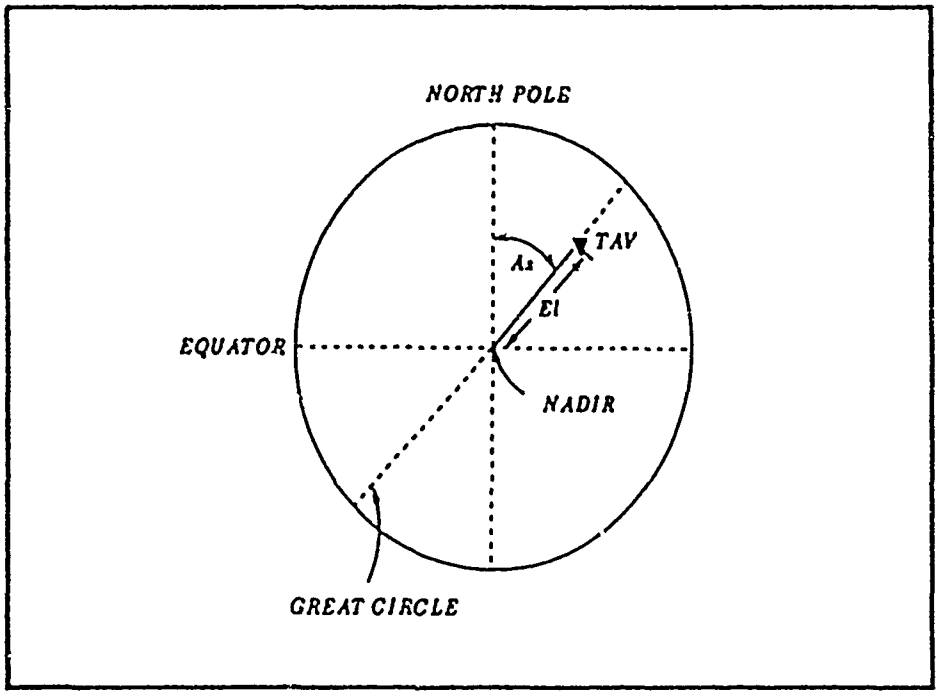

Figure 3.1. Azimuth and Elevation Data Angles

Azimuth is defined as the measured angle from the sensor platform's constant longitudinal position to the great circle connecting the platform's equatorial nadir and the TAV itself. It is measured positive in the clockwise direction. Conveniently, any great circle running through the platform's nadir appears as a straight line from the sensor platform. This ensures that, regardless of the TAV's position along any such great circle, the azimuth is identical.

The elevation angle locates the TAV's precise position along the identified great circle. It is measured from the nadir to the TAV directly. It can be alternately thought of as the angle subtended by the nadir-TAV segment when measured from the sensor platform. The elevation is always a positive angle by convention and never exceeds 8.6°.

Associated with the sensor data is some uncertainty due to sensor position inaccuracies, pointing inaccuracies, sensor platform jitter etc. These effects will not be considered independently, but their sum effect will be modelled in terms of the introduced standard deviation (σ) to the data. Osedacz (2:3), estimates the nominal data standard deviations as 3.5×10^{-3} radians for azimuth measurements and 4.3×10^{-4} radians for elevation. These values will be carried forward into this thesis, as well, and correspond to variances in the data covariance matrix [Q]. If the azimuth and elevation angles are assumed to be statistically independent of one another in a given set of data, then all covariances in [Q] are zero. This information completes [Q] :

$$[Q] = \begin{bmatrix} \sigma^2_{Az} & 0 \\ 0 & \sigma^2_{El} \end{bmatrix} = \begin{bmatrix} 1.225 \times 10^{-5} & 0 \\ 0 & 1.849 \times 10^{-11} \end{bmatrix} \quad (3.1)$$

Preprocessing of the Data Stream

The azimuth and elevation angles have TAV position information imbedded in them. Instead of processing the raw data angles in the Kalman estimation algorithm, it is very advantageous to extract this position information by transforming the angle data to raw longitude/latitude data. In doing so, the data now directly provides two of the six dynamic parameters characterizing TAV motion (λ and δ). Inputting this longitude/latitude data to the Kalman estimation algorithm greatly simplifies two of the matrices required by that algorithm. These matrices, [G] and [H], are discussed in detail next chapter. The remainder of this section pursues the data transformation itself.

Consider the planar triangle (Figure 3.2) with vertices at the sensor, earth's center, and the TAV:

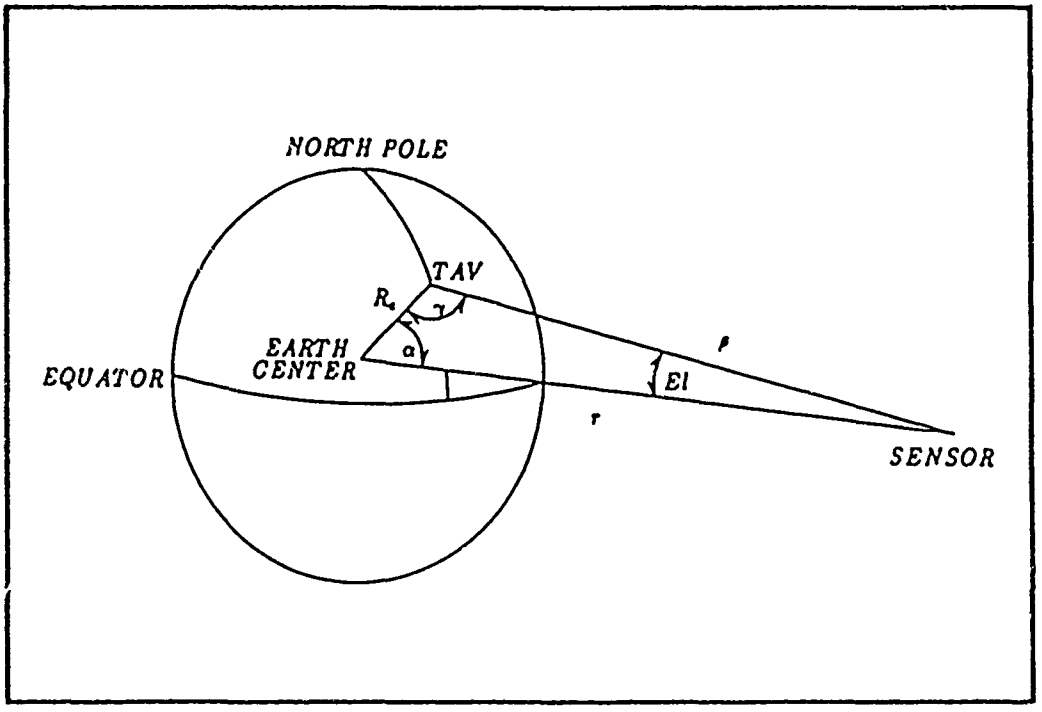

Figure 3.2. Planar Sensor-Earth's Center-TAV Triangle

From the law of sines for planar triangles

$$\frac{r}{\sin \gamma} = \frac{R_e}{\sin El} \tag{3.2}$$

where

r is the distance from the sensor to the earth's center
R_e is the radius of the earth

Solving for the interior angle γ

$$\gamma = \sin^{-1} \left[\frac{r \cdot \sin El}{R_e} \right] \tag{3.3}$$

From the geometry of Figure 3.2, it is evident at $\gamma = 90^\circ$, the TAV is imminently fading over the horizon from the sensor's point of view. Indeed, for $\gamma < 90^\circ$, the sensor "sees" the TAV as behind the earth. In view of these observations, the range of values for γ is restricted:

$$90^\circ < \gamma < 180^\circ \tag{3.4}$$

where $\gamma = 180^\circ$ is achieved when the TAV is directly over the sensor nadir point ($El = 0^\circ$). With γ determined, α is evaluated from the observation that interior angles of a planar triangle sum to 180° :

$$\alpha = 180^\circ - (El + \gamma) \tag{3.5}$$

Now that γ and α are evaluated in terms of r, R_e and El, the more complicated spherical geometry of the problem will provide the relationships expressing longitude and latitude as a function of the azimuth and elevation angles. This spherical geometry is depicted in Figure 3.3.

Applying the law of sines for oblique spherical triangles relative to Figure 3.3

$$\frac{\sin \delta}{\sin (90^\circ - Az)} = \frac{\sin \alpha}{\sin 90^\circ} \tag{3.6}$$

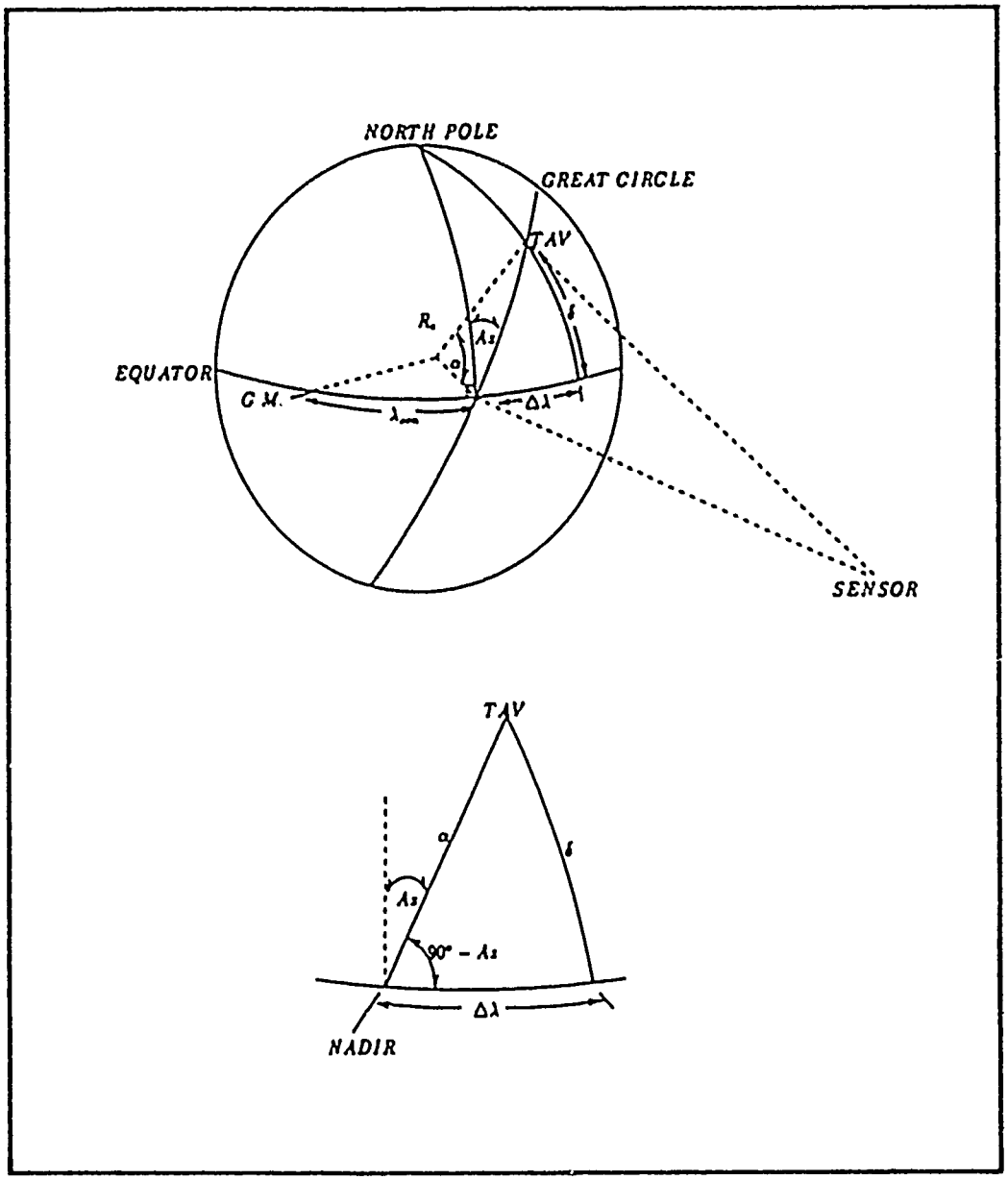

Figure 3.3. Spherical Geometry of TAV Tracking Problem

or

$$\sin \delta = \sin \alpha \cdot \sin (90^\circ - \alpha) \qquad (3.7)$$

which by trigonometric identity and further manipulation reduces to

$$\delta = \sin^{-1} (\sin \alpha \cdot \cos Az) \qquad (3.8)$$

Substituting Eqs (3.3) and (3.5) for α in Eq (3.8) results in the first

of two desired data transformations:

$$\delta = \sin^{-1}\left\{\sin\left[El + \sin^{-1}\left(\frac{r}{R_e}\cdot \sin El\right)\right]\cos Az\right\} \qquad (3.9)$$

The second transformation must produce a relationship expressing λ as a function of Az and El. This relationship can again be determined from the geometry of Figure 3.3. It is clear from the figure that

$$\lambda = \lambda_{sen} + \Delta\lambda \qquad (3.10)$$

where

λ is the TAV longitude position
λ_{sen} is the longitude position of the sensor
$\Delta\lambda$ is the longitudinal distance measured from the sensor to the TAV

Since λ_{sen} is predetermined, calculation of $\Delta\lambda$ will complete this data transformation to the TAV s longitudinal coordinate. Recognizing the spherical triangle of Figure 3.3 as a right spherical triangle

$$\sin \Delta\lambda = \tan \delta \cdot \cot (90^{\circ} - Az) \qquad (3.11)$$

which by trigonometric identity and further manipulation reduces to

$$\Delta\lambda = \sin^{-1}\left[\tan \delta \cdot \tan Az\right] \qquad (3.12)$$

Substituting Eqs (3.9) and (3.12) into Eq (3.10) completes the transformation from data angles to longitude:

$$\lambda = \lambda_{sen} + \sin^{-1}\left[\tan\left\{\sin^{-1}\left\{\sin\left[El + \sin^{-1}\left(\frac{r}{R_e}\cdot \sin El\right)\right]\cdot \cos Az\right\}\right\}\tan Az\right] \qquad (3.13)$$

Given any Az and El data set, Eqs (3.9) and (3.13) transform the data set to λ and δ data. Since the geometry of the problem ensures both δ and $\Delta\lambda$ will always lie in the interval $[-\pi/2,\pi/2]$, these equations have no complicated quadrant uncertainties.

Recall the Az and El data had an associated data covariance matrix, [Q], with variances reflecting the error imbedded in the data

measurements. No such data covariance matrix for the λ and δ data exists to this point. By transforming [O], however, with the Jacobian, [J], of the mathematical relationship between Az/El data and λ/δ data, the data covariance for λ and δ is determined. That is

$$[O]' = [J]\cdot[O]\cdot[J]^T \tag{3.14}$$

where

[O] is the data covariance associated with the Az and El data
[J] is the Jacobian matrix for the system
$[O]'$ is the data covariance associated with the λ and δ data

Recognizing that Eqs (3.9) and (3.13) are of the form

$$\lambda = f_1(Az,El) \tag{3.15}$$

$$\delta = f_2(Az,El) \tag{3.16}$$

the [J] and its transpose $[J]^T$ have elements derived from partial derivatives:

$$[J] = \begin{bmatrix} \frac{\partial f_1}{\partial Az} & \frac{\partial f_1}{\partial El} \\ \frac{\partial f_2}{\partial Az} & \frac{\partial f_2}{\partial El} \end{bmatrix} \tag{3.17}$$

$$[J]^T = \begin{bmatrix} \frac{\partial f_1}{\partial Az} & \frac{\partial f_2}{\partial Az} \\ \frac{\partial f_1}{\partial El} & \frac{\partial f_2}{\partial El} \end{bmatrix} \tag{3.18}$$

where

$$\frac{\partial f_1}{\partial Az} = \left\{ 1 - \left[\tan\left(\sin^{-1}\left\{ \sin\left[El + \sin^{-1}\left(\frac{r}{R_e}\cdot \sin El \right) \right] \cos Az \right\} \right) \tan Az \right]^2 \right\}^{-1/2}$$

$$\cdot \left[\sec^2\left(\sin^{-1}\left\{ \sin\left[El + \sin^{-1}\left(\frac{r}{R_e}\cdot \sin El \right) \right] \cos Az \right\} \right) \right.$$

$$\cdot \left[1 - \left\{ \sin\left[El + \sin^{-1}\left(\frac{r}{R_e} \cdot \sin El \right) \right] \cos Az \right\}^2 \right]^{-1/2}$$

$$\cdot (-\sin Az) \cdot (\tan Az) \cdot \left\{ \sin\left[El + \sin^{-1}\left(\frac{r}{R_e} \cdot \sin El \right) \right] \right\}$$

$$\cdot (\sec^2 Az) \cdot \tan\left(\sin^{-1}\left\{ \sin\left[El + \sin^{-1}\left(\frac{r}{R_e} \cdot \sin El \right) \right] \cos Az \right\} \right) \Bigg]$$

$$\frac{\partial f_1}{\partial El} = \left\{ 1 - \left[\tan\left(\sin^{-1}\left\{ \sin\left[El + \sin^{-1}\left(\frac{r}{R_e} \cdot \sin El \right) \right] \cos Az \right\} \right) \tan Az \right]^2 \right\}^{-1/2}$$

$$\cdot \Bigg[\sec^2\left(\sin^{-1}\left\{ \sin\left[El + \sin^{-1}\left(\frac{r}{R_e} \cdot \sin El \right) \right] \cos Az \right\} \right)$$

$$\cdot \left[1 - \left\{ \sin\left[El + \sin^{-1}\left(\frac{r}{R_e} \cdot \sin El \right) \right] \cos Az \right\}^2 \right]^{-1/2}$$

$$\cdot \cos Az \cdot \cos\left[El + \sin^{-1}\left(\frac{r}{R_e} \cdot \sin El \right) \right]$$

$$\cdot \left\{ 1 + \left[1 - \left(\frac{r}{R_e} \cdot \sin El \right)^2 \right]^{-1/2} \cdot \frac{r}{R_e} \cdot \cos El \right\} \tan Az \Bigg]$$

$$\frac{\partial f_2}{\partial Az} = \left[1 - \left\{ \sin\left[El + \sin^{-1}\left(\frac{r}{R_e} \cdot \sin El \right) \right] \cdot \cos Az \right\}^2 \right]^{-1/2}$$

$$\cdot \sin\left[El + \sin^{-1}\left(\frac{r}{R_e} \cdot \sin El \right) \right] \cdot \left[-\sin Az \right]$$

$$\frac{\partial f_2}{\partial El} = \left[1 - \left\{ \sin\left[El + \sin^{-1}\left(\frac{r}{R_e} \cdot \sin El \right) \right] \cdot \cos Az \right\}^2 \right]^{-1/2}$$

$$\cdot \cos Az \cdot \cos\left[El + \sin^{-1}\left(\frac{r}{Re} \cdot \sin El \right) \right]$$

$$\cdot \left\{ 1 + \left[1 - \left(\frac{r}{R_e} \cdot \sin El \right)^2 \right]^{-1/2} \cdot \frac{r}{R_e} \cdot \cos El \right\}$$

Eqs (3.17) and (3.18) complete the elements required for Eq (3.14). The data covariance for longitude and latitude data is now resolvable from Eq (3.14). This data covariance matrix and the attendant longitude and latitude data is now ready for processing within the Kalman estimation algorithm.

IV. Six State Element Kalman Filter Development

In selecting the optimal estimator appropriate to the TAV tracking problem, it is essential to first recognize that estimation of the TAV parameters is a stochastic process. The unpredictability with which the TAV may maneuver, at a given instant, rules out any possibility of deterministically this problem deterministically. In light of this stochastic nature, a sequential estimator is preferred over a batch estimation algorithm like a least squares method.

Two sequential estimators considered were the Bayes filter and the Kalman filter. Although the Bayes filter retains advantages over the Kalman filter in start up with the initial data, the advantage enjoyed by the Kalman filter in processing demands clinched its selection. This advantage in processing stems from the fact that the Bayes filter algorithm requires matrix inversions on the order of the state vector, which for this problem amounts to a 6x6 matrix inversion. The Kalman filter, on the other hand, requires inversions on the order of the data vector; in this case a 2x2 matrix inversion (4:102).

This chapter derives the six state Kalman filter that will process longitude and latitude data from an observed TAV trajectory and output estimates for the TAV's current position, heading, velocity, and acceleration. A detailed description of the specifically tailored elements that make up the Kalman filter for this tracking and estimation task will be presented. All techniques and symbology of estimation theory implemented in this thesis are derived from Wiesel (3:1-146) except when annotated otherwise.

Data Vector

The data vector, $\bar{z}$, input to the Kalman filter is a two element vector consisting of the current longitude (λ) and latitude (δ) of the TAV:

$$\bar{z} = (\lambda \; \delta) \tag{4.1}$$

The data elements in this vector result from the preprocessing of raw sensor azimuth and elevation angles. They are presented to the filter in units of radians. Associated with each input, $\bar{z}$, is the data covariance matrix $[Q]'$ developed in Chapter III, Eqs (3.14)-(3.18).

State Vector

The state vector, $\bar{x}$, being estimated by the Kalman filter algorithm is a 6x1 vector consisting of the six TAV dynamic parameters developed in Chapter II:

$$\bar{x} = (\lambda \;\; \delta \;\; h \;\; V \;\; a_l \;\; a_T) \tag{4.2}$$

At each data time (t_1) the filter propagates $\bar{x}$ over the data interval (Δt) as an initial estimate of the TAV's current state. This initial estimate would be extremely precise if $\bar{x}$ was propagated using a numerical integration package such as Haming. Although Haming was well suited for the task of generating the truth model for the TAV state over time, it has drawbacks to its use in the filter algorithm. Executing the Haming integrator over *every data* interval is computationally very burdensome and best avoided if possible. A better alternative is to propagate $\bar{x}$ using a discrete time approximation. This approximation implies that if the data interval is made sufficiently small, the Kalman filter can accurately propagate $\bar{x}$ linearly, in lieu of direct integration of the equations of motions. This is true even if the

equations of motion, themselves, are nonlinear. For this thesis, data intervals of 10 seconds or less were employed, an interval range found to be small enough to allow linear propagation of the TAV state vector.

The discrete time approximation propagates $\bar{x}$ from t_i to t_{i+1} by

$$\bar{x}_{i+1} = \dot{\bar{x}}_i \cdot \Delta t + \bar{x}_i \tag{4.3}$$

Incorporating the first order equations of motion for each state vector element from Eqs (2.3), (2.7), (2.32), (2.33), (2.34), and (2.35)

$$\begin{bmatrix} \lambda_{i+1} \\ \delta_{i+1} \\ h_{i+1} \\ V_{i+1} \\ a_{Ii+1} \\ a_{Ti+1} \end{bmatrix} = \begin{bmatrix} (V_i \cdot \sin h_i / R_e \cdot \cos \delta_i) - \omega_e \\ (V_i \cdot \cos h_i) / R_e \\ -a_{Ti} \cdot V_i + [(V_i \cdot \sin h_i \cdot \sin \delta_i) / R_e \cdot \cos \delta_i] \\ a_{Ii} \\ 0 \\ 0 \end{bmatrix} \cdot \Delta t + \begin{bmatrix} \lambda_i \\ \delta_i \\ h_i \\ V_i \\ a_{Ii} \\ a_{Ti} \end{bmatrix} \tag{4.4}$$

State Transition Matrix

The discrete time propagation of $\bar{x}$ detailed in Eq (4.4) provides an approximate solution to the TAV equations of motion in closed form:

$$\bar{x}_{i+1}(t) = f\,[\bar{x}_i(t),\ t] \tag{4.5}$$

where $f\,[\bar{x}_i(t),\ t]$ represents the right hand sides of the six equations in Eq (4.4). Since the state transition matrix, $[\Phi]$, describes a small change in the initial conditions of $\bar{x}$ propagating into a change in the final conditions:

$$[\Phi(i+1,i)] = \nabla_{x_i} \left[f\,[\bar{x}_i(t),\ t] \right] \tag{4.6}$$

or

$$[\Phi] = \begin{bmatrix} \frac{\partial \lambda_{t+1}}{\partial \lambda_t} & \frac{\partial \lambda_{t+1}}{\partial \delta_t} & \frac{\partial \lambda_{t+1}}{\partial h_t} & \frac{\partial \lambda_{t+1}}{\partial V_t} & \frac{\partial \lambda_{t+1}}{\partial a_{It}} & \frac{\partial \lambda_{t+1}}{\partial a_{Tt}} \\ \frac{\partial \delta_{t+1}}{\partial \lambda_t} & \frac{\partial \delta_{t+1}}{\partial \delta_t} & \frac{\partial \delta_{t+1}}{\partial h_t} & \frac{\partial \delta_{t+1}}{\partial V_t} & \frac{\partial \delta_{t+1}}{\partial a_{It}} & \frac{\partial \delta_{t+1}}{\partial a_{Tt}} \\ \frac{\partial h_{t+1}}{\partial \lambda_t} & \frac{\partial h_{t+1}}{\partial \delta_t} & \frac{\partial h_{t+1}}{\partial h_t} & \frac{\partial h_{t+1}}{\partial V_t} & \frac{\partial h_{t+1}}{\partial a_{It}} & \frac{\partial h_{t+1}}{\partial a_{Tt}} \\ \frac{\partial V_{t+1}}{\partial \lambda_t} & \frac{\partial V_{t+1}}{\partial \delta_t} & \frac{\partial V_{t+1}}{\partial h_t} & \frac{\partial V_{t+1}}{\partial V_t} & \frac{\partial V_{t+1}}{\partial a_{It}} & \frac{\partial V_{t+1}}{\partial a_{Tt}} \\ \frac{\partial a_{It+1}}{\partial \lambda_t} & \frac{\partial a_{It+1}}{\partial \delta_t} & \frac{\partial a_{It+1}}{\partial h_t} & \frac{\partial a_{It+1}}{\partial V_t} & \frac{\partial a_{It+1}}{\partial a_{It}} & \frac{\partial a_{It+1}}{\partial a_{Tt}} \\ \frac{\partial a_{Tt+1}}{\partial \lambda_t} & \frac{\partial a_{Tt+1}}{\partial \delta_t} & \frac{\partial a_{Tt+1}}{\partial h_t} & \frac{\partial a_{Tt+1}}{\partial V_t} & \frac{\partial a_{Tt+1}}{\partial a_{It}} & \frac{\partial a_{Tt+1}}{\partial a_{Tt}} \end{bmatrix} \tag{4.7}$$

where from Eq (4.4)

$$\frac{\partial \lambda_{t+1}}{\partial \delta_t} = \frac{V_t \cdot \sin h_t \cdot \sin \delta_t}{R_e \cdot \cos \delta_t^2} \cdot \Delta t$$

$$\frac{\partial \lambda_{t+1}}{\partial h_t} = \frac{V_t \cdot \cos h_t}{R_e \cdot \cos \delta_t} \cdot \Delta t$$

$$\frac{\partial \lambda_{t+1}}{\partial V_t} = \frac{\sin h_t}{R_e \cdot \cos \delta_t} \cdot \Delta t$$

$$\frac{\partial \delta_{t+1}}{\partial h_t} = \frac{-V_t \cdot \sin h_t}{R_e} \cdot \Delta t$$

$$\frac{\partial \delta_{t+1}}{\partial V_t} = \frac{\cos h_t}{R_e} \cdot \Delta t$$

$$\frac{\partial h_{t+1}}{\partial \delta_t} = \left[\frac{V_t \cdot \sin h_t}{R_e} + \frac{V_t \cdot \sin h_t \cdot \sin^2 \delta_t}{R_e \cdot \cos^2 \delta_t} \right] \cdot \Delta t$$

$$\frac{\partial h_{t+1}}{\partial h_t} = \frac{V_t \cdot \cos h_t \cdot \sin \delta_t}{R_e \cdot \cos \delta_t} \cdot \Delta t + 1$$

$$\frac{\partial h_{t+1}}{\partial V_t} = \left[\frac{a_{Tt}}{V_t^2} + \frac{\sin h_t \cdot \sin \delta_t}{R_e \cdot \cos \delta_t} \right] \cdot \Delta t$$

$$\frac{\partial h_{t+1}}{\partial a_{Tt}} = \frac{-\Delta t}{V_t}$$

$$\frac{\partial V_{t+1}}{\partial a_{It}} = \Delta t$$

$$\frac{\partial \lambda_{t+1}}{\partial \lambda_t} = \frac{\partial \delta_{t+1}}{\partial \delta_t} = \frac{\partial V_{t+1}}{\partial V_t} = \frac{\partial a_{It+1}}{\partial a_{It}} = \frac{\partial a_{Tt+1}}{\partial a_{Tt}} = 1$$

and all remaining partial derivatives are equal to zero.

Observation Function

The Observation Function, [G], is the mathematical relationship that expresses the data vector $\bar{z}$ as a function of the state vector elements $\bar{x}$:

$$\bar{z} = G(\bar{x}, t) \tag{4.8}$$

Benefiting from the preprocessing of the angles data to longitude and latitude data, [G] is simply the product of a scalar matrix and the state vector. This product reflects that the longitude and latitude data are identically the first two state elements (λ and δ):

$$\bar{z} = \begin{bmatrix} 1 & 0 & 0 & 0 & 0 & 0 \\ 0 & 1 & 0 & 0 & 0 & 0 \end{bmatrix} \cdot \bar{x} \tag{4.9}$$

where

$$G = \begin{bmatrix} 1 & 0 & 0 & 0 & 0 & 0 \\ 0 & 1 & 0 & 0 & 0 & 0 \end{bmatrix} \cdot \bar{x} \qquad (4.10)$$

H Matrix

The H Matrix, [H], relates the error in the current state estimate to the error in the reference trajectory. It is essentially the linearization of [G] with respect to the state vector and is mathematically expressed

$$[H] = \frac{\partial [G]}{\partial \bar{x}} = \begin{bmatrix} 1 & 0 & 0 & 0 & 0 & 0 \\ 0 & 1 & 0 & 0 & 0 & 0 \end{bmatrix} \qquad (4.11)$$

State Covariance Matrix

The State Covariance Matrix, [P], is a 6x6 matrix of covariances and variances associated with the state vector elements at a given point in time. It essentially measures how good the current state vector estimate is. [P] is initialized, upon target acquisition, assuming statistical independence between the elements of $\bar{x}$. This assumption reduces [P] to diagonal form:

$$[P] = \begin{bmatrix} \sigma_\lambda^2 & \sigma_\delta^2 & \sigma_h^2 & \sigma_V^2 & \sigma_{a_I}^2 & \sigma_{a_T}^2 \end{bmatrix} \qquad (4.12)$$

Again, this assumption is true only for the initial data point in a trajectory. Subsequent iterations and data points will result in nonzero covariances in [P].

Kalman filters require a reasonable initial estimate of [P] to begin productive processing. The initial guess involves a compromise between a [P] reflecting accurate data and a [P] reflecting inordinately inaccurate data. The Kalman filter will not start properly in the event of either extreme. A suitable [P] for initializing the filter for this

thesis sets all variances equal to 3×10^{-2}, where σ_λ^2 , σ_δ^2 and σ_h^2 have units of rad^2, σ_V^2 units of DU^2/TU^2 and the acceleration variances ($\sigma_{a_I}^2$ and $\sigma_{a_T}^2$) units of DU^2/TU^4 or G^2.

During the interval between data points, the goodness of the last state estimate degrades as the TAV remains dynamic. This degradation in the accuracy of the estimate is reflected through the propagation of [P] over the data interval. In executing this propagation of [P], a subtlety of Kalman filters must be reckoned with: the variances of [P] must be prevented from going to zero. Should the zeros occur, increasing state residuals are ignored and the filter estimates cease to be useful. This result is particularly unacceptable for the problem at hand because the TAV system is modelled by *stochastic dynamics*. This infers the variances should never be zero, but must always reflect the reality of unpredictable dynamic inputs. In order to estimate stochastic dynamics the Kalman filter must be "advised" of the constant uncertainty through non-zero variances. Since the filter, with each successive data point, tends to drive $[P] \rightarrow 0$, techniques are employed to inject additional uncertainty into the [P] elements. For this filter, that technique will be noisy dynamics.

The equation for propagation of [P] using noisy dynamics is

$$[P] = [\Phi][P][\Phi]^T + [C][Q_n][C]^T \qquad (4.13)$$

where

[C] is a matrix of ones and zeros serving to "noise" the desired elements of [P] with the desired noise value from the noise matrix $[Q_n]$. Simplifying for this scenario

$$[C][Q_n][C]^T = \begin{bmatrix} Q_{n_\lambda} & Q_{n_\delta} & Q_{n_h} & Q_{n_V} & Q_{n_{aI}} & Q_{n_{aT}} \end{bmatrix} \qquad (4.14)$$

The values of the diagonal elements in $[Q_n]$ are specified through the tuning process addressed in the next chapter.

Filter Equations and Algorithm

The Kalman filter employed in this thesis is in its iterated form and is not extended. As discussed, the dynamics and the observation relationships have been linearized and convergence will rarely, if ever, be attained in one iteration (2:7).

Three equations constitute the core of the Kalman filter algorithm:

$$[K] = [P(-)]\cdot[T]^T\cdot\left([Q]' + [T]\cdot[P(-)]\cdot[T]^T\right)^{-1} \tag{4.15}$$

$$[P(+)] = \left([I] - [K]\cdot[T]\right)\cdot[P(-)] \tag{4.16}$$

$$\delta\bar{x}(+) = \delta\bar{x}(-) + [K]\cdot\left(\bar{r}_z - [T]\cdot\delta\bar{x}(-)\right) \tag{4.17}$$

where

$[K]$ ≡ Kalman Gain Matrix
$[P(-)]$ ≡ State Covariance Matrix from the previous estimate
$[P(+)]$ ≡ State Covariance Matrix of the new estimate
$\delta\bar{x}(-)$ ≡ previous correction to the state estimate
$\delta\bar{x}(+)$ ≡ new correction to the state estimate
$[T] \equiv [H]\cdot[\Phi]$
$[I]$ ≡ identity matrix of order of the state vector
$\bar{r}_z$ ≡ data residual

In applying these equations in the most general Kalman filter algorithm, $[\Phi]$, $[K]$, and $[P(+)]$ are recalculated for each iteration over a single data point. The considerable computational effort involved in such a scheme was eliminated, without detriment, by assuming that the previous estimate is close to the true state. This allows for a single reevaluation of the filter linearizations, $[K]$, and $[P(+)]$ for each data point versus every iteration within a data point. The small data intervals used in observing the TAV are critical to the validity of this assumption.

The complete data processing algorithm, including the preprocessing of the azimuth and elevation data, and the Kalman filter discussed in this section is incorporated as a flowchart in Appendix A.

V. Tuning the Kalman Filter

The process of tuning the Kalman filter involves the evaluation of the individual matrix elements in the simplified noise matrix of Eq (4.14). The objective of the tuning process is to select a combination of the six noise elements producing the best filter estimates over the conceivable envelope of TAV operations. This section elaborates on the strategy driving the tuning process for the TAV tracking scenario and details the final tuning results for the six state Kalman filter.

Tuning Approach

Each diagonal element of the simplified noise matrix in Eq (4.14) reflects the degree of uncertainty that is being injected into the variances for each state element. Since each of the six diagonal elements have a possible range of values from zero to infinity, evaluation of all possible combinations is impossible. Even the starting point from which to begin the search for a set of noise elements is difficult without some initial approach. The approach for the tuning accomplished in this thesis was based on observations of the TAV equations of motion.

The TAV equations of motion for the intrack and transverse acceleration are very limited in application. In words, zero jerk implies the accelerations in both directions are not changing — an assumption that would never allow the TAV pilot to alter the intrack and transverse acceleration initial conditions for the rest of the flight! If the value of the variances are thought of, in an intuitive sense, as the degree of permission granted the Kalman filter to adjust the

corresponding state elements, then the values of $Q_{n_{aI}}$ and $Q_{n_{aT}}$ are expected to be large. Large acceleration noise components translate to large acceleration variances, which in turn allow the filter to significantly adjust acceleration estimates that could be severely inaccurate.

For λ, δ, h, and V, the dynamics are well defined and over the small data intervals between updates considered in this thesis, the estimates can be expected to be reasonably close. Whereas the TAV can change acceleration from 3.0 to -3.0 Gs, almost instantaneously, it cannot drastically change λ, δ, h, and V unless a long data interval is employed. As a result, the Q_n elements being added to the variances for λ, δ, h, and V should be small, allowing only enough noise to precipitate small corrections and prohibit the variances from going to zero.

Following these two rules of thumb, the tuning process was started at $Q_{n_\lambda} = Q_{n_\delta} = Q_{n_h} = 0$ rads^2, $Q_{n_V} = 0$ DU^2/TU^2, and $Q_{n_{aI}} = Q_{n_{aT}} = 100$ DU^2/TU^4.

As alluded to earlier, tuning is the search for noise elements that produce the best filter estimates over a conceivable flight envelope for the TAV. Consequently, the range of TAV flight profiles that the Kalman filter can expect to observe must be defined. This thesis considers TAV profiles that approach orbital velocity (approximately 1 DU/TU) and incorporate accelerations of up to eight G's. This acceleration envelope is very liberal for any TAV developed in the near future. Transverse G's are on the order of eight G's for the best fighter aircraft, a mission role that the TAV is not envisioned for, and eight intrack G's should cover even the worst case reentry scenarios of this

manned system.

Having established the flight envelope the Kalman filter is designed to observe, a single set of noise elements (Q_n's) permitting accurate estimation of the TAV trajectory at all accelerations is required. For a given data interval, a noise matrix that works for an eight G profile and a zero G, great circle should also work for the intermediate values of acceleration. As a result, for a given data interval, the Kalman filter was independently tuned to meet these two cases by themselves. This method produced two sets of noise elements which were then compromised to allow reasonable filter estimation of both cases with one set of noise values.

Tuning Parameters

Three parameters were particularly useful in evaluating tuning runs made for a given data interval. These parameters were acceleration response, maximum error, and average error.

Acceleration response, A_r, measures the speed with which the filter recognizes a sudden change in the TAV acceleration. It is defined as the time measured from the instant the TAV's acceleration changes to the instant the filter's estimate is 95% of the true acceleration value (Figure 5.1).

Maximum error, e_{max}, is the largest deviation of the filter state estimate from the truth model. Mathematically,

$$e_{max} = \left| \bar{x}_{EST}(t_m) - \bar{x}_{TRUTH}(t_m) \right|_{MAX} \qquad (5.1)$$

where t_m is the time the maximum error occured for the state element being specified. For each tuning run, e_{max} was evaluated for λ, δ, h, V, a_I, and a_T.

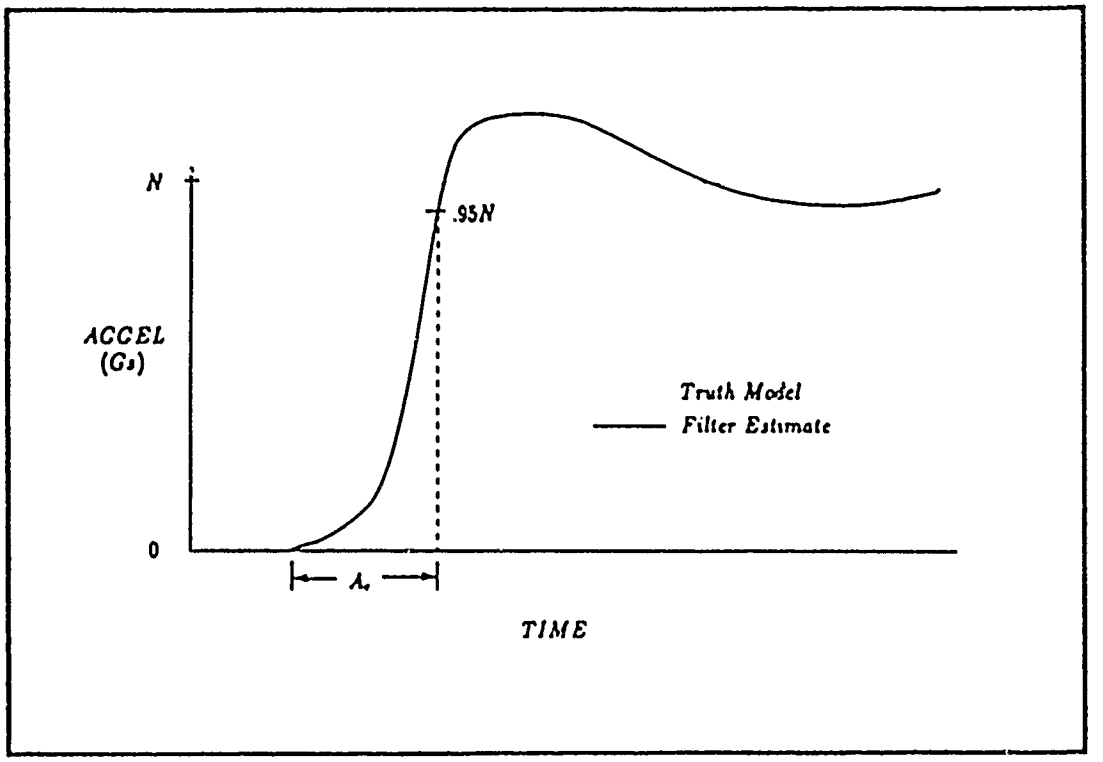

Figure 5.1. Acceleration Response Definition

Average error, e_{ave}, is the average error between the filter state estimate and the truth model over an entire flight profile:

$$\sum_{i}^{N} \frac{\left| \bar{x}_{EST}(t_i) - \bar{x}_{TRUTH}(t_i) \right|}{N} \qquad (5.2)$$

where

N ≡ the number of total data points from the trajectory observed

t_i ≡ time of the i^{th} data point

Average error was also calculated for all six state elements.

Tuning Flight Profile

To standardize the tuning process and allow a framework within which to evaluate a variety of noise sets over a number of accelerations and data intervals, a standard flight profile was created. All tuning runs were accomplished with this profile serving as the truth model.

The tuning flight profile, in all cases, consisted of data over a 480 second duration. During the first 60 seconds of the flight, the TAV flew a great circle, constant speed trajectory. Following this, an intrack acceleration of 1 to 8 G's was executed for 120 seconds. This intrack maneuver was followed by a 120 second interval of great circle, constant speed flight. Over the subsequent 120 second interval, a 1 to 8 G transverse acceleration was executed. To complete the profile, a great circle constant speed trajectory was flown. Table V.1 summarizes the standard flight profile:

Table V.1. Tuning Flight Profile

Time Interval (sec)	Duration (sec)	Trajectory
0 - 60	60	Great Circle, Constant Speed
61 - 180	120	Intrack Acceleration
181 - 300	120	Great Circle, Constant Speed
301 - 420	120	Transverse Acceleration
421 - 480	60	Great Circle, Constant Speed

Results

Having established the flight profile and parameters to evaluate tuning runs with, tuning results can now be addressed.

The standard flight profile was used to tune Kalman filters running with three different data intervals: 1, 5 and 10 seconds. Tuning was initiated with the Q_n values defined earlier and subsequent Q_n values were selected and tested as changes in the tuning parameters dictated. Tuning was stopped when average error parameters ceased to improve with changes to the first two significant digits in the acceleration Q_n terms. Filters were tuned separately over the the data intervals to

optimally track the 1 G and 8 G acceleration profiles, where an N G profile infers that both intrack and transverse accelerations were input as N Gs. Although the 0 G case is the true low end of the acceleration range, it does not provide acceleration response data. Therefore, a 1 G profile was used to validate the lower acceleration limit. In all cases, the tuned noises for the 1 G acceleration case and the 0 G acceleration case were identical for a given data interval.

The final values for the Q_n elements are tabulated in Table V.2 by

Table V.2. Optimal Q_n Values for Data Interval/Accelerations Cases

	1 Sec Data Int		5 Sec Data Int		10 Sec Data Int	
	1 G	8 G	1 G	8 G	1 G	8G
Tuned Q_n Values						
Q_{n_λ} $(rads^2)$	.01	.01	.01	.01	.01	.01
Q_{n_δ} $(rads^2)$	.01	.01	.01	.01	.01	.01
Q_{n_h} $(rads^2)$	0.0	0.0	0.0	0.0	0.0	0.0
Q_{n_V} (DU^2/TU^2)	0.0	0.0	0.0	0.0	0.0	0.0
$Q_{n_{aI}}$ (DU^2/TU^4)	$2x10^{10}$	$2x10^{10}$	$2.5x10^{7}$	$2.5x10^{7}$	$2.5x10^{6}$	$2.5x10^{6}$
$Q_{n_{aT}}$ (DU^2/TU^4)	$2x10^{10}$	$2x10^{10}$	$2.5x10^{7}$	$2.5x10^{7}$	$3.0x10^{6}$	$2.5x10^{6}$

data interval/acceleration case. The tuning results for these six cases, including the values calculated for the tuning parameters, are detailed in Appendix B.

The objective of tuning separate filters for each data interval at the expected boundaries of acceleration was to choose noise values (Q_n) suitable for estimation over the entire TAV flight envelope. Now that the noise values at the acceleration boundaries have been specified, these all encompassing noise values can be selected. Using Table V.2, the noise values appropriate for operating a Kalman filter at each of the data intervals are listed in Table V.3:

Table V.3. Optimal Q_n Values for Data Intervals

	Q_{n_λ} (RADS^2)	Q_{n_δ} (RADS^2)	Q_{n_h} (RADS^2)	Q_{n_V} (DU/TU)	$Q_{n_{aI}}$ (DU^2/TU^4)	$Q_{n_{aT}}$ (DU^2/TU^4)
Data Int (sec)						
1	.01	.01	0.0	0.0	2×10^{10}	2×10^{10}
5	.01	.01	0.0	0.0	2.5×10^{7}	2.5×10^{7}
10	.01	.01	0.0	0.0	2.5×10^{6}	2.5×10^{6}

VI. Six State Kalman Filter Results

The six state Kalman filter was tested for performance at three different data intervals: 1 second, 5 seconds, and 10 seconds. Values for the filter's noise elements were derived from Table V.3, implying that each data interval specific filter differed in the $[Q_n]$ set employed. Once the three Kalman filters were tailored to incorporate their unique data intervals and noise elements, each filter was tested against flight profiles varying in acceleration from 0 to 8 Gs. This range was tested at acceleration intervals of one, producing 9 estimation runs per TAV trajectory type tested. In addition to this acceleration range, a special test of the filter was conducted for 20 G accelerations. Although, 20 Gs are beyond the reasonable operational envelope of a manned TAV, this case opens the door to considering this filter design for tracking problems involving high G maneuvers.

Two TAV trajectories were flown in simulation of data coming into the sensor. The first was the trajectory used to tune the six state filter in Chapter V. It consists of an intrack acceleration followed by a transverse acceleration of like magnitude. The second trajectory simulates simultaneous intrack and transverse accelerations of equal magnitude.

Serial Acceleration Results

The TAV trajectory tested in this section consisted of an intrack acceleration followed separately by a transverse acceleration of equal magnitude. This 480 second data profile is summarized in detail in Table VI.1:

Table VI.1. Serial Acceleration Test Trajectory

Time Interval (sec)	Duration (sec)	Trajectory
0 - 60	60	Great Circle, Constant Speed
61 - 180	120	Intrack Acceleration
181 - 300	120	Great Circle, Constant Speed
301 - 420	120	Transverse Acceleration
421 - 480	60	Great Circle, Constant Speed

As a visual aid to grasping the trajectories, this thesis produced code that receives the truth model longitude and latitude as input and outputs the TAV trajectory on a 2-D projection of the earth as seen from the sensor platform. The trajectory of the 20 G serial acceleration case is included in Figure 6.1.

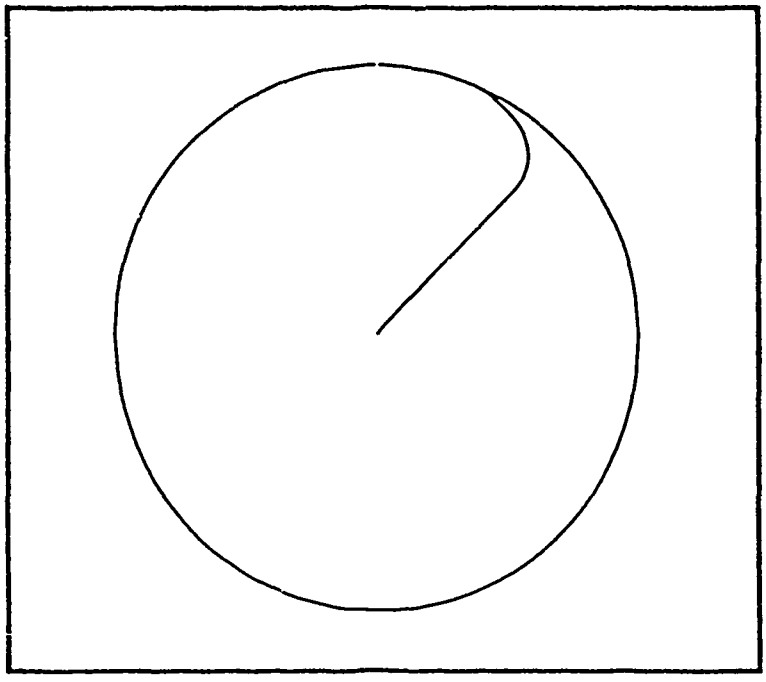

Figure 6.1. Sensor View of Serial 20 G TAV Trajectory

The 20 G case was selected because of the exaggerated trajectory it

produces, making it possible to distinguish the intrack and transverse acceleration phases. Note, the trajectory begins at the sensor nadir on the equator and ends in the northern latitudes.

Each data interval specific Kalman filter was tested against the serial trajectory for a total of 30 filter estimation runs. Results for these runs are tabulated by data interval in Tables VI.2 - VI.7 using the tuning parameters defined in Chapter V as performance parameters.

In addition to the average error, maximum error, and acceleration response parameters, a detailed data point by data point comparison of the TAV trajectory truth model and the Kalman filter state estimates is invaluable. By overlaying the truth model and estimate in graphical form, a visual sense of where the filter estimates are close and where the filter estimates diverge emerges. This graphical technique could have been included as results for every data run. Not only would the volume of graphs have been overwhelming, however, but it soon would be apparent that all the graphical comparisons per state are identical in form. Only the values associated with the particular graphs would significantly change. Since Tables VI.2 - VI.7 already provide these numbers in detail, only a single set of graphs will be incorporated here. A 5 second data interval and 4 G acceleration profile was selected to be representative of all the serial acceleration tests. Its position in the center of the acceleration and data interval ranges make it a solid choice. In addition, 4 Gs is also fairly representative of the maximum acceleration expected for most TAV trajectories. The acceleration range was expanded to 8 Gs to be very conservative.

Table VI.2. Serial Acceleration Errors for 1 Second Data Interval

Accel (Gs)	$\frac{e_{ave_\lambda}}{e_{max_\lambda}}$ (DEG)	$\frac{e_{ave_\delta}}{e_{max_\delta}}$ (DEG)	$\frac{e_{ave_h}}{e_{max_h}}$ (DEG)	$\frac{e_{ave_V}}{e_{max_V}}$ (MPH)	$\frac{e_{ave_{aI}}}{e_{max_{aI}}}$ (Gs)	$\frac{e_{ave_{aT}}}{e_{max_{aT}}}$ (Gs)
0	3.3E-10 9.3E-10	1.3E-10 3.8E-10	2.0E-09 4.0E-03	1.0E-01 2.1E-01	2.0E-05 5.0E-05	9.8E-05 2.3E-04
1	9.3E-10 4.9E-08	6.7E-10 3.7E-08	1.4E-02 5.9E-02	2.9279i 12.6069	6.4E-03 1.00000	6.4E-03 1.00021
2	1.6E-09 1.1E-07	1.2E-09 7.1E-08	2.3E-02 9.7E-02	5.7689i 25.1853	1.3E-02 2.00014	1.3E-02 2.00040
3	2.4E-09 1.9E-07	1.6E-09 1.1E-07	2.9E-02 0.12210	8.6394i 37.7659	1.9E-02 3.00026	1.9E-02 3.00067
4	3.9E-09 2.9E-07	2.1E-09 1.4E-07	3.4E-02 0.13965	11.5282 50.3458	2.6E-02 4.00041	2.6E.02 4.00105
5	4.2E-09 4.0E-07	2.6E-09 1.8E-07	3.7E-02 0.15220	14.4600 62.9243	3.2E-02 5.00062	3.2E-02 5.00193
6	5.3E-09 5.4E-07	3.0E-09 2.2E-07	4.0E-02 0.16123	17.4959 75.5045	3.9E-02 6.00088	3.9E-02 6.00319
7	6.6E-09 7.2E-07	3.5E-09 2.6E-07	4.2E-02 0.16766	20.4637 88.0848	4.6E-02 7.00121	4.6E-02 7.00483
8	8.4E-09 9.5E-07	4.0E-09 3.0E-07	4.3E-02 0.17208	23.5531 100.665	5.3E-02 8.00160	5.3E-02 8.00687
20	1.3E-08 1.8E-06	1.1E-09 7.3E-08	6.5E-02 0.29125	77.1827 334.790	0.18417 20.0142	0.17917 20.0934

Table VI.3. Serial Acceleration Errors for 5 Second Data Interval

	$\frac{e_{ave_\lambda}}{e_{max_\lambda}}$ (DEG)	$\frac{e_{ave_\delta}}{e_{max_\delta}}$ (DEG)	$\frac{e_{ave_h}}{e_{max_h}}$ (DEG)	$\frac{e_{ave_V}}{e_{max_V}}$ (MPH)	$\frac{e_{ave_{aI}}}{e_{max_{aI}}}$ (Gs)	$\frac{e_{ave_{aT}}}{e_{max_{aT}}}$ (Gs)
Accel (Gs)						
0	1.7E-9 6.3E-9	1.1E-9 4.2E-9	1.0E-2 2.0E-2	5.2E-1 1.04051	1.0E-4 2.1E-4	4.9E-4 9.9E-4
1	4.6E-8 6.3E-7	3.9E-8 4.6E-7	7.2E-2 0.27207	14.7697 58.2664	3.2E-2 1.00093	3.2E-2 1.00107
2	9.2E-8 1.3E-6	7.2E-8 9.3E-7	0.11584 0.44741	29.1182 116.381	6.3E-2 2.00069	6.4E-2 2.00200
3	1.3E-7 2.3E-6	1.1E-7 1.3E-6	0.14605 0.56425	43.6436 174.495	9.7E-2 3.00129	9.6E-2 3.00935
4	2.0E-7 3.7E-6	1.4E-7 2.0E-6	0.16809 0.64590	58.9389 232.595	0.19067 4.00196	0.12905 4.00524
5	2.7E-7 5.3E-6	1.7E-7 2.3E-6	0.18504 0.70457	73.2145 290.722	0.16415 5.00292	0.16197 5.00879
6	3.5E-7 7.2E-6	2.1E-7 3.1E-6	0.19841 0.74714	88.3041 348.831	0.19790 6.00419	0.19542 6.01466
7	4.4E-7 9.8E-6	2.4E-7 3.6E-6	0.20919 0.77768	103.670 406.957	0.23198 7.00563	0.22944 7.02228
8	5.6E-7 1.3E-5	2.8E-7 4.2E-6	0.21800 0.79899	119.939 465.066	0.26644 8.00743	0.26497 8.03172
20	3.3E-6 6.0E-5	2.2E-7 3.1E-6	0.31081 1.44998	398.841 1698.97	0.94968 20.0626	0.84372 20.1691

Table VI.4. Serial Acceleration Errors for 10 Second Data Interval

Accel (Gs)	$\frac{e_{ave_\lambda}}{e_{max_\lambda}}$ (DEG)	$\frac{e_{ave_\delta}}{e_{max_\delta}}$ (DEG)	$\frac{e_{ave_h}}{e_{max_h}}$ (DEG)	$\frac{e_{ave_V}}{e_{max_V}}$ (MPH)	$\frac{e_{ave_{aI}}}{e_{max_{aI}}}$ (Gs)	$\frac{e_{ave_{aT}}}{e_{max_{aT}}}$ (Gs)
0	1.4E-8 / 6.1E-8	6.7E-9 / 3.2E-8	2.0E-2 / 4.0E-2	1.04671 / 2.96411	2.0E-4 / 5.3E-4	9.9E-4 / 2.6E-3
1	1.1E-6 / 8.0E-6	9.6E-7 / 6.2E-6	0.14412 / 0.57049	31.0404 / 124.765	6.8E-2 / 1.00394	6.2E-2 / 1.00182
2	2.3E-6 / 1.8E-5	1.9E-6 / 1.3E-5	0.29349 / 0.99048	69.2408 / 249.182	0.14208 / 2.00798	0.12109 / 2.00914
3	3.7E-6 / 3.0E-5	2.8E-6 / 1.9E-5	0.29487 / 1.16316	96.0697 / 373.588	0.21748 / 3.01236	0.18121 / 3.00501
4	5.2E-6 / 4.3E-5	3.8E-6 / 2.5E-5	0.39868 / 1.31912	129.089 / 498.011	0.29352 / 4.01714	0.24200 / 4.00765
5	6.9E-6 / 6.3E-5	4.9E-6 / 3.1E-5	0.97065 / 1.42466	162.909 / 622.452	0.36958 / 5.02297	0.30942 / 5.01102
6	8.8E-6 / 8.4E-5	5.9E-6 / 3.8E-5	0.99419 / 1.59100	195.548 / 746.876	0.44579 / 6.02811	0.36655 / 6.01522
7	1.1E-5 / 1.1E-4	7.0E-6 / 4.4E-5	0.41916 / 1.64989	228.705 / 871.299	0.52089 / 7.03442	0.43456 / 7.02029
8	1.4E-5 / 1.4E-4	8.1E-6 / 5.1E-5	0.42995 / 1.77846	261.709 / 995.740	0.59445 / 8.04135	0.51069 / 8.02626
20	2.1E-5 / 5.6E-4	9.5E-6 / 5.6E-5	0.61496 / 2.06911	816.956 / 2870.69	1.62896 / 20.1117	1.47281 / 20.9423

Table VI.5. Acceleration Response for 1 Second Data Interval

Accel (Gs)	A_{r_I} (DATA POINTS)	A_{r_I} (SEC)	A_{r_T} (DATA POINTS)	A_{r_T} (SEC)
0	N/A	N/A	N/A	N/A
1	3	3	3	3
2	3	3	3	3
3	3	3	3	3
4	3	3	3	3
5	3	3	3	3
6	3	3	3	3
7	3	3	3	3
8	3	3	3	3
20	4	4	4	4

Table VI.6. Acceleration Response for 5 Second Data Interval

Accel (Gs)	A_{r_I} DATA (POINTS)	A_{r_I} (SEC)	A_{r_T} DATA (POINTS)	A_{r_T} (SEC)
0	N/A	N/A	N/A	N/A
1	3	15	3	15
2	3	15	3	15
3	3	15	3	15
4	3	15	3	15
5	3	15	3	15
6	3	15	3	15
7	3	15	3	15
8	3	15	3	15
20	4	20	4	20

Table VI.7. Acceleration Response for 10 Second Data Interval

Accel (Gs)	A_{r_I} (DATA POINTS)	A_{r_I} (SEC)	A_{r_T} (DATA POINTS)	A_{r_T} (SEC)
0	N/A	N/A	N/A	N/A
1	3	30	3	30
2	3	30	3	30
3	3	30	3	30
4	3	30	3	30
5	3	30	3	30
6	3	30	3	30
7	3	30	3	30
8	3	30	3	30
20	4	40	4	40

Figures 6.2 - 6.7 show this typical estimation vs. truth model profile for λ, δ, h, V, a_I, and a_T in a serial trajectory. From the

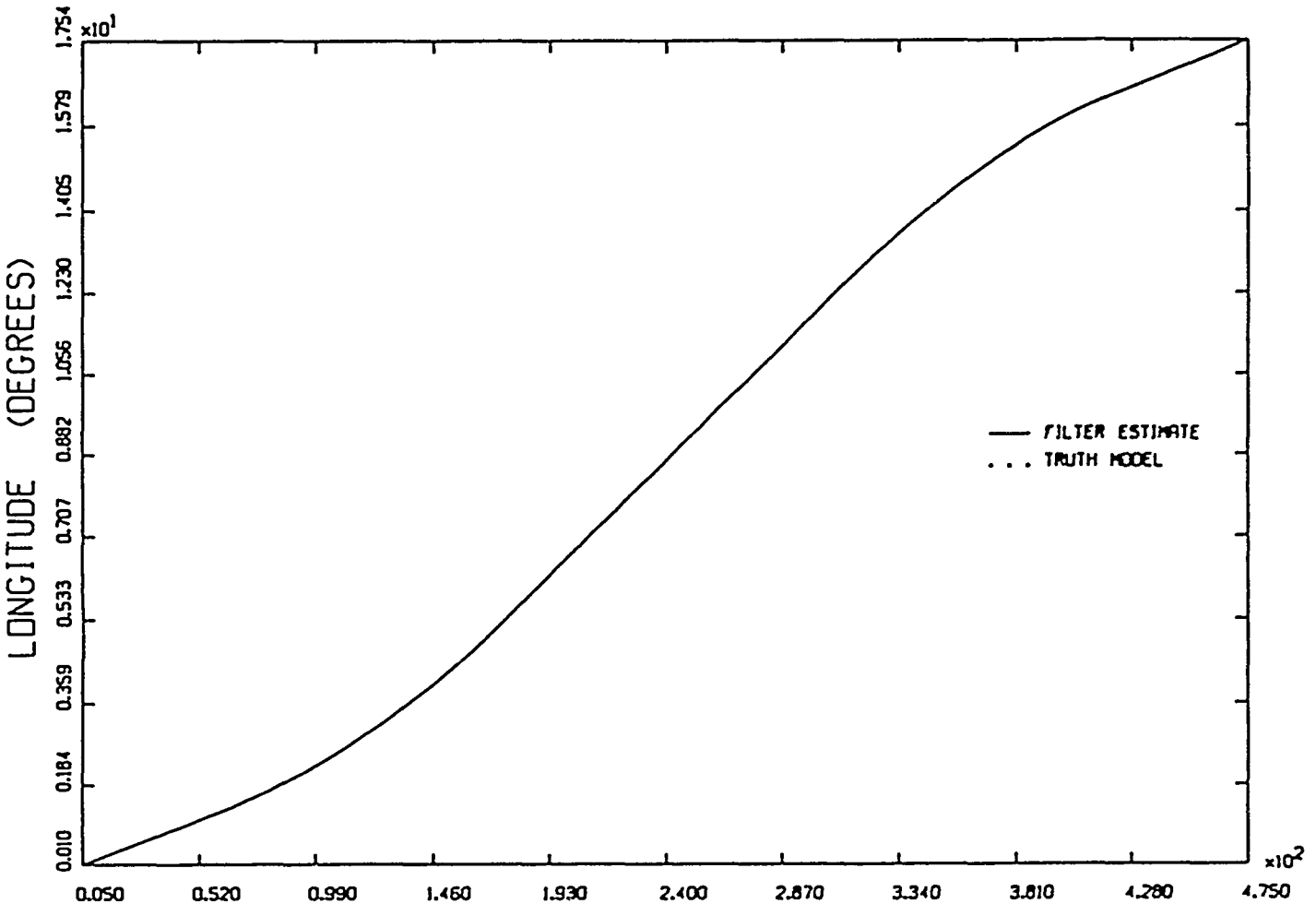

Figure 6.2. Kalman Longitude Estimate
(Serial 4 G : Data Interval = 5 Sec)

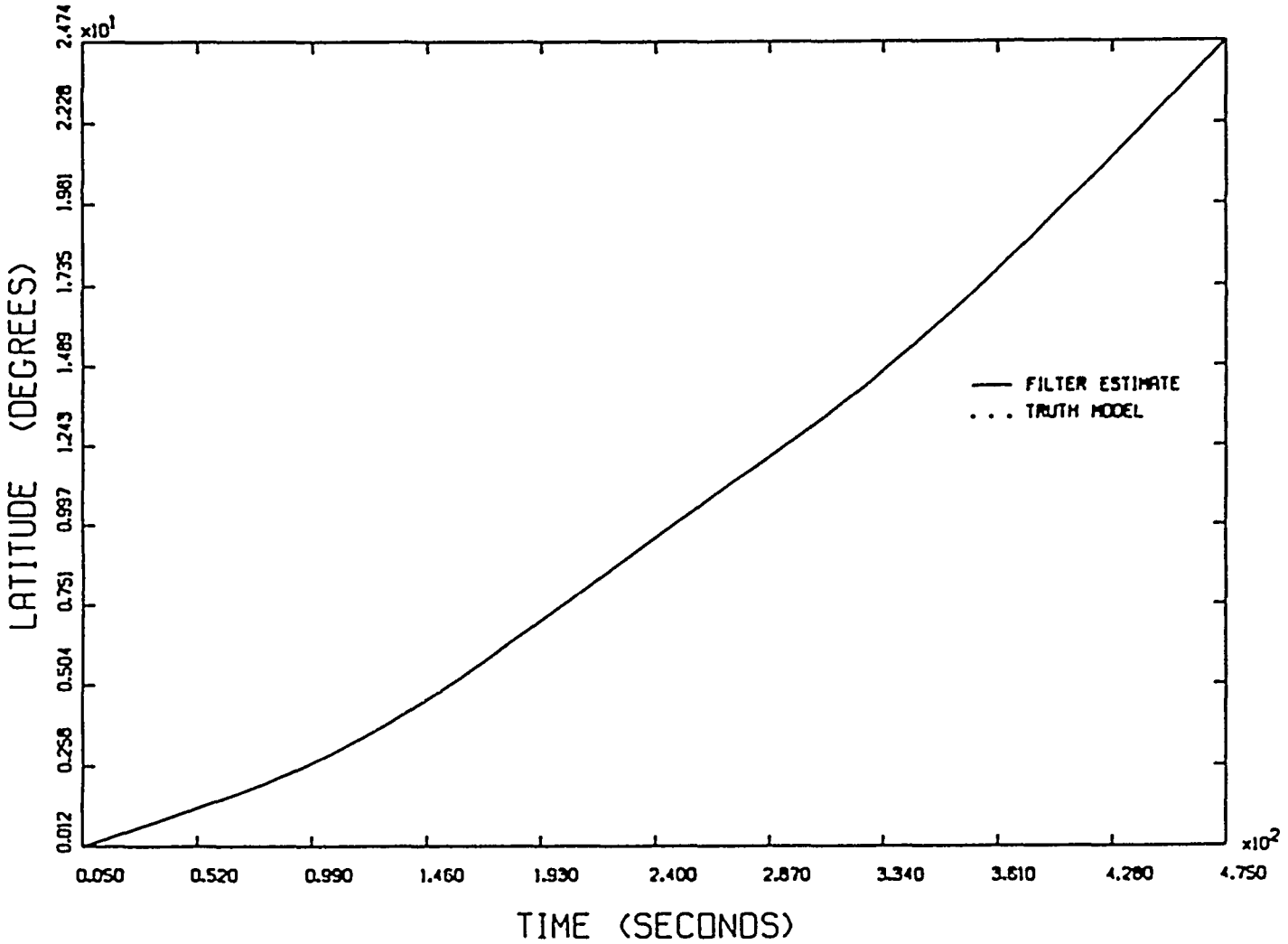

Figure 6.3. Kalman Latitude Estimate
(Serial 4 G : Data Interval = 5 Sec)

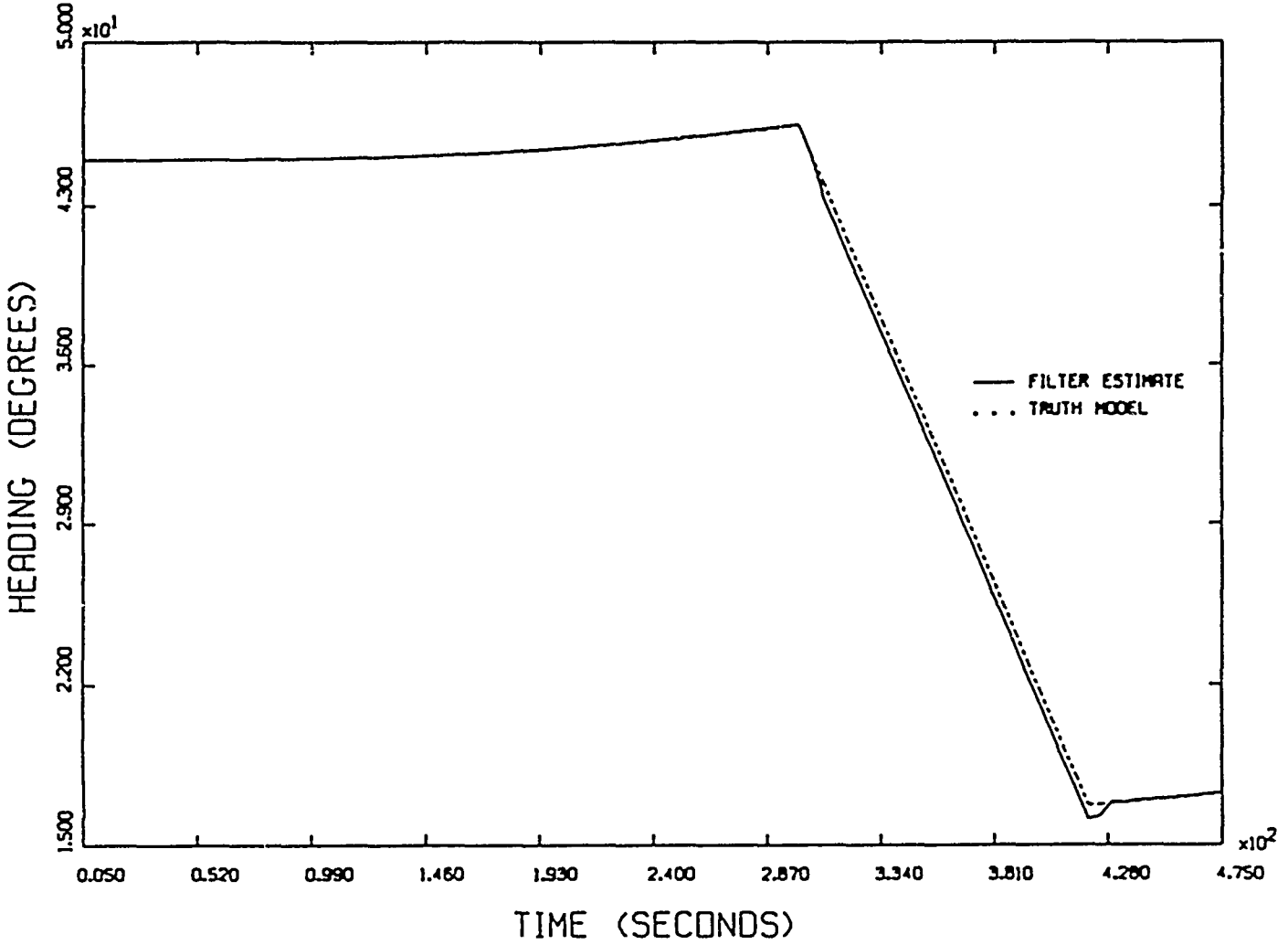

Figure 6.4. Kalman Heading Estimate
(Serial 4 G : Data Interval = 5 Sec)

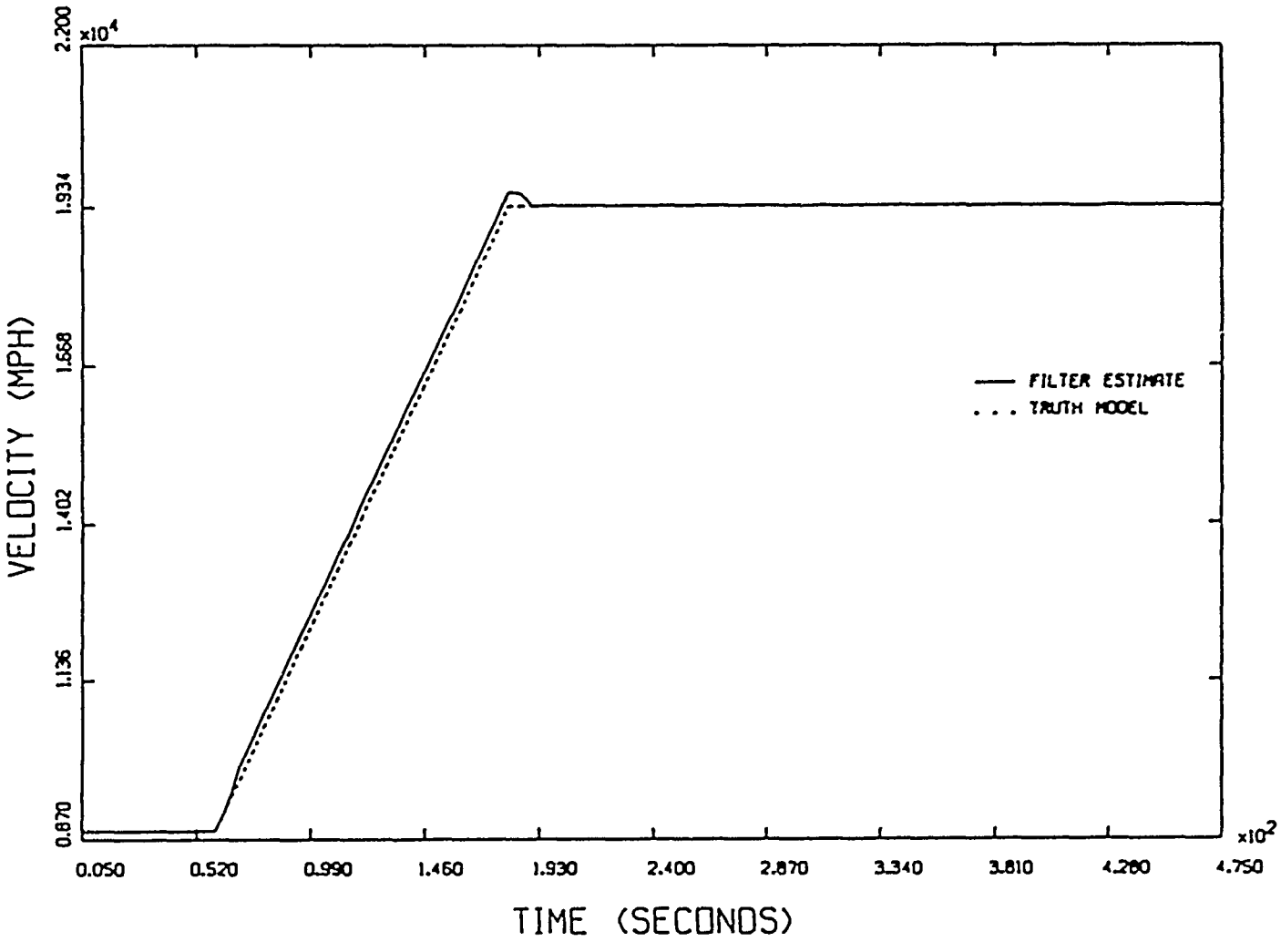

Figure 6.5. Kalman Velocity Estimate
(Serial 4 G : Data Interval = 5 Sec)

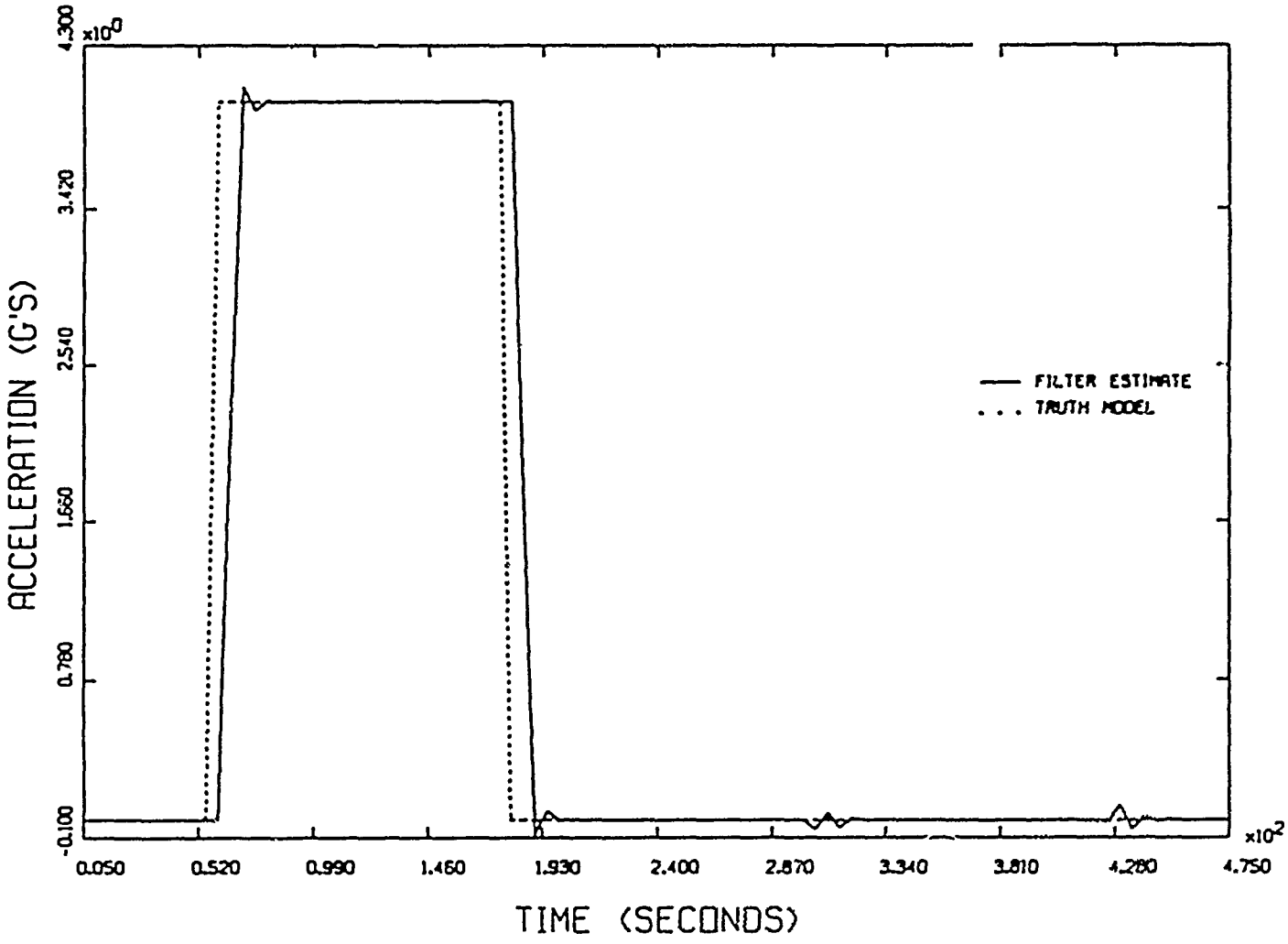

Figure 6.6. Kalman Intrack Acceleration Estimate (Serial 4 G : Data Interval = 5 Sec)

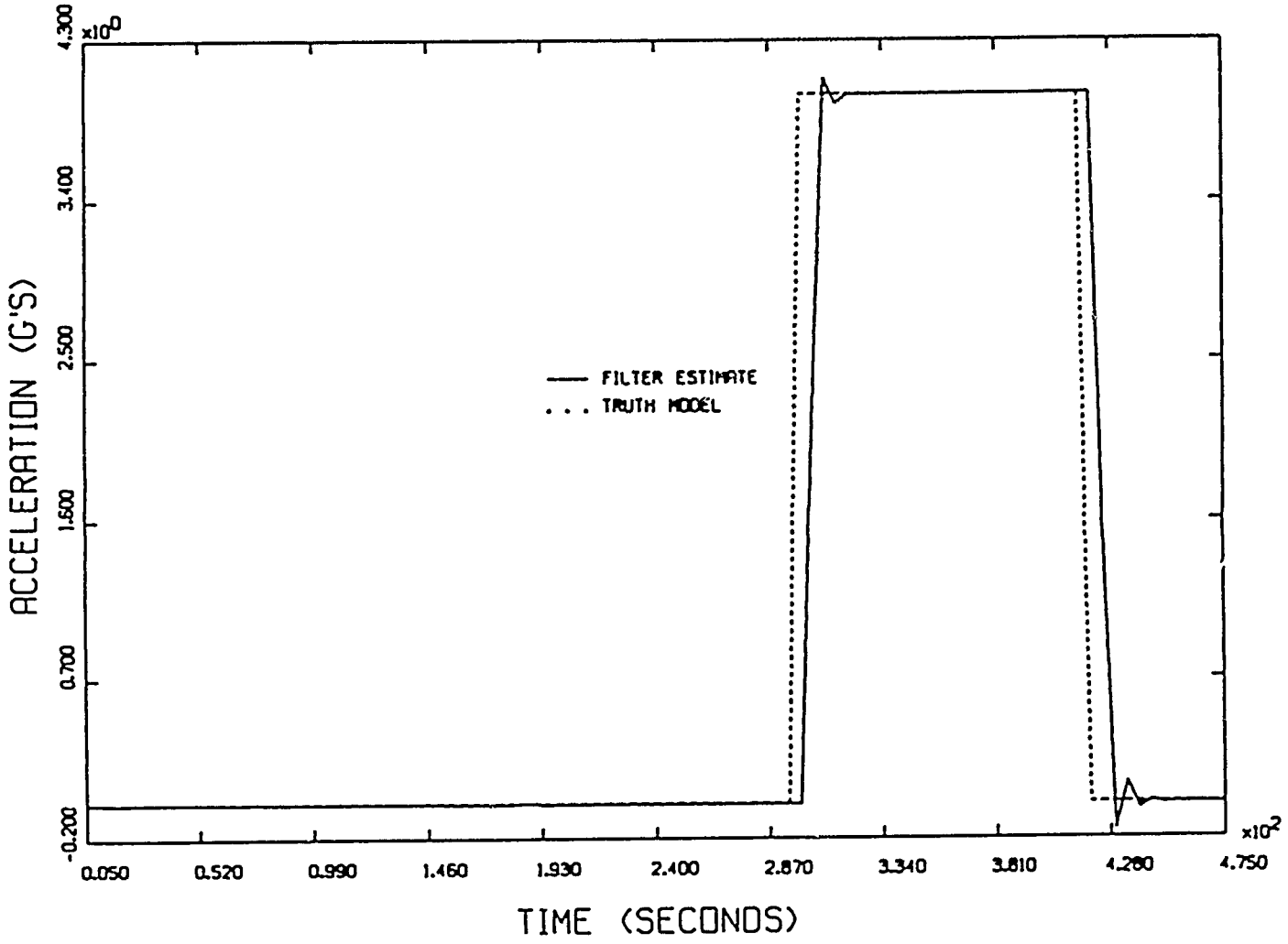

Figure 6.7. Kalman Transverse Acceleration Estimate (Serial 4 g : Data Interval = 5 Sec)

figures for the two position parameters, λ and ϕ, the accuracy hinted at by the previously tabulated average error values are borne out. The truth model and estimated values of these states were so close as to make the two lines indistinguishable. The figures for heading and velocity show estimates very close to the truth model values as well. For the serial acceleration cases, intrack accelerations precipitated a divergence of the velocity estimate from the velocity truth model. Similarly, input of transverse accelerations precipitated an interval of divergence between the heading estimate and truth model. Both intervals of divergence begin as soon as the related accelerations are input. The maximum divergence between the estimate and truth model usually occured two data points following termination of the accelerations, at which point the divergence quickly diminishes as the estimate recovers to follow the truth model again. The figures representing the acceleration trends show the greatest estimate error around both the inception and completion of an acceleration interval. Maximum error always occured one data point after the acceleration was begun and completed. As in the case of heading and velocity, however, the acceleration estimates quickly corrected back to the truth models in roughly three to four data points. This behavior was independent of the size of the data interval.

Simultaneous Acceleration Results

Testing of the simultaneous trajectory consisted of equal intrack and transverse accelerations, simultaneously initiated and terminated over the same data span. This profile is also 480 seconds in length and is summarized in Table VI.8:

Table VI.8. Simultaneous Acceleration Test Trajectory

Time Interval (sec)	Duration (sec)	Trajectory
0 - 60	60	Great Circle, Constant Speed
61 - 180	120	Intrack and Transverse Accel.
181 - 300	120	Great Circle, Constant Speed
301 - 420	120	Great Circle, Constant Speed
421 - 480	60	Great Circle, Constant Speed

The trajectory is illustrated in Figure 6.8. The 20 G acceleration profile was again selected for its length and exaggerated characteristics. The direction of the TAV motion is again from the equatorial nadir to northern latitudes.

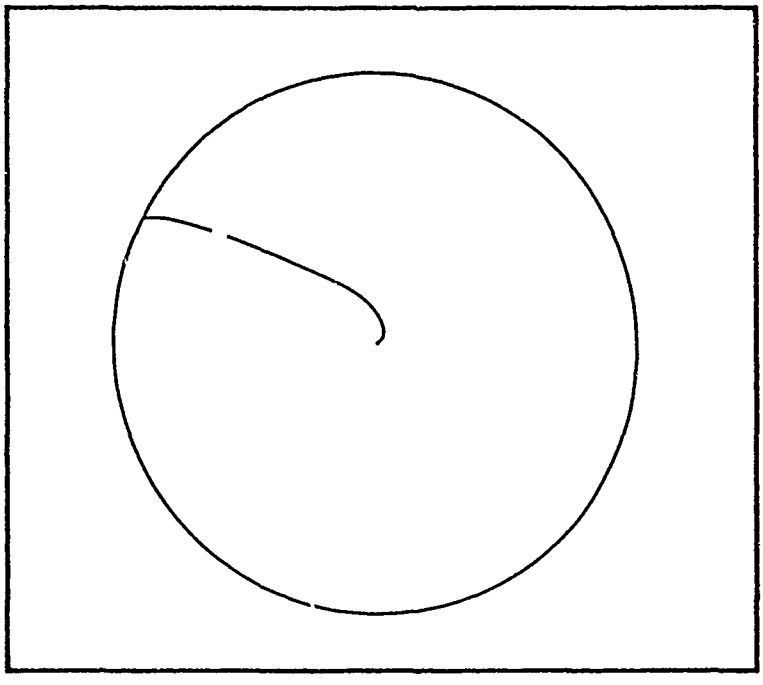

Figure 6.8. Sensor View of Simultaneous 20 G TAV Trajectory

Like the serial case, each data interval specific Kalman filter was

tested against the simultaneous trajectory set. Results for these runs appear in Tables VI.9 - VI.14., where data is again expressed by data interval in terms of the tuning parameters discussed in Chapter V.

Table VI.9. Simultaneous Acceleration Errors for 1 Second Data Interval

	$\frac{e_{ave_\lambda}}{e_{max_\lambda}}$ (DEG)	$\frac{e_{ave_\delta}}{e_{max_\delta}}$ (DEG)	$\frac{e_{ave_h}}{e_{max_h}}$ (DEG)	$\frac{e_{ave_V}}{e_{max_V}}$ (MPH)	$\frac{e_{ave_{aI}}}{e_{max_{aI}}}$ (Gs)	$\frac{e_{ave_{aT}}}{e_{max_{aT}}}$ (Gs)
Accel (Gs)						
0	3.3E-10 / 9.3E-10	1.3E-10 / 3.8E-10	2.0E-03 / 4.0E-03	1.0E-01 / 2.1E-01	2.0E-05 / 5.0E-05	9.8E-05 / 2.3E-04
1	3.1E-10 / 1.7E-06	7.6E-10 / 7.0E-08	1.8E-02 / 8.0E-02	2.90121 / 12.6729	6.3E-03 / 1.00002	6.6E-03 / 1.00010
2	5.4E-10 / 6.2E-08	1.2E-09 / 1.4E-07	3.0E-02 / 0.15076	5.69494 / 25.4505	1.3E-02 / 1.99999	1.4E-02 / 2.00010
3	8.1E-10 / 1.2E-07	1.6E-09 / 2.1E-07	4.0E-02 / 0.29354	8.91775 / 38.9579	1.9E-02 / 2.99998	2.1E-02 / 3.00010
4	1.2E-09 / 2.0E-07	2.0E-09 / 2.8E-07	4.6E-02 / 0.31039	11.01896 / 51.3909	2.5E-02 / 3.99910	2.8E-02 / 4.00010
5	1.6E-09 / 2.9E-07	2.4E-09 / 3.5E-07	5.7E-02 / 0.38928	19.8471 / 64.54	3.2E-02 / 5.00017	3.6E-02 / 5.00010
6	2.0E-09 / 3.8E-07	2.6E-09 / 4.2E-07	6.8E-02 / 0.45419	16.9229 / 77.8158	3.8E-02 / 6.00054	4.4E-02 / 6.00010
7	2.5E-09 / 4.7E-07	2.9E-09 / 4.9E-7	7.9E-02 / 0.52910	20.9399 / 91.2007	4.5E-02 / 7.00111	5.2E-02 / 7.00010
8	3.0E-09 / 5.7E-07	3.1E-09 / 5.6E-07	8.9E-02 / 0.58997	24.1296 / 104.693	5.1E-02 / 8.00189	6.1E-02 / 8.00010
20	7.2E-10 / 1.3E-07	7.1E-10 / 1.2E-07	0.14637 / 1.18201	61.0905 / 924.710	0.16008 / 20.0043	0.20048 / 20.0001

Table VI.10. Simultaneous Acceleration Errors for 5 Second Data Interval

Accel (Gs)	$\frac{e_{ave_\lambda}}{e_{max_\lambda}}$ (DEG)	$\frac{e_{ave_\delta}}{e_{max_\delta}}$ (DEG)	$\frac{e_{ave_h}}{e_{max_h}}$ (DEG)	$\frac{e_{ave_V}}{e_{max_V}}$ (MPH)	$\frac{e_{ave_{aI}}}{e_{max_{aI}}}$ (Gs)	$\frac{e_{ave_{aT}}}{e_{max_{aT}}}$ (Gs)
0	1.7E-9 6.5E-9	1.1E-9 4.2E-9	1.0E-2 2.0E-2	5.2E-1 1.04051	1.0E-4 2.1E-4	4.9E-4 9.9E-4
1	8.6E-9 2.4E-7	4.0E-8 9.2E-7	8.9E-2 0.95619	14.6158 59.7607	9.2E-2 1.00014	9.9E-2 1.00049
2	2.8E-8 8.2E-7	7.2E-8 1.8E-6	0.14989 0.67850	28.9616 122.202	6.4E-2 1.99999	6.9E-2 2.00049
3	5.0E-8 1.6E-6	1.0E-7 2.7E-6	0.19491 0.96091	41.8328 187.190	9.5E-2 2.99990	0.10519 3.00049
4	8.0E-8 2.6E-6	1.2E-7 3.7E-6	0.22517 1.25595	55.9892 254.152	0.12749 4.00001	0.14294 4.00049
5	1.1E-7 9.6E-6	1.5E-7 4.6E-6	0.27450 1.55879	69.5805 322.859	0.16017 5.00079	0.18911 5.00049
6	1.5E-7 4.6E-6	1.7E-7 5.5E-6	0.32462 1.86561	85.0078 392.704	0.19956 6.00249	0.22604 6.00049
7	1.9E-7 5.7E-6	1.8E-7 6.4E-6	0.37460 2.17776	102.149 469.210	0.22780 7.00504	0.27099 7.00049
8	2.3E-7 6.8E-6	2.0E-7 7.4E-6	0.42299 2.49609	121.145 593.821	0.26290 8.00860	0.31787 8.00049
20	1.2E-7 9.1E-6	6.0E-8 1.8E-6	0.69845 3.24947	319.405 1598.92	0.81418 20.0300	1.04685 20.0005

Table VI.11. Simultaneous Acceleration Errors for 10 Second Data Interval

Accel (Gs)	$\frac{e_{ave_\lambda}}{e_{max_\lambda}}$ (DEG)	$\frac{e_{ave_\phi}}{e_{max_\phi}}$ (DEG)	$\frac{e_{ave_h}}{e_{max_h}}$ (DEG)	$\frac{e_{ave_V}}{e_{max_V}}$ (MPH)	$\frac{e_{ave_{aI}}}{e_{max_{aI}}}$ (Gs)	$\frac{e_{ave_{aT}}}{e_{max_{aT}}}$ (Gs)
0	1.4E-8 / 6.1E-8	6.7E-9 / 3.2E-8	2.0E-2 / 4.0E-2	1.04671 / 2.06411	2.0E-4 / 5.5E-4	9.9E-4 / 2.6E-3
1	4.0E-7 / 2.5E-6	9.2E-7 / 1.2E-5	0.18517 / 0.68331	29.7459 / 130.453	6.9E-2 / 1.00275	6.6E-2 / 1.00083
2	1.4E-6 / 8.1E-6	1.7E-6 / 2.4E-5	0.31782 / 1.34880	57.3927 / 267.963	0.12172 / 1.99984	0.14823 / 2.00083
3	2.5E-6 / 1.5E-5	2.6E-6 / 3.6E-5	0.41671 / 2.16314	83.0936 / 406.197	0.18627 / 2.99984	0.24687 / 3.00083
4	4.0E-6 / 2.2E-5	3.8E-6 / 4.8E-5	0.49962 / 3.06624	111.263 / 537.959	0.26629 / 3.99984	0.35894 / 4.00083
5	6.9E-6 / 3.0E-5	5.5E-6 / 6.0E-5	0.59204 / 4.04577	141.154 / 698.599	0.36794 / 4.99984	0.48825 / 5.13677
6	1.0E-5 / 4.1E-5	8.0E-6 / 7.2E-5	0.69700 / 5.09902	175.480 / 933.351	0.48956 / 6.14545	0.66179 / 6.33612
7	1.8E-5 / 1.0E-4	1.1E-5 / 8.4E-5	0.81908 / 6.20928	218.147 / 1232.91	0.66229 / 7.45839	0.88939 / 7.54843
8	2.7E-5 / 2.2E-4	1.5E-5 / 1.0E-4	0.94659 / 7.37359	274.912 / 1592.96	0.89522 / 8.93146	1.14267 / 8.73334
20	9.2E-6 / 4.5E-5	2.4E-6 / 1.9E-5	1.51679 / 19.6138	598.933 / 3132.80	1.73928 / 20.0685	2.19240 / 20.0010

Table VI.12. Simultaneous Acceleration Response for 1 Sec Data Interval

Accel (Gs)	A_{r_I} (DATA POINTS)	A_{r_I} (SEC)	A_{r_T} (DATA POINTS)	A_{r_T} (SEC)
0	N/A	N/A	N/A	N/A
1	3	3	3	3
2	3	3	3	3
3	3	3	3	3
4	3	3	3	3
5	3	3	3	3
6	3	3	3	3
7	3	3	3	3
8	3	3	3	3
20	4	4	5	5

Table VI.13. Simultaneous Acceleration Response for 5 Sec Data Interval

Accel (Gs)	A_{r_I} DATA (POINTS)	A_{r_I} (SEC)	A_{r_T} DATA (POINTS)	A_{r_T} (SEC)
0	N/A	N/A	N/A	N/A
1	3	15	3	15
2	3	15	3	15
3	3	15	3	15
4	3	15	4	20
5	3	15	4	20
6	3	15	4	20
7	3	15	4	20
8	3	15	4	20
20	4	20	4	20

Table VI.14. Simultaneous Acceleration Response for 10 Sec Data Interval

Accel (Gs)	A_{r_I} (DATA POINTS)	A_{r_I} (SEC)	A_{r_T} (DATA POINTS)	A_{r_T} (SEC)
0	N/A	N/A	N/A	N/A
1	3	30	3	30
2	3	30	4	40
3	3	30	4	40
4	3	30	4	40
5	3	30	4	40
6	3	30	4	40
7	3	30	4	40
8	3	30	4	40
20	4	40	4	40

Graphical depictions of the 5 second data interval and 4 G acceleration case for simultaneous accelerations are given in Figures 6.9 - 6.14. Again, the shape of these plots are equivalent in form to

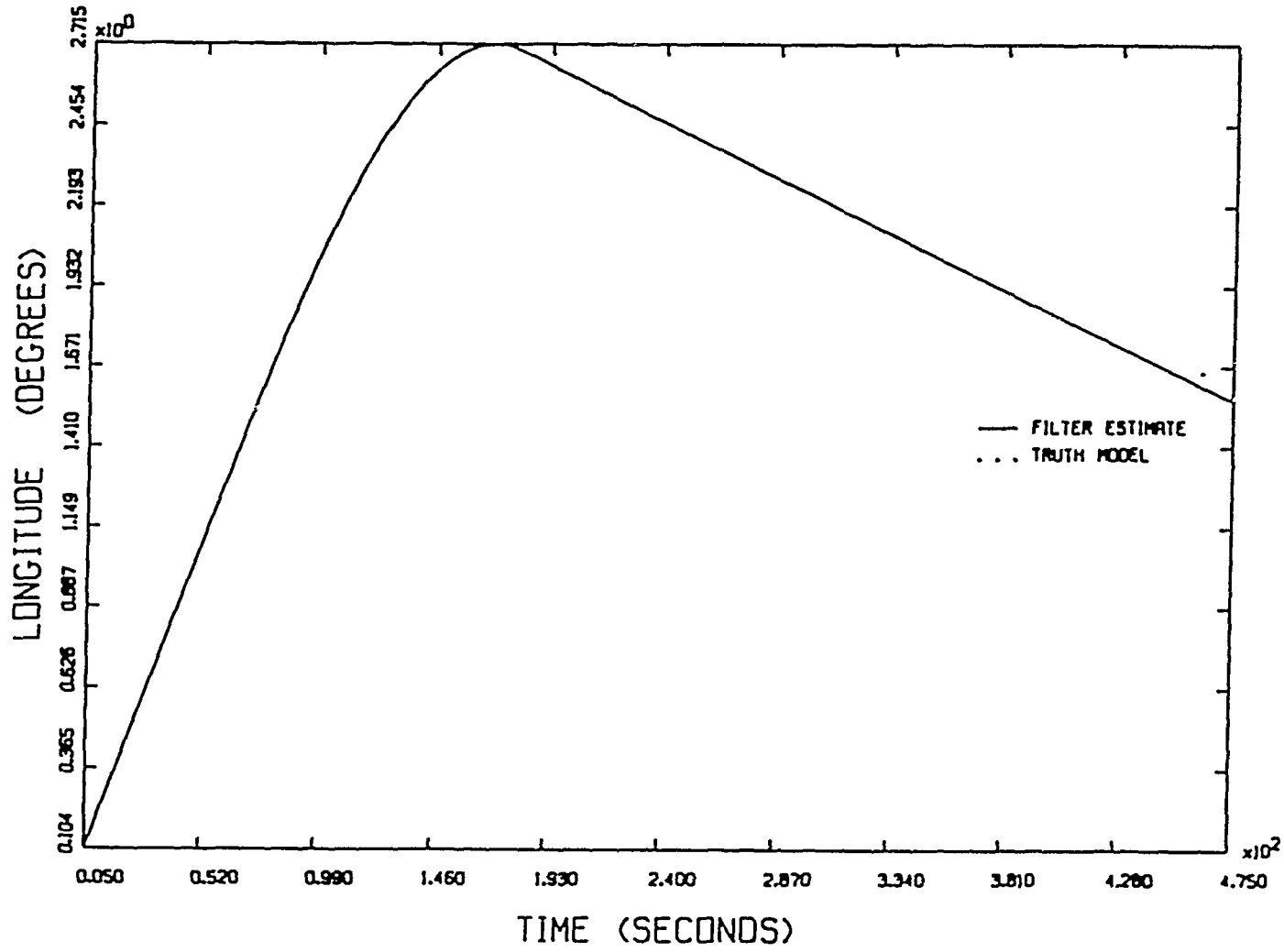

Figure 6.9. Kalman Longitude Estimate (Simultaneous 4 G : Data Interval = 5 Sec)

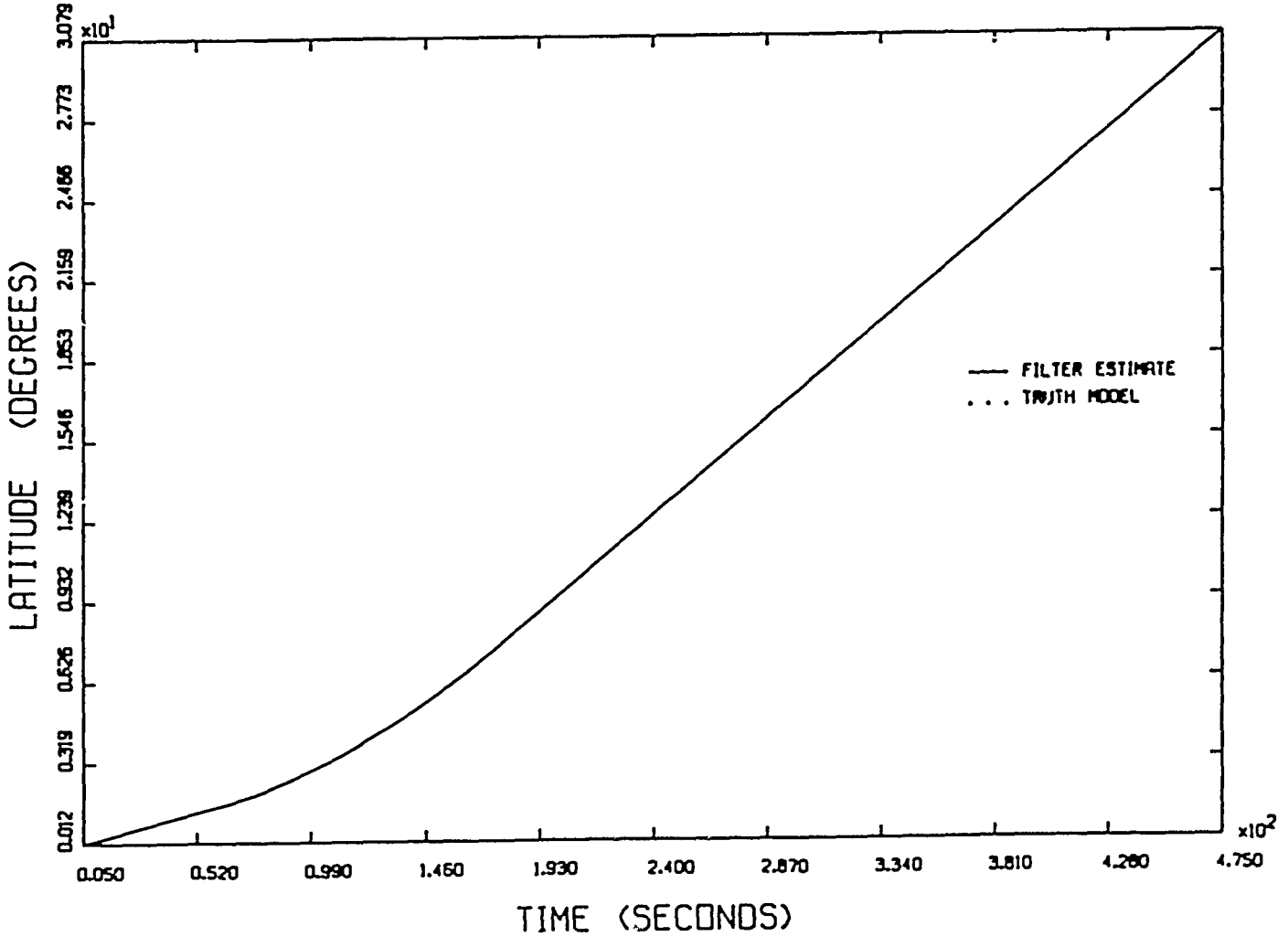

Figure 6.10. Kalman Latitude Estimate (Simultaneous 4 G : Data Interval = 5 Sec)

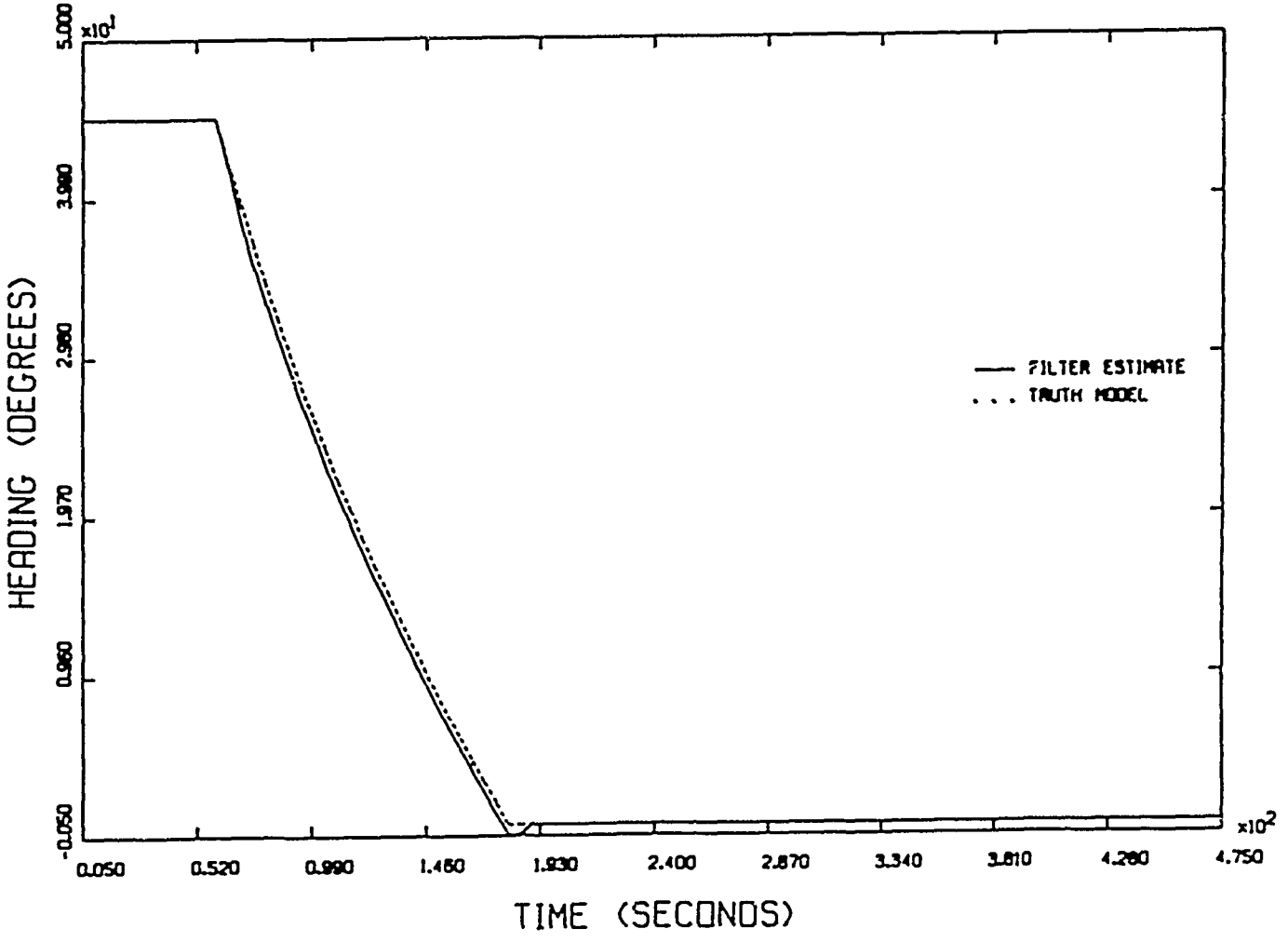

Figure 6.11. Kalman Heading Estimate (Simultaneous 4 G : Data Interval = 5 Sec)

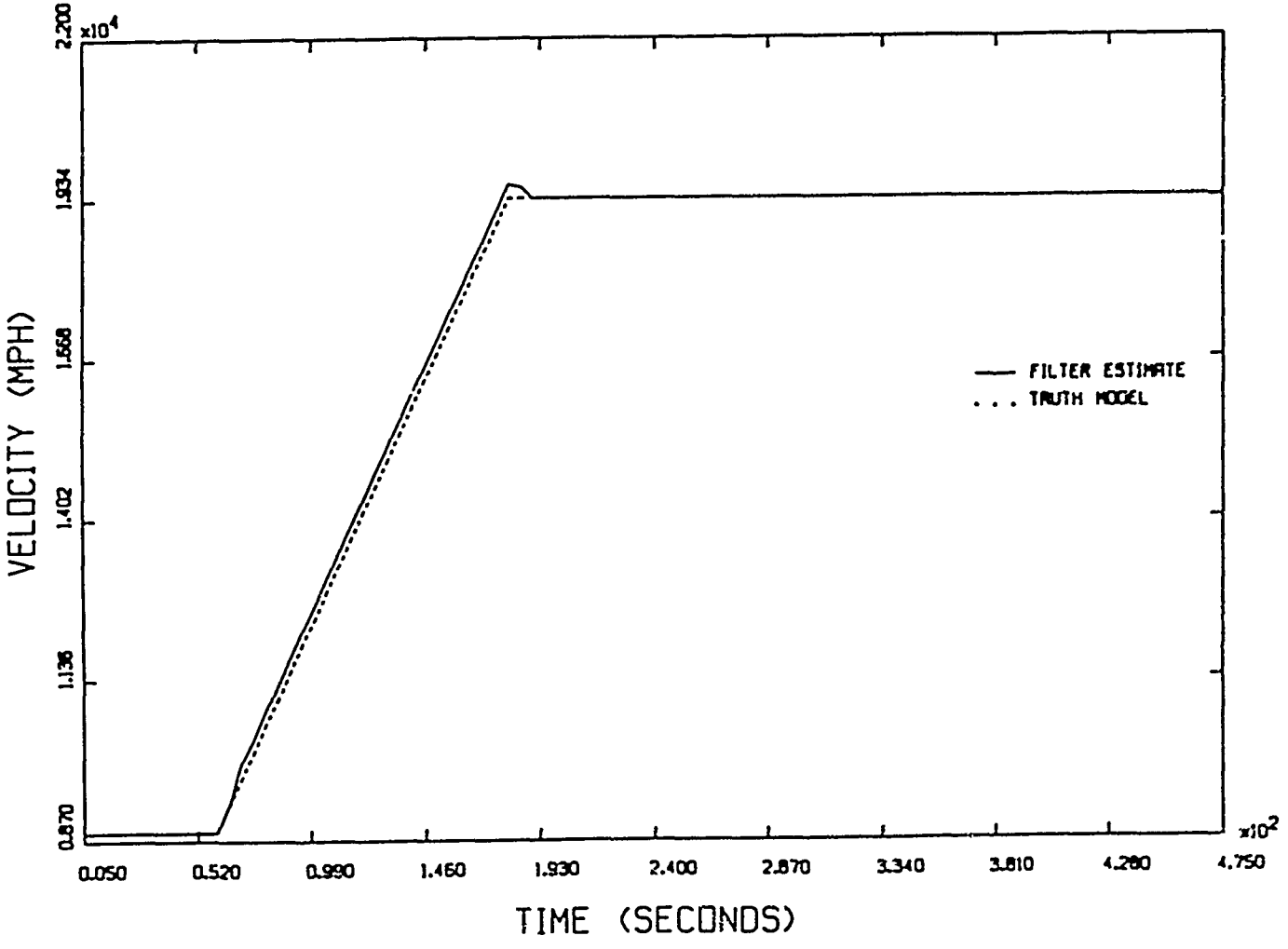

Figure 6.12. Kalman Velocity Estimate (Simultaneous 4 G : Data Interval = 5 Sec)

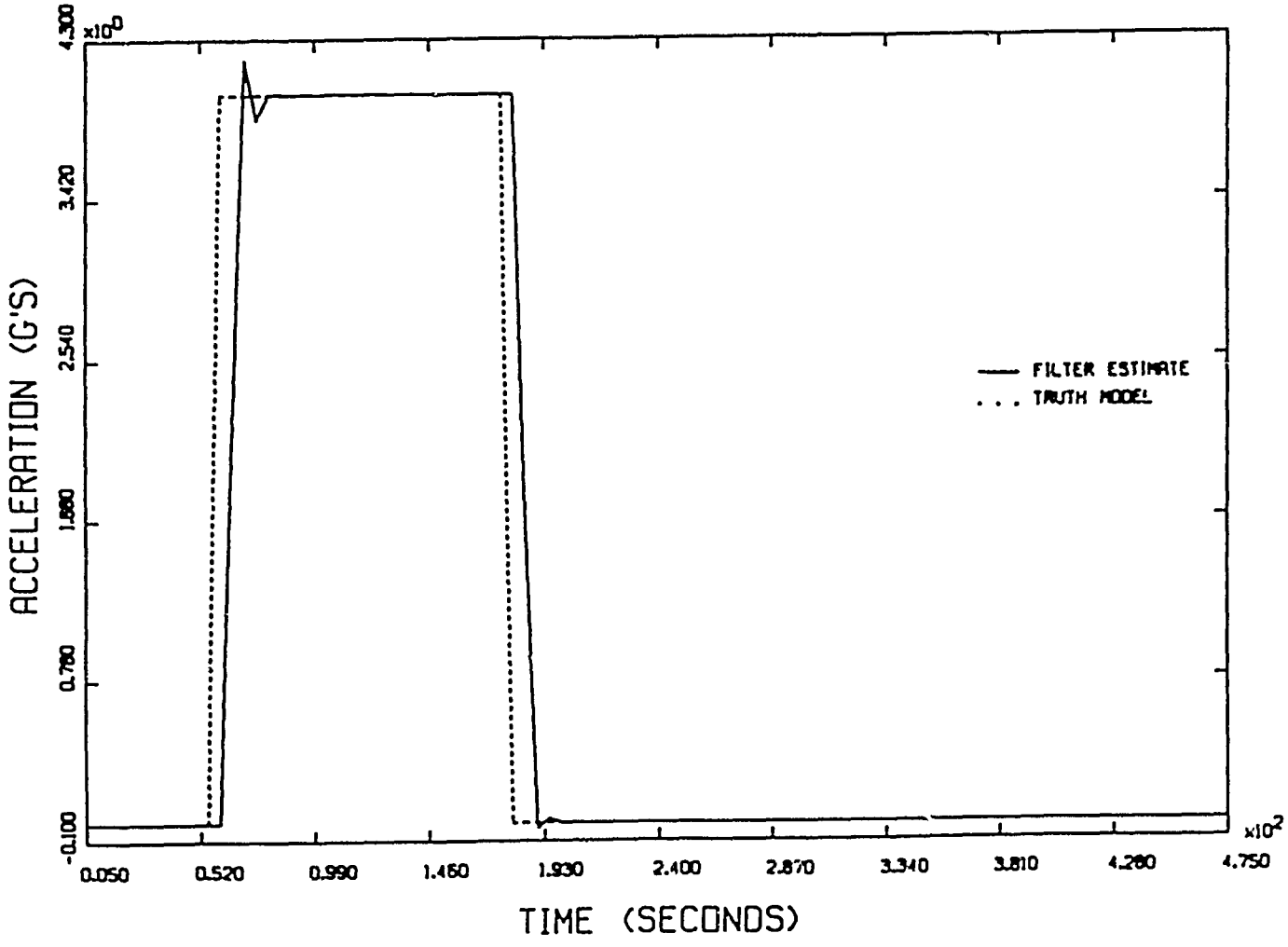

Figure 6.13. Kalman Intrack Acceleration Estimate (Simultaneous 4 G : Data Interval = 5 Sec)

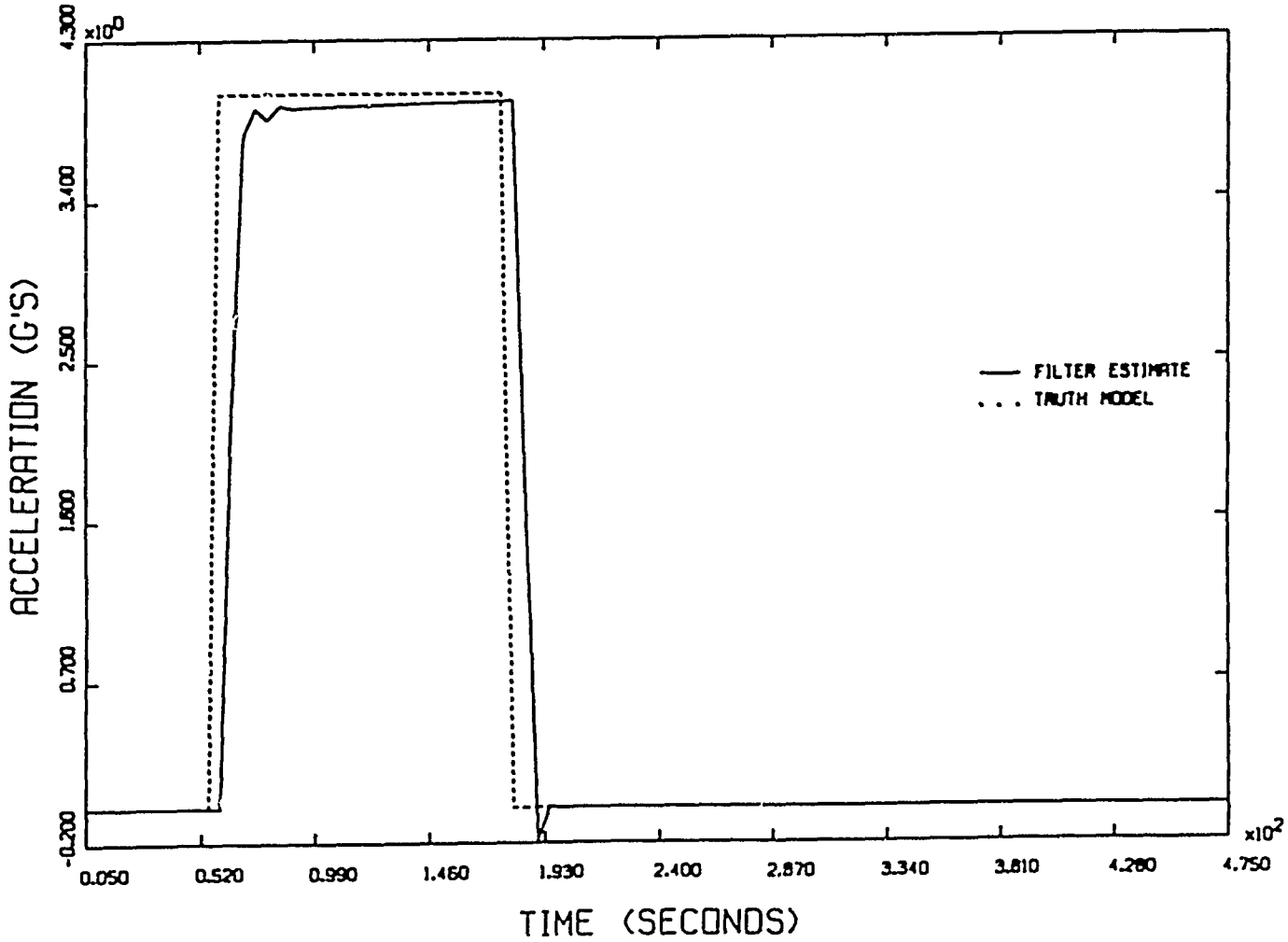

Figure 6.14. Kalman Transverse Acceleration Estimate (Simultaneous 4 g : Data Interval = 5 Sec)

the remaining data interval and acceleration cases. Only the relative values vary from case to case as reflected in the preceding tables.

Discussion

On the whole, the results from the six state Kalman filter are very good, indicating the filter design may be very appropriate for the TAV tracking problem. In terms of average error over the expected 0 to 8 G TAV flight envelope, the 10 second data interval filter estimating an 8 G simultaneous acceleration trajectory fared the poorest. Even the data from this case, however, provides healthy accuracy for estimating the TAV state. In this case, the longitude and latitude estimates, determined to 10^{-6} degree average accuracy, translate to position errors of only 6 meters at the equator. The average heading error measured a scant .94 degrees. The average velocity error of 275 mph is only 1 percent of the 24735 mph velocity averaged by the TAV over this profile. The intrack acceleration error of .89 Gs is only 11 percent of the 8 G maneuver that introduced it and finally the transverse acceleration error of 1.14 Gs is 14 percent of the 8 G maneuver that introduced it. These acceleration errors are but a fraction of the magnitude of the acceleration maneuvers themselves, despite the complete unpredictability of the maneuvers. It should be stressed, again, this data represents the poorest estimate from the data tables. By dropping to a 1 second data interval, for example, the errors for the same simultaneous 8 G acceleration trajectory are reduced by at least a factor of 10! Although applications can be imagined where these errors are unacceptable, for tracking and analysis of TAV capabilities this filter is sufficient.

Further analysis of the results show three distinct trends. First, the filter s performance over serial acceleration trajectories was, in general, better than its performance over the simultaneous trajectories. Second, as the magnitude of the acceleration maneuvers increased, both estimation errors (maximum and average) and the acceleration response increased. Third, decreasing the data interval effectively reduced both errors and the acceleration response.

The superiority of the Kalman filter estimates for the serial acceleration profiles over the simultaneous acceleration profiles is intuitively expected. Simultaneous accelerations essentially introduce sudden step inputs to two of the six TAV states. It is not surprising this results in dynamics more difficult to estimate than the dynamics associated with introducing the step inputs to the states one at a time. It is important to note, however, that the differences in the estimate quality are very slight. In addition, whether the simultaneous or the serial trajectories are being estimated, changing the data interval or the acceleration maneuver magnitudes effects the estimation errors and acceleration response similarly. This fact is used to simplify the discussion of the remaining two data trends. Only the results for the simultaneous intrack and transverse accelerations will be examined in support of the discussion of these two trends. The trends found to be true for the simultaneous trajectory are also identically true for the serial trajectories. Detailed analysis of both would prove redundant.

The effect on the filter estimates of altering TAV acceleration magnitude or changing the data interval is graphically demonstrated in Figures 6.15-6.21:

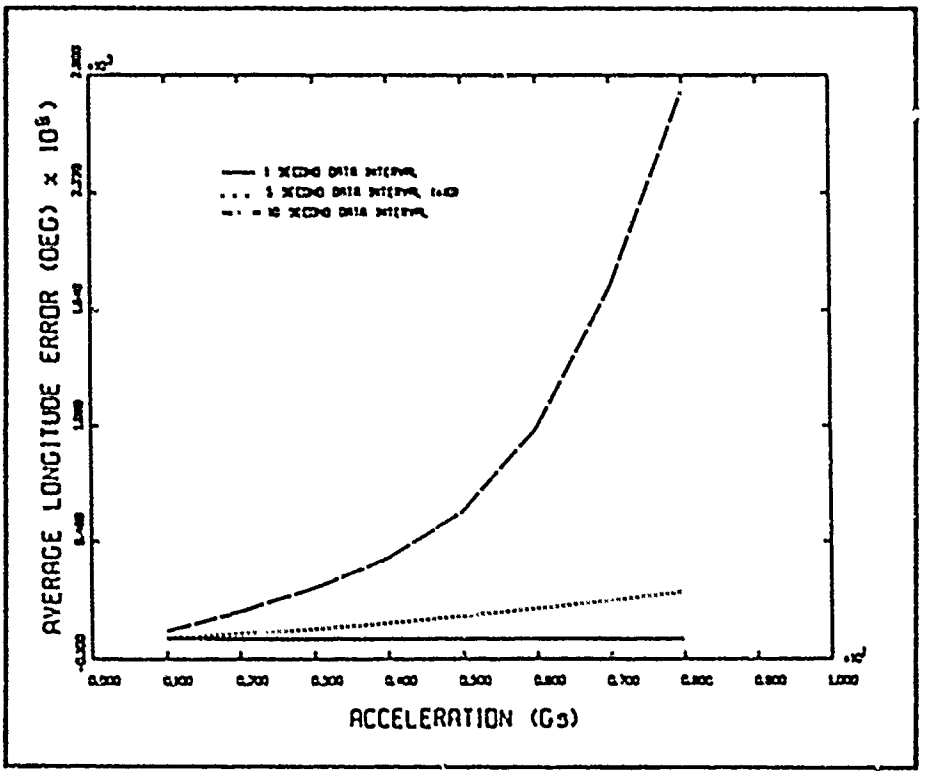

Figure 6.15. Longitude Average Error Vs. TAV Acceleration

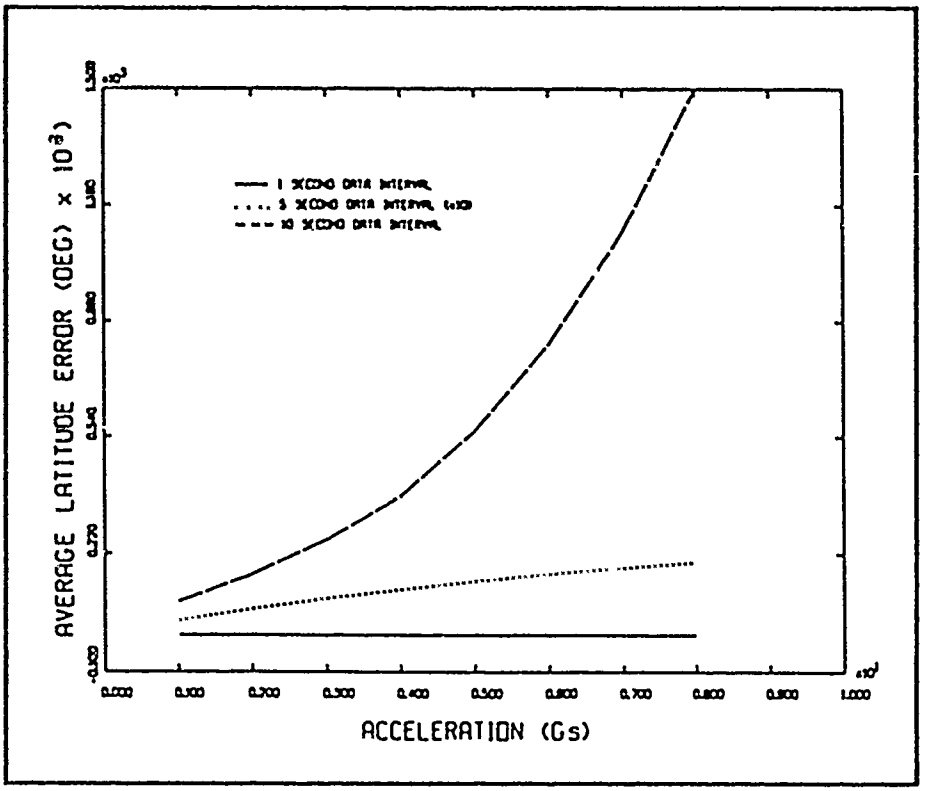

Figure 6.16. Latitude Average Error Vs. TAV Acceleration

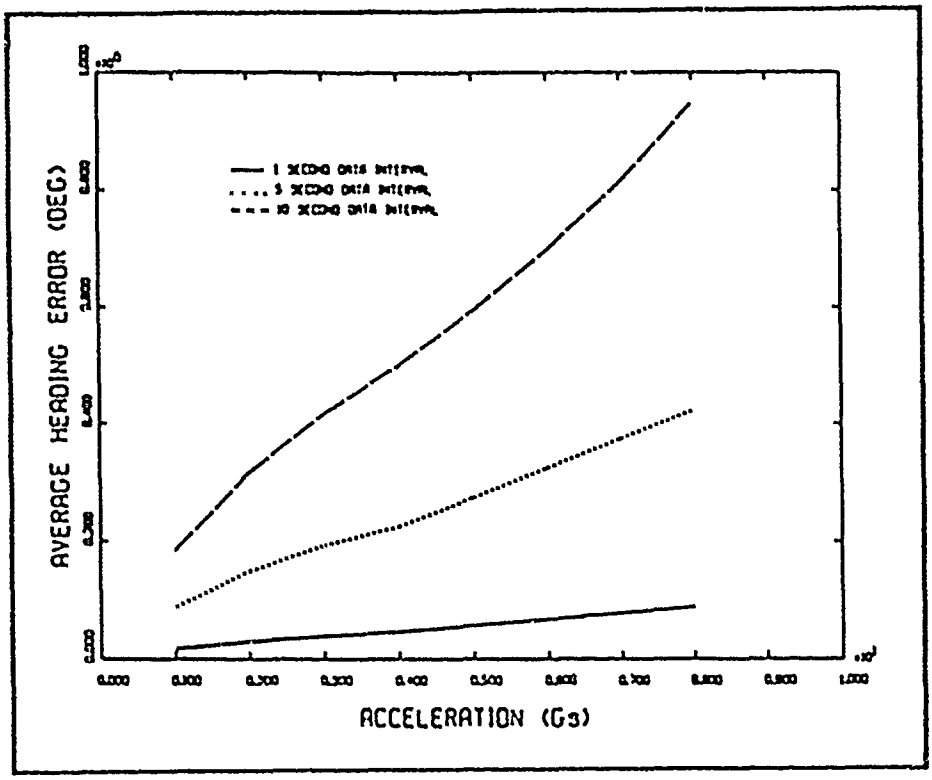

Figure 6.17. Heading Average Error Vs. TAV Acceleration

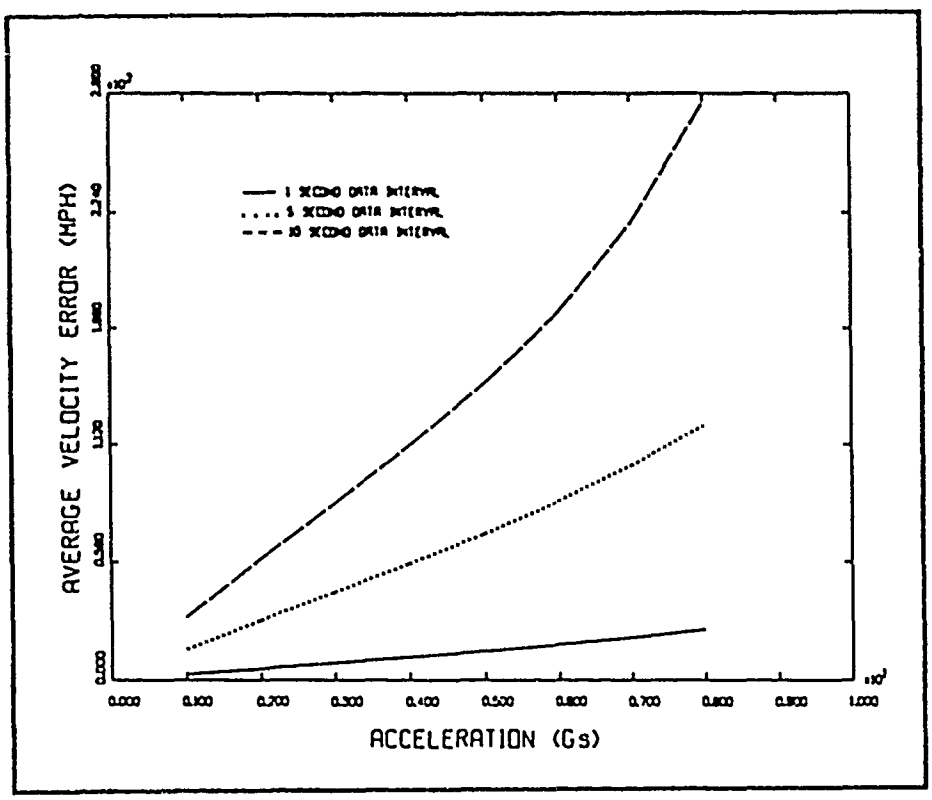

Figure 6.18. Velocity Average Error Vs. TAV Acceleration

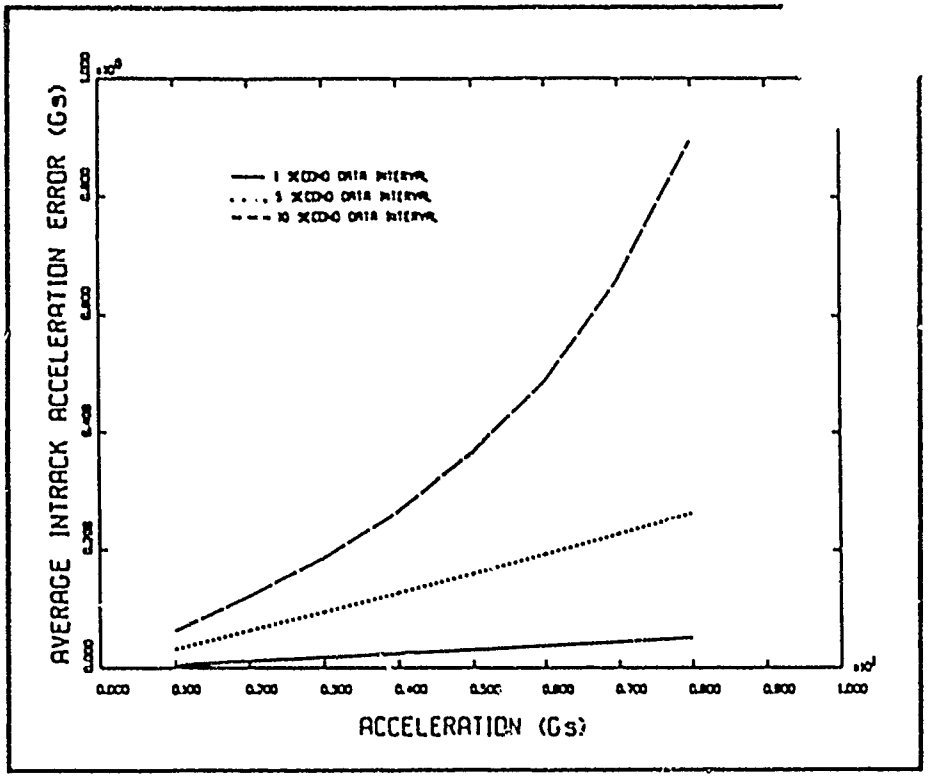

Figure 6.19. A_I Average Error Vs. TAV Acceleration

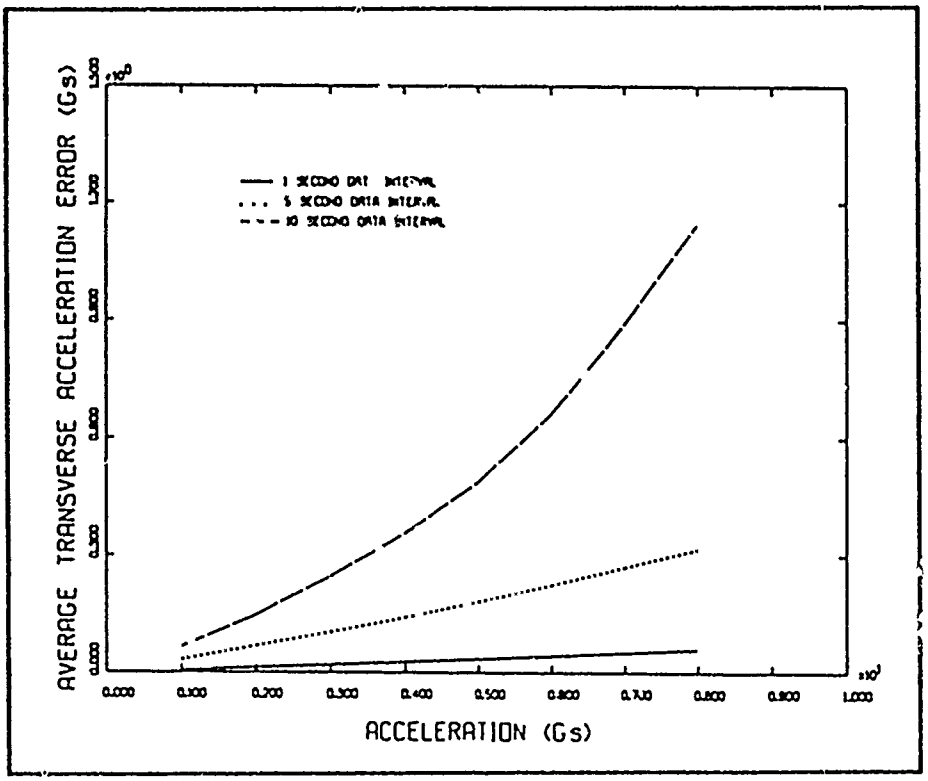

Figure 6.20. A_T Average Error Vs. TAV Acceleration

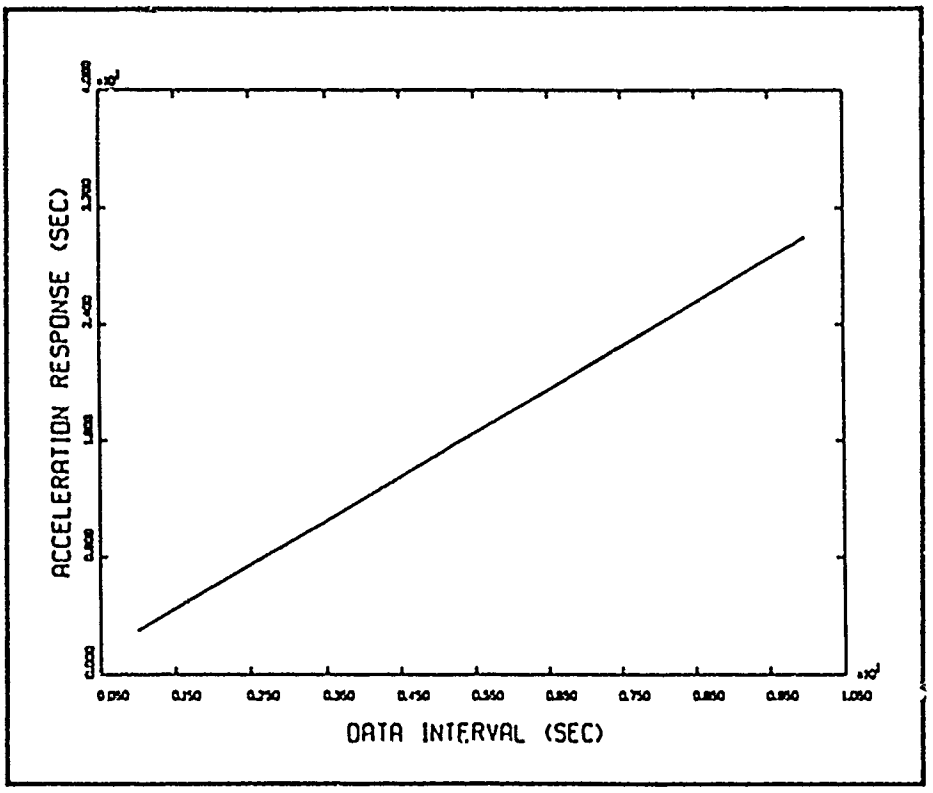

Figure 6.21. Acceleration Response Vs. Data Interval Size

These figures clearly support the remainder of the data trends. Specifically:

1) As the magnitude of the accelerations increased, the average error for all of the state elements increased. (Figures 6.15- 6.20)

2) As the size of the data intervals decreased, the average error for all state elements decreased. (Figures 6.15-6.20)

3) As the size of the data interval increased, the acceleration response, in seconds, increased. (Figure 6.21)

Reproducing Figures 6.15-6.20, with the vertical axis reflecting maximum error, would result in similiar graphical relationships between data interval size, acceleration magnitudes, and e_{max} for all state elements. As the magnitude of accelerations increased, maximum error for all state elements increased, and as the data interval decreased, the maximum

error decreased.

The most important implication of the results of this section is the critical impact data interval size has on filter performance. According to these results, filter designers can theoretically drive the average error and acceleration response to zero by implementing filters with infinitesimally small data intervals. In the case of the average error, a smaller data interval allows less time for the true TAV state to diverge from the estimated state before a fresh data point updates the state. In the case of the acceleration response, the number of data points required to recover 95 percent of the new acceleration value doesn't change, but the sum duration of the three intervals do. Therefore the smaller the data interval, the shorter the acceleration response. Unfortunately for designers, budget constraints and computer processing requirements usually prevent actual specifications from achieving theoretical ideals. Nevertheless, the data interval provides the designer with a powerful tool to control filter accuracy and response speed.

20 G Acceleration Case

Accelerations of 20 Gs represent a substantial departure from the 0 to 8 G flight envelope already tested. The departure was so substantial that a Kalman filter tuned to noise elements tabulated in Table V.3 was unable to estimate this acceleration case. Instead, tuning iterations for each of the data intervals were repeated for the filter. The new noise elements incorporated into the filter for the 20 G acceleration case appear in Table VI.15:

Table VI.15. Optimal Q_n Values for Data Intervals (20 G Accelerations)

	Q_{n_λ} $(RADS^2)$	Q_{n_δ} $(RADS^2)$	Q_{n_h} $(RADS^2)$	Q_{n_V} (DU/TU)	$Q_{n_{aI}}$ (DU^2/TU^4)	$Q_{n_{aT}}$ (DU^2/TU^4)
Data Int (sec)						
1	.01	.01	0.0	0.0	7.2×10^{0}	7.2×10^{0}
5	.01	.01	0.0	0.0	1.1×10^{7}	1.1×10^{7}
10	.01	.01	0.0	0.0	1.0×10^{6}	1.0×10^{6}

The filter results for the case of 20 G intrack and transverse accelerations were natural extensions of the results for the TAV range of accelerations. From Tables VI.2 - VI.7, it is apparent that the higher accelerations for this case significantly increased the maximum and average errors relative to errors from less dramatic acceleration magnitudes. This is predictable, given the relationship already defined between acceleration magnitude and error. What the data tables also show, however, is that the errors and acceleration response remain sensitive to the data interval size, even at these extremely high levels of acceleration. This is an encouraging result -- once again the data interval can be decreased to achieve relatively accurate error and speed specifications. Review of the filter performance at 20 simultaneous Gs and a data interval of 1 second bears this out. For that case, average position errors on the order of 10^{-10} degrees, average heading error on the order of 10^{-1} degrees, average velocity error on the order of 61.1 mph and average acceleration errors on the order of 2 G's, are excellent

results. These results support the use of this six state filter against high acceleration systems.

VII. Four State Element Kalman Filter

In addition to developing a six state Kalman filter to estimate the TAV trajectory, a Kalman filter with four state elements was attempted. This chapter explains the impetus behind this second filter, the filter s design, and finally, the drawbacks of the filter's performance in a TAV estimation problem.

Design Intentions

The six state Kalman filter estimated the intrack and transverse accelerations by including them as state elements with equations of motion

$$\dot{a}_I = 0 \tag{2.34}$$

$$\dot{a}_T = 0 \tag{2.35}$$

Because of the unpredictable nature of the TAV accelerations, these equations of motion are a crude approximation to propagating the accelerations over time. By adding very high levels of noise to the acceleration variances, however, the six state filter did remarkably well in estimating the acceleration states over the TAV trajectory. The acceleration estimates corresponded very accurately with the acceleration truth model, with one notable exception -- the data points coinciding and immediately following a step change in the truth model accelerations.

Chapter VI results show that the acceleration estimates recovered 95% of the true acceleration values only after three data points were processed by the six state filter. In light of this finding, designing and testing a four state filter considers the following questions:

1) Could the accelerations be estimated explicitly by using slope information from velocity and heading estimates (eg. $a_I = \Delta V/\Delta t$) instead of incorporating the accelerations as state elements?

2) Would this four state filter improve the acceleration response?

3) Are the estimates for λ, δ, h, V, a_I, and a_T better than those of the six element filter?

State Vector

The four state vector, $\bar{x}$, being estimated by the Kalman filter algorithm is a 4x1 vector consisting of four of the TAV dynamic parameters developed in Chapter II:

$$\bar{x} = (\lambda \quad \delta \quad h \quad V) \tag{7.1}$$

As in the design of the six state filter, a discrete time approximation is used to propagate $\bar{x}$ from t_i to t_{i+1} by

$$\bar{x}_{i+1} = \dot{\bar{x}}_i \cdot \Delta t + \bar{x}_i$$

Incorporating the first order equations of motion for each state vector element from Eqs (2.3), (2.7), (2.32) and (2.33)

$$\begin{bmatrix} \lambda_{i+1} \\ \delta_{i+1} \\ h_{i+1} \\ V_{i+1} \end{bmatrix} = \begin{bmatrix} (V_i \cdot \sin h_i / R_e \cdot \cos \delta_i) - \omega_e \\ (V_i \cdot \cos h_i)/ R_e \\ -a_{Ti} / V_i + [(V_i \cdot \sin h_i \cdot \sin \delta_i)/ R_e \cdot \cos \delta_i] \\ a_{Ii} \end{bmatrix} \cdot \Delta t + \begin{bmatrix} \lambda_i \\ \delta_i \\ h_i \\ V_i \end{bmatrix} \tag{7.3}$$

Note that the values for a_I and a_T are not propagated by this relationship. Instead, slope information from the last two TAV estimates are used to calculate these quantities. The values for a_{Ii} and a_{Ti} in Eq (7.3) would be computed

$$a_{Ii} = (V_i - V_{i-1})/\Delta t \tag{7.4}$$

and

$$a_{T1} = \left\{\left[h_i - h_{i-1}\right]/\Delta t - \left[\left[S \cdot \sin H \cdot \sin D\right]/(R_e \cdot \cos Di\right]\right\} \cdot (-S) \quad (7.5)$$

where

$$D = (\delta_i + \delta_{i-1})/2$$
$$H = (h_i + h_{i-1})/2$$
$$S = (V_i + V_{i-1})/2$$

Although complicated in appearance, Eq (7.5) simply recognizes that the TAV's total change in heading includes a contribution from the earth's rotation. This contribution must be subtracted out to exclusively determine the contribution made to $\dot{h}$ by any transverse acceleration.

State Transition Matrix

The discrete time propagation of $\bar{x}$, detailed in Eq (7.3), provides an approximate solution to the TAV equations of motion in closed form:

$$\bar{x}_{i+1}(t) = f\,[\bar{x}_i(t),\ t] \quad (7.6)$$

where $f\,[\bar{x}_i(t),\ t]$ represents the right hand sides of the four equations in Eq (7.3). Since the state transition matrix, $[\Phi]$, describes a small change in the initial conditions of $\bar{x}$ propagating into a change in the final conditions:

$$[\Phi(i+1,i)] = \nabla_{x_i}\left[\, f\,[\bar{x}_i(t),\ t]\right] \quad (7.7)$$

or

$$[\Phi] = \begin{bmatrix} \frac{\partial \lambda_{i+1}}{\partial \lambda_i} & \frac{\partial \lambda_{i+1}}{\partial \delta_i} & \frac{\partial \lambda_{i+1}}{\partial h_i} & \frac{\partial \lambda_{i+1}}{\partial V_i} \\ \frac{\partial \delta_{i+1}}{\partial \lambda_i} & \frac{\partial \delta_{i+1}}{\partial \delta_i} & \frac{\partial \delta_{i+1}}{\partial h_i} & \frac{\partial \delta_{i+1}}{\partial V_i} \\ \frac{\partial h_{i+1}}{\partial \lambda_i} & \frac{\partial h_{i+1}}{\partial \delta_i} & \frac{\partial h_{i+1}}{\partial h_i} & \frac{\partial h_{i+1}}{\partial V_i} \\ \frac{\partial V_{i+1}}{\partial \lambda_i} & \frac{\partial V_{i+1}}{\partial \delta_i} & \frac{\partial V_{i+1}}{\partial h_i} & \frac{\partial V_{i+1}}{\partial V_i} \end{bmatrix} \tag{7.8}$$

where from Eq (7.3)

$$\frac{\partial \lambda_{i+1}}{\partial \delta_i} = \frac{V_i \cdot \sin h_i \cdot \sin \delta_i}{R_e \cdot \cos \delta_i^2} \cdot \Delta t$$

$$\frac{\partial \lambda_{i+1}}{\partial h_i} = \frac{V_i \cdot \cos h_i}{R_e \cdot \cos \delta_i} \cdot \Delta t$$

$$\frac{\partial \lambda_{i+1}}{\partial V_i} = \frac{\sin h_i}{R_e \cdot \cos \delta_i} \cdot \Delta t$$

$$\frac{\partial \delta_{i+1}}{\partial h_i} = \frac{-V_i \cdot \sin h_i}{R_e} \cdot \Delta t$$

$$\frac{\partial \delta_{i+1}}{\partial V_i} = \frac{\cos h_i}{R_e} \cdot \Delta t$$

$$\frac{\partial h_{i+1}}{\partial \delta_i} = \left[\frac{V_i \cdot \sin h_i}{R_e} + \frac{V_i \cdot \sin h_i \cdot \sin^2 \delta_i}{R_e \cdot \cos^2 \delta_i} \right] \cdot \Delta t$$

$$\frac{\partial h_{i+1}}{\partial h_i} = \frac{V_i \cdot \cos h_i \cdot \sin \delta_i}{R_e \cdot \cos \delta_i} \cdot \Delta t + 1$$

$$\frac{\partial h_{t+1}}{\partial V_t} = \left[\frac{a_{Tt}}{V_t^2} + \frac{\sin h_t \cdot \sin \delta_t}{R_e \cdot \cos \delta_t} \right] \cdot \Delta t$$

$$\frac{\partial \lambda_{t+1}}{\partial \lambda_t} = \frac{\partial \delta_{t+1}}{\partial \delta_t} = \frac{\partial V_{t+1}}{\partial V_t} = 1$$

and all remaining partial derivatives equal zero.

Observation Function

As in the case of the six state filter, the observation function for the four state filter benefits from the preprocessing of the angles data to longitude and latitude data. Since the longitude and latitude data remain identically the first two state elements (λ and δ):

$$G = \begin{bmatrix} 1 & 0 & 0 & 0 \\ 0 & 1 & 0 & 0 \end{bmatrix} \cdot \bar{x} \qquad (7.9)$$

H Matrix

The H matrix, [H], relates the error in the current state estimate to the error in the reference trajectory. It is essentially the linearization of [G] with respect to the state vector and is mathematically expressed for the four state Kalman filter

$$[H] = \frac{\partial [G]}{\partial \bar{x}} = \begin{bmatrix} 1 & 0 & 0 & 0 \\ 0 & 1 & 0 & 0 \end{bmatrix} \qquad (7.10)$$

State Covariance Matrix

For the four state Kalman filter, the state covariance matrix is a 4x4 matrix of covariances and variances associated with the state vector elements at a given point in time. Again assuming statistical independence between the elements of $\bar{x}$ at target acquisition

$$[P] = \begin{bmatrix} \sigma_\lambda^2 & \sigma_\delta^2 & \sigma_h^2 & \sigma_V^2 \end{bmatrix} \qquad (7.11)$$

where units of the variances are identical to those of the six state

filter. As in the case of the six state filter, [P] was initialized with all variances equal to $3x10^{-2}$ and propagated using noisy dynamics by

$$[P] = [\Phi][P][\Phi]^T + [C][Q_n][C]^T \tag{7.12}$$

where

$$[C][Q_n][C]^T = \begin{bmatrix} Q_{n_\lambda} & & & & & \\ & Q_{n_\delta} & & & & \\ & & Q_{n_h} & & & \\ & & & Q_{n_V} & & \\ & & & & Q_{n_{aI}} & \\ & & & & & Q_{n_{aT}} \end{bmatrix} \tag{7.13}$$

The values of the diagonal elements in $[Q_n]$ were again specified through the process of tuning.

Filter Equations and Algorithm

With the exception of the means used to propagate a_I and a_T for the four state Kalman filter, the filter equations and the hosting algorithm are identical to those of the six state Kalman filter already discussed. The equations remain

$$[K] = [P(-)]\cdot[T]^T\cdot\left([Q]' + [T]\cdot[P(-)]\cdot[T]^T\right)^{-1} \tag{7.14}$$

$$[P(+)] = \left([I] - [K]\cdot[T]\right)\cdot[P(-)] \tag{7.15}$$

$$\delta\bar{x}(+) = \delta\bar{x}(-) + [K]\cdot\left(\bar{r}_z - [T]\cdot\delta\bar{x}(-)\right) \tag{7.16}$$

where

[K] ≡ Kalman Gain Matrix
[P(-)] ≡ State Covariance Matrix from the previous estimate
[P(+)] ≡ State Covariance Matrix of the new estimate
$\delta\bar{x}(-)$ ≡ previous correction to the state estimate
$\delta\bar{x}(+)$ ≡ new correction to the state estimate
$[T] \equiv [H]\cdot[\Phi]$
[I] ≡ identity matrix of order of the state vector
$\bar{r}_z$ ≡ data residual

Once again it was assumed, without detriment, that the previous estimate is close to the true state, allowing for a single reevaluation of the filter linearizations, [K], and [P(+)] for each data point versus every iteration within a data point. Small data intervals again made

this assumption viable.

The complete data processing algorithm, including the preprocessing of the azimuth and elevation data, and the four state Kalman filter discussed in this section is incorporated as a flow chart in Appendix C.

Results

Very early in the testing of the four state Kalman filter, it became obvious this filter s estimation of TAV trajectories was generally inferior to the estimates of the six element filter. Detailed testing was discontinued as soon as it was determined that the results being generated by the four state filter were consistently inferior across the spectrum of data intervals and acceleration ranges. Because of the reasonableness of the thought process that led to the development of this four element filter, however, typical results from the filter have been incorporated in this section. These results serve to answer the questions posed at the beginning of the chapter where the impetus to designing this alternative to the six state filter was discussed.

Figures 7.1 - 7.6 illustrate the pattern of estimation typical of a four element filter operating over the data intervals and accelerations discussed in Chapter VI. Like the six element filter, the estimated longitude (Figure 7.1) and latitude (Figure 7.2) values coincided nicely with the position truth models. The estimates for the remaining four state elements, however, continuously fluctuated about the truth model lines. These fluctuations were particularly severe in the case of the acceleration estimates, where the method of estimating accelerations through slope information is seen to produce drastic adjustments over short time intervals. The estimates for heading and velocity, both

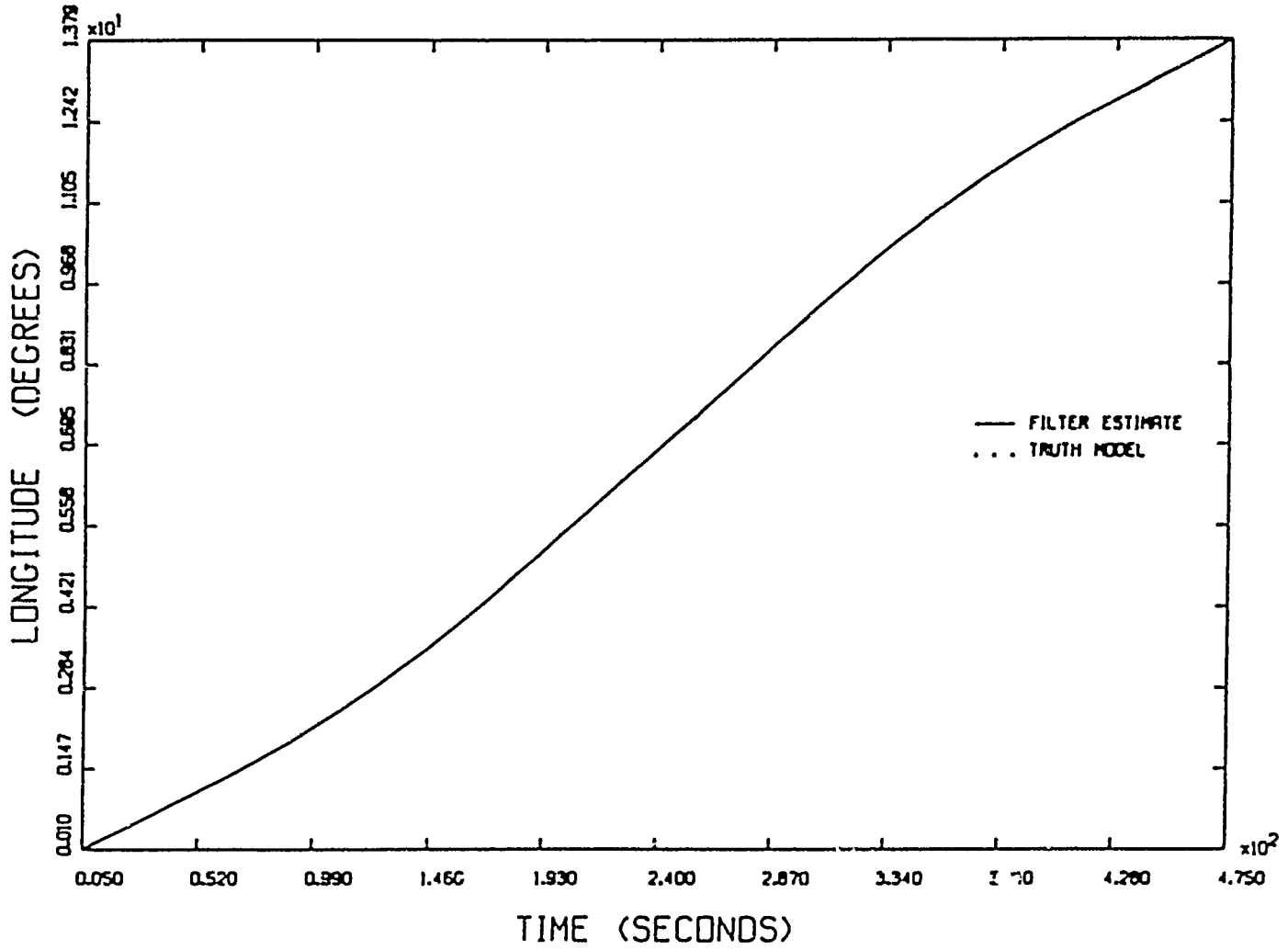

Figure 7.1. Kalman Longitude Estimate
(4 State : Serial 2 G : Data Interval = 5 Sec)

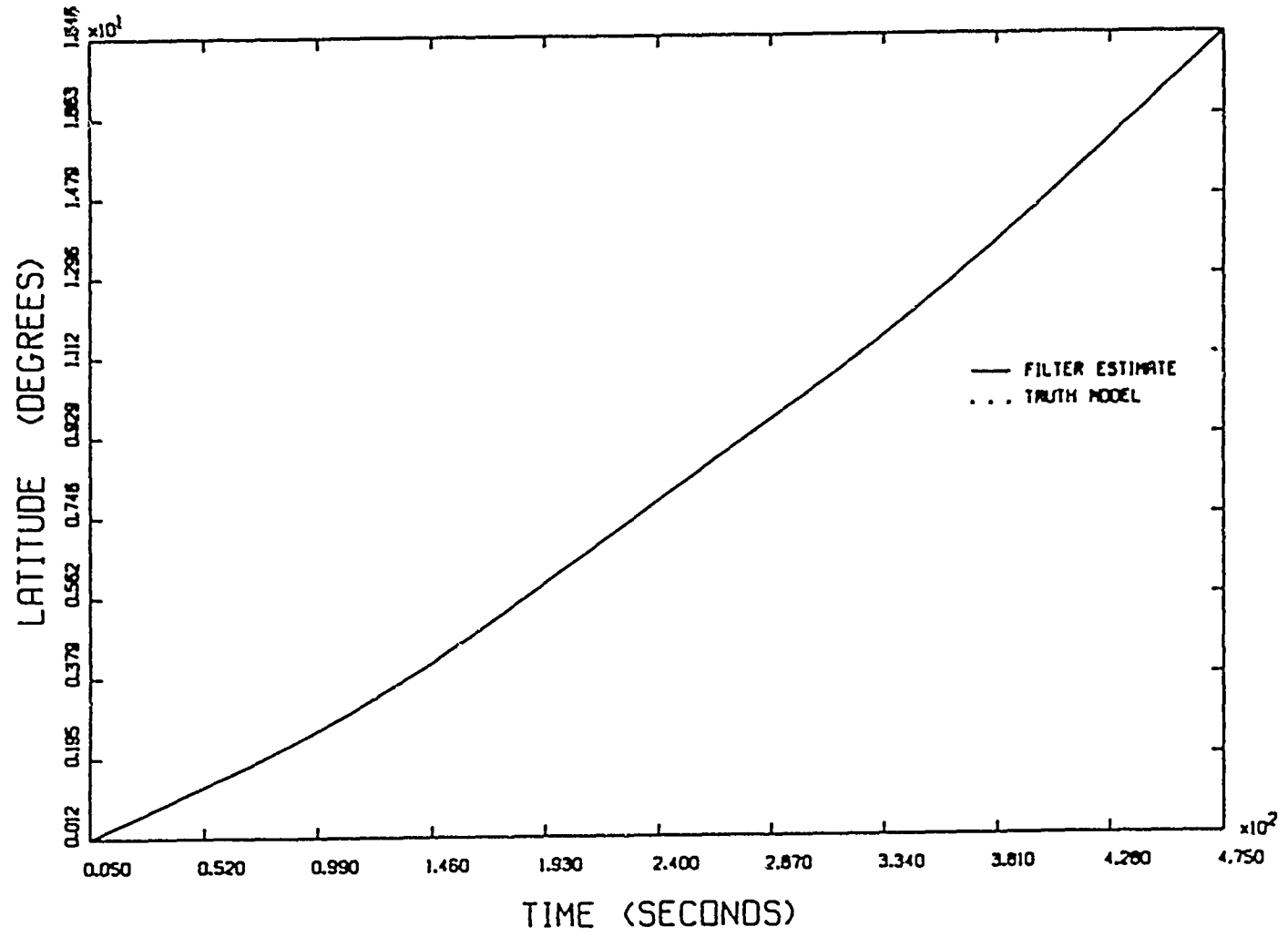

Figure 7.2. Kalman Latitude Estimate
(4 State : Serial 2 G : Data Interval = 5 Sec)

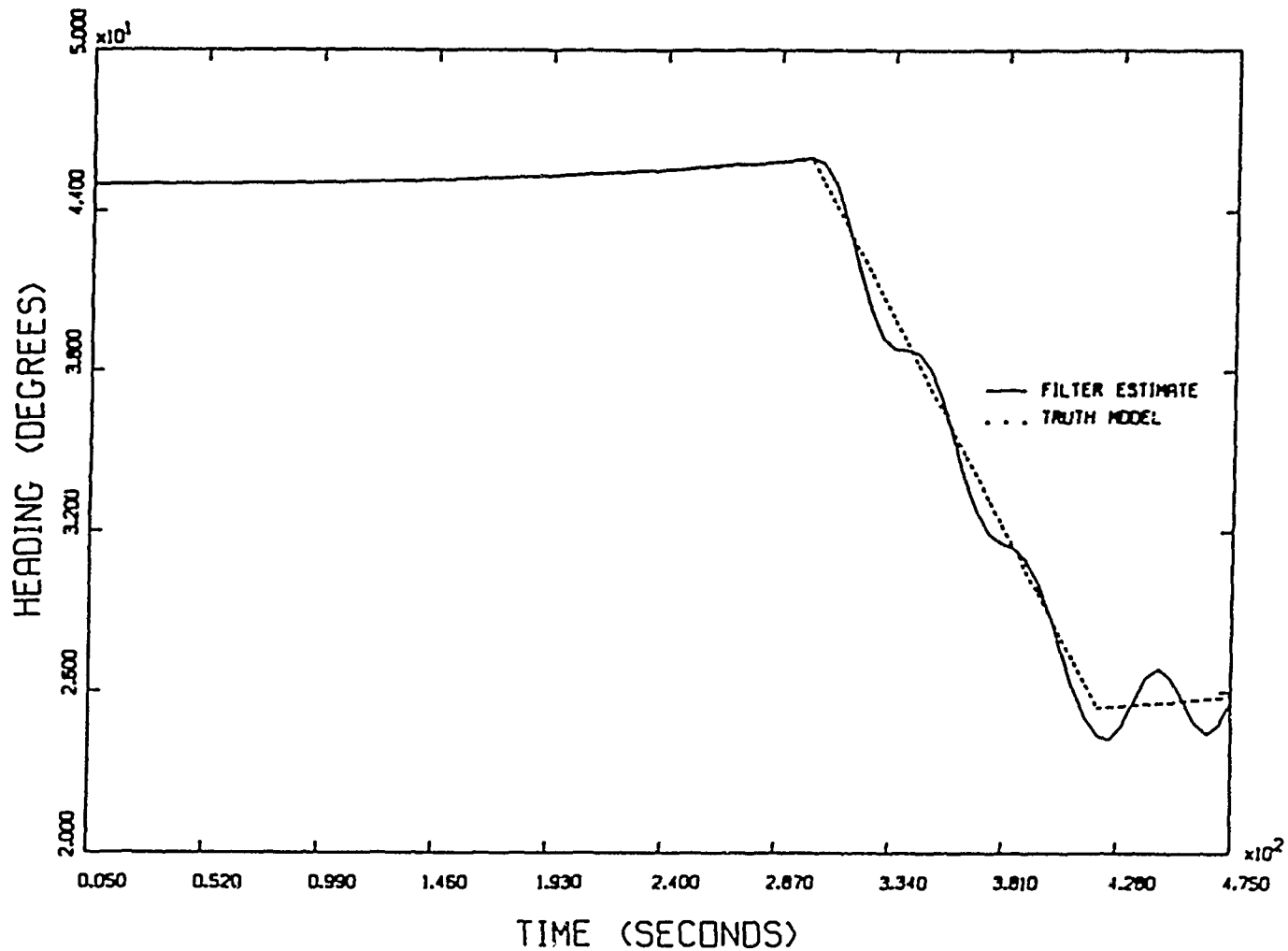

Figure 7.3. Kalman Heading Estimate
(4 State : Serial 2 G : Data Interval = 5 Sec)

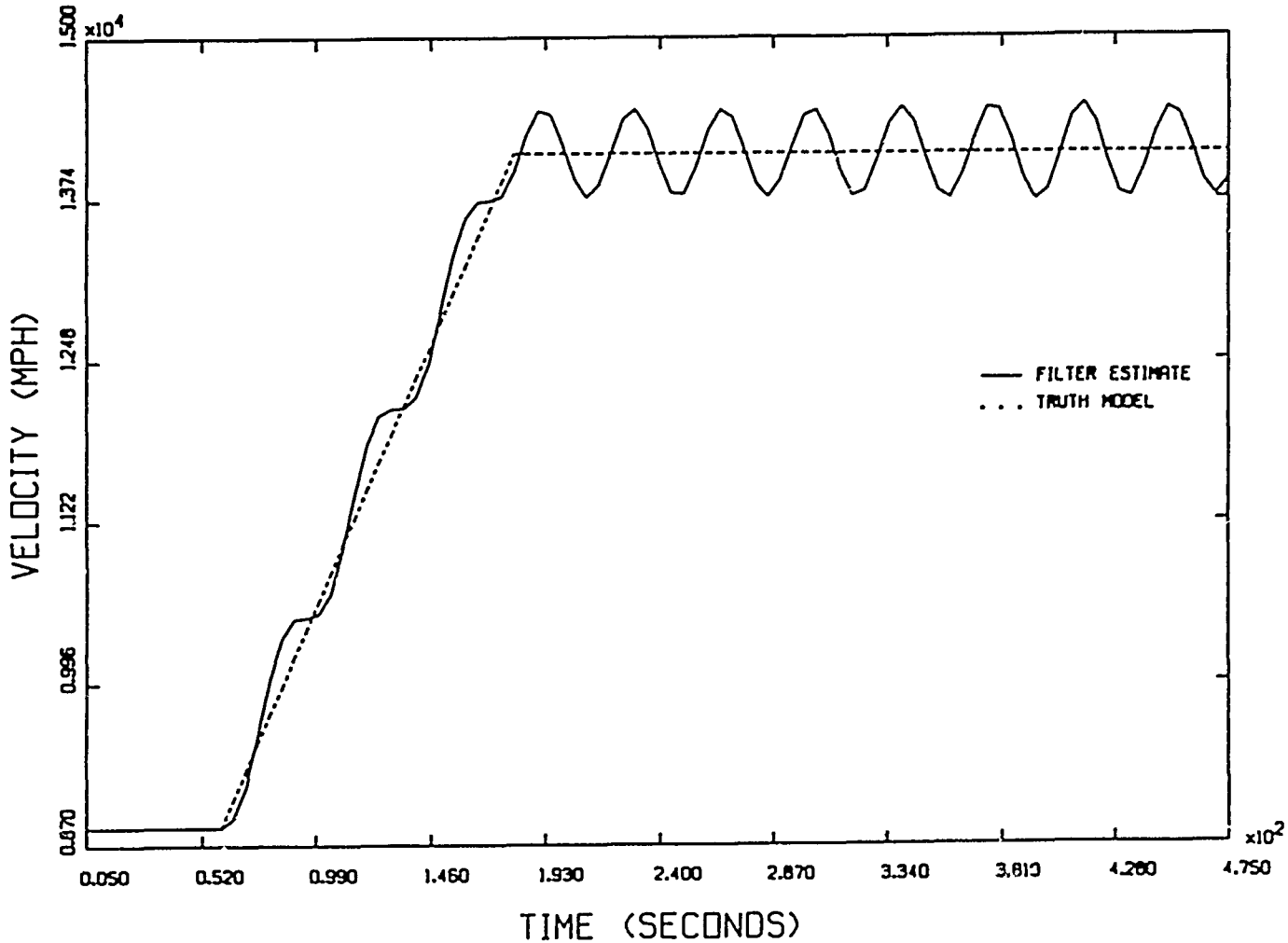

Figure 7.4. Kalman Velocity Estimate
(4 State : Serial 2 G : Data Interval = 5 Sec)

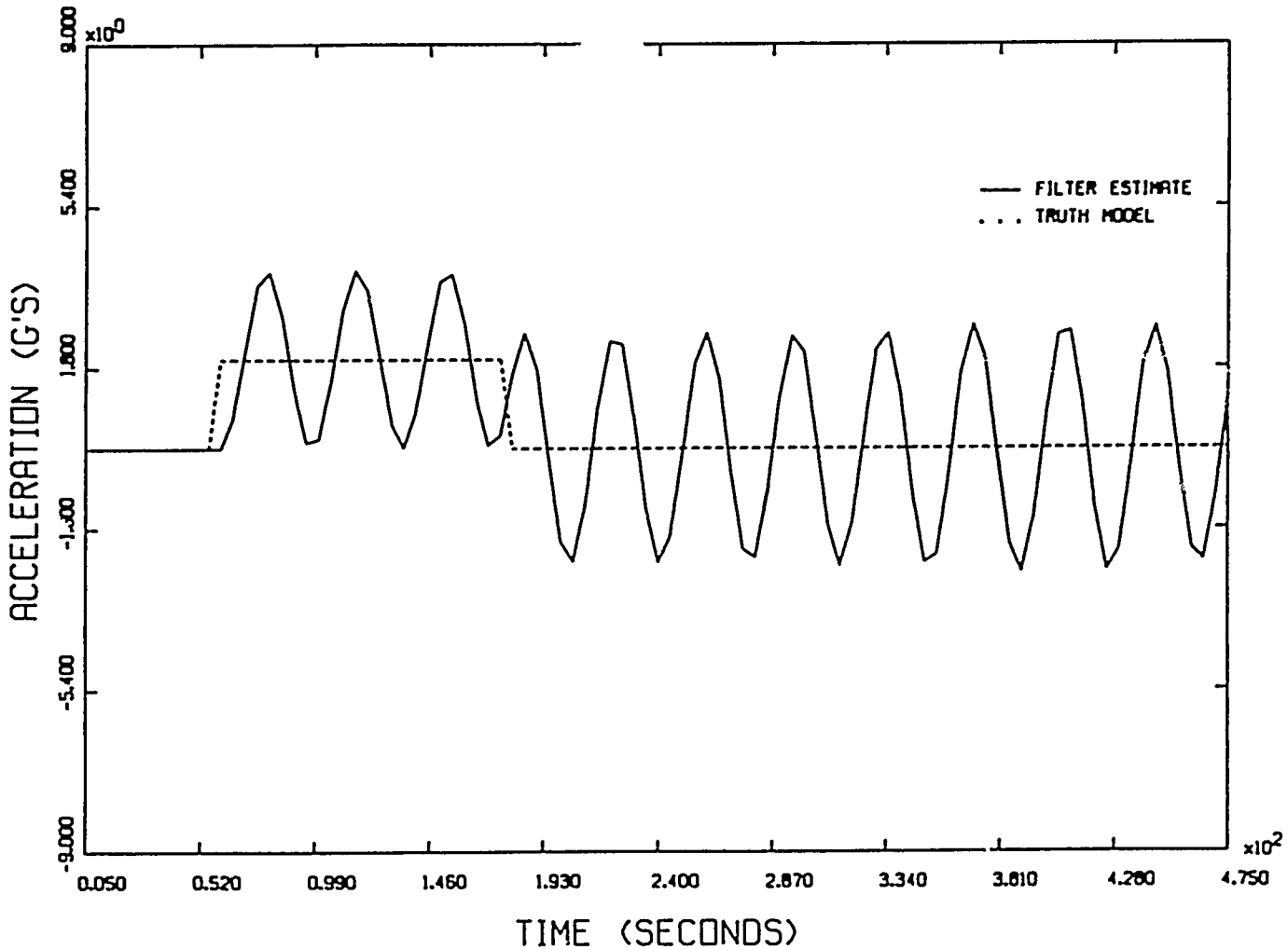

Figure 7.5. Kalman Intrack Acceleration Estimate (4 State : Serial 2 G : Data Interval = 5 Sec)

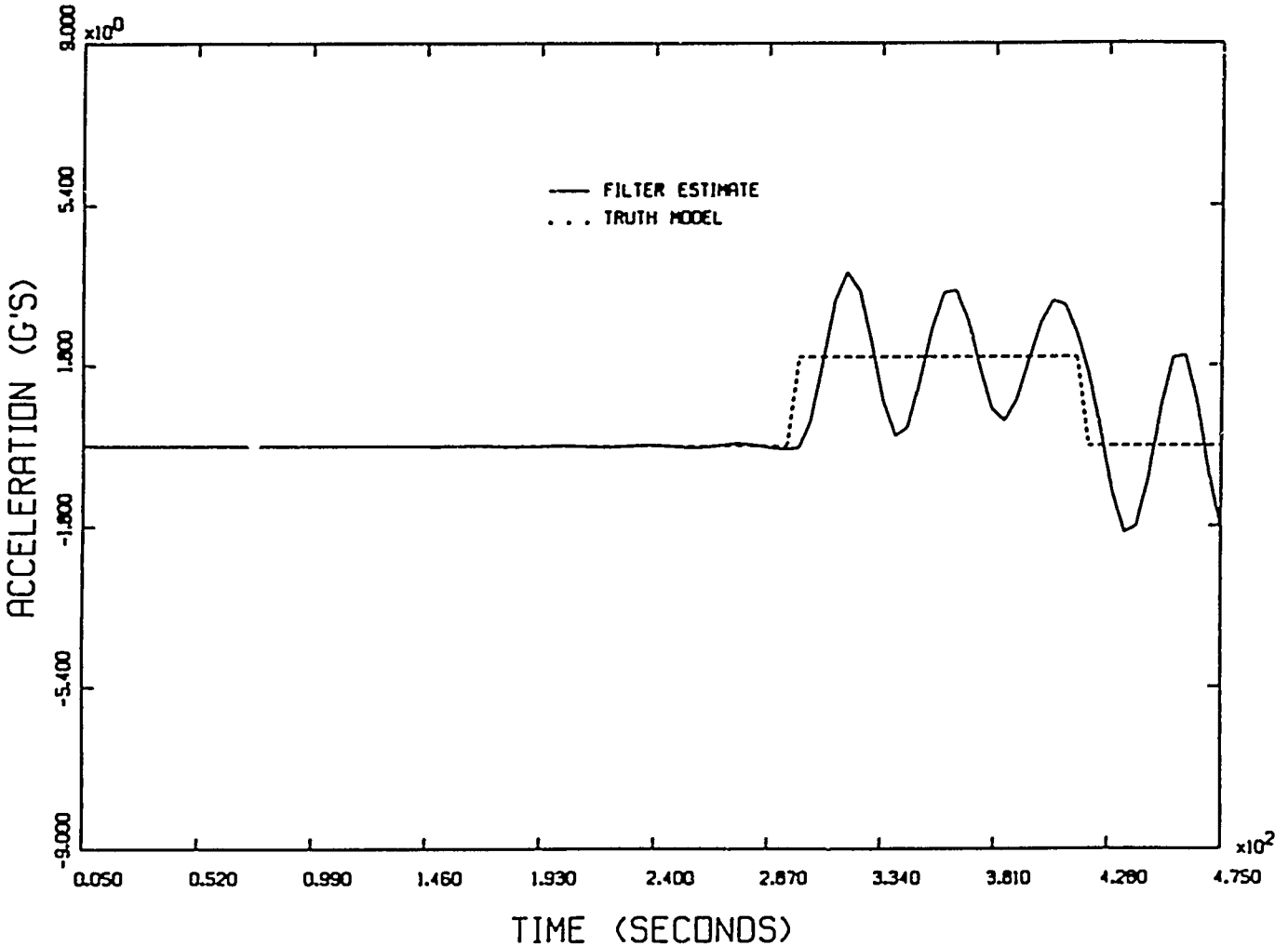

Figure 7.6. Kalman Transverse Acceleration Estimate (4 State : Serial 2 g : Data Interval = 5 Sec)

functions of the accelerations, are immediately influenced by these acceleration fluctuations and begin to fluctuate in tandem with the acceleration cycles.

Although, the oscillatory behavior exhibited by the four element behavior is not desirable in an estimator, it nevertheless must be concluded the accelerations can be estimated explicitly using the heading and velocity slopes. From data point to data point, the four state filter is erratic in a dynamic acceleration environment, but from an overall trajectory perspective the estimates do contain the same information as those of the six element filter. By employing averaging techniques, the four element estimates can conceivably be smoothed out to estimates closely following the truth models. This "smoothing" was not attempted in this thesis but may be an area for further study.

In terms of acceleration response, A_r, the four element filter did offer an improvement over the six element filter, although the improvement was slight. For a given data interval, the four element filter often reflected 95% of the value of a recent acceleration change one data point before the six element filter. This difference was especially consistent in the intrack acceleration estimates. The disadvantage of this response time, however, was the tendency of the four state filter to overshoot the true acceleration value as soon as it had attained it. Although one data point behind in acceleration response, the six state filter settled to the acceleration truth model very quickly. These results again reinforce the finding that although filters operating with the same data intervals can have their acceleration responses compared in terms of data points, it is wiser to consider acceleration response as a function of data intervals. Instead

of selecting the four state filter over the six state filter for its faster acceleration response, one should instead modify the six state filter to operate at the data interval providing the desired response.

In summary, the six state filter was superior to the four state filter for the TAV estimation problem. Both filters were equally matched in terms of position estimates, but in terms of heading, velocity, and acceleration estimates, the six element filter was much more precise from a data point to data point perspective.

VIII. Recommendations

According to the results presented in this thesis, the six state Kalman filter offers accurate and flexible estimation of a typical TAV trajectory observed from a space platform. Position, heading, velocity, and acceleration information provided by the filter give not only a strong grasp of the whereabouts and intentions of a TAV target, but are also an accurate tool by which to assess the capabilities of such a system when other means of access are prohibited. Consideration of this filter for use in the space to TAV tracking problem is encouraged.

Further work to improve the six state filter could focus on making the model more realistic. The assumptions of this thesis regarding platform jitter and positional uncertainty might be replaced by models predicting such effects in more detailed fashion. The assumption making the TAV an isotropically radiating point source might also be replaced by models representing the thermal signature of the TAV in greater complexity. Software could then be written to recognize this signature against the earth background, determine the TAV's center of mass and begin the tracking estimation process. The means by which the Kalman filter first initializes after acquiring the TAV could also be made more realistic. This thesis provided the filter with an initial state estimate very close to the truth model initial state. In reality, the filter must determine this initial state vector itself, perhaps by constructing position, velocity, heading, and acceleration approximations from the first few data points. These are but a few of the possible refinements necessary should this concept ever go operational.

Without altering the model and filter presented in this thesis, a considerable amount of additional testing is very desirable for the six state Kalman filter. Although rudimentary tuning was accomplished while constructing a Kalman filter suitable for accurate estimation of a TAV trajectory, a concerted Monte Carlo analysis was not conducted. Such an analysis should be performed to ensure the filter estimator is, on the average, unbiased and that the state covariance elements are representative of the uncertainty in the estimate. Once this analysis is completed in sufficient detail, many more variations to the TAV trajectory can be tested. These variations could then more deeply investigate Kalman filter performance and isolate the limitations of the filter near the apparent earth horizon, at increasingly higher accelerations, and over smaller time intervals between significant changes to acceleration.

Additional study can also be committed to improving the performance of the four state Kalman filter. As noted in Chapter VII, optimal smoothing may make the estimation from this filter more useable. In general, however, study emphasis on the six state filter is recommended over the four state filter.

As a final note, additional work may be appropriate in addressing the Kalman filter's propensity to lag acceleration changes by the TAV. It might be possible to build a number of discrete Kalman filters, each operating at a distinct acceleration value. This filter set, working in conjunction with software tasked to select the appropriate acceleration, could then have specific filters swapped in and out like filters over a camera lens. This method might improve the acceleration response and assist in initializing the filter when the TAV is first spotted.

Appendix A: Six State Kalman Filter Flowchart

This appendix details the flowchart for the six state Kalman filter algorithm used to process incoming sensor data. It includes the preprocessing of data angles to latitude and longitude.

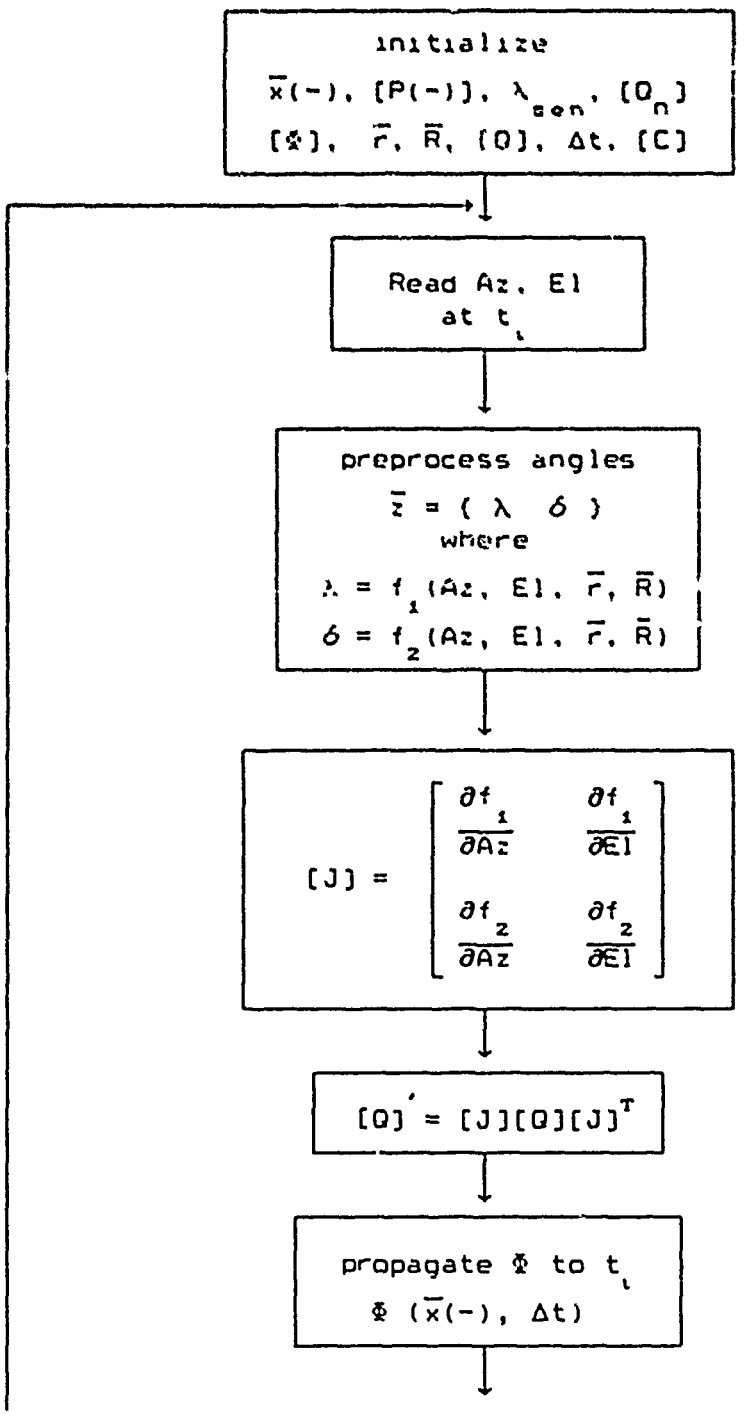

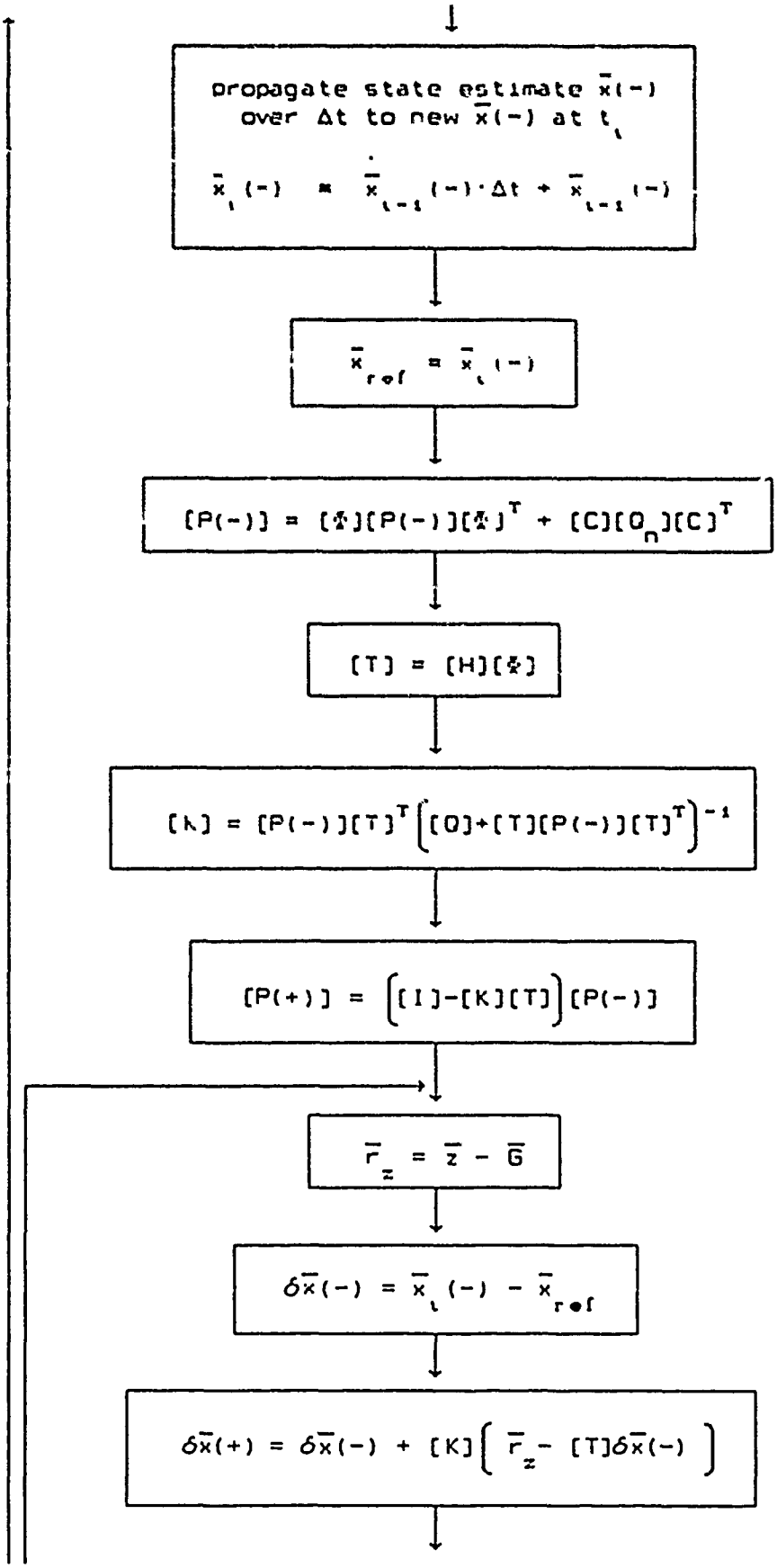
propagate state estimate $\bar{x}(-)$ over Δt to new $\bar{x}(-)$ at t_i
$\bar{x}_i(-) = \bar{x}_{i-1}(-)\cdot\Delta t + \bar{x}_{i-1}(-)$
$\bar{x}_{ref} = \bar{x}_i(-)$
$[P(-)] = [\Phi][P(-)][\Phi]^T + [C][Q_n][C]^T$
$[T] = [H][\Phi]$
$[K] = [P(-)][T]^T\left([Q]+[T][P(-)][T]^T\right)^{-1}$
$[P(+)] = \left([I]-[K][T]\right)[P(-)]$
$\bar{r}_z = \bar{z} - \bar{G}$
$\delta\bar{x}(-) = \bar{x}_i(-) - \bar{x}_{ref}$
$\delta\bar{x}(+) = \delta\bar{x}(-) + [K]\left(\bar{r}_z - [T]\delta\bar{x}(-)\right)$

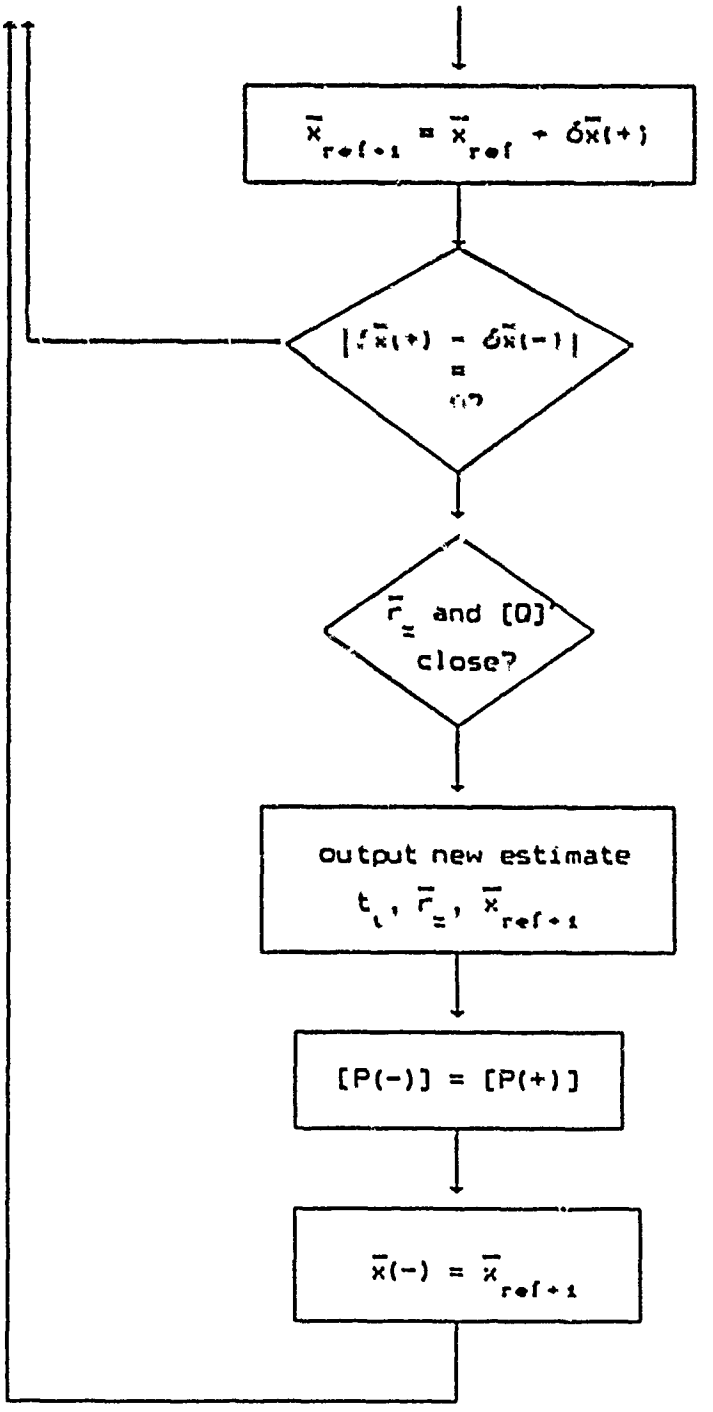

Constants employed (1:429): $\bar{R}$ = 1 DU = 6378.145 km

$\bar{r}$ = 42162.93133 km

$\bar{\omega}_{\bullet}$ = 0.0588336565 rad/TU

Appendix B: Six State Kalman Filter Tuning Output

In Chapter 5, the six state Kalman filter Q_n values were tuned over six data interval and acceleration profiles. This appendix details the optimal Q_n values determined for each case along with the values for the associated tuning parameters.

Table B.1. Optimal Q_n Values for Data Interval/Accelerations Cases

	1 Sec Data Int		5 Sec Data Int		10 Sec Data Int	
	1 G	8 G	1 G	8 G	1 G	8G
Tuned Q_n Values						
Q_{n_λ} $(rads^2)$	.01	.01	.01	.01	.01	.01
Q_{n_δ} $(rads^2)$	.01	.01	.01	.01	.01	.01
Q_{n_h} $(rads^2)$	0.0	0.0	0.0	0.0	0.0	0.0
Q_{n_V} (DU^2/TU^2)	0.0	0.0	0.0	0.0	0.0	0.0
$Q_{n_{aI}}$ (DU^2/TU^4)	$2x10^{10}$	$2x10^{10}$	$2.5x10^7$	$2.5x10^7$	$2.5x10^6$	$2.5x10^6$
$Q_{n_{aT}}$ (DU^2/TU^4)	$2x10^{10}$	$2x10^{10}$	$2.5x10^7$	$2.5x10^7$	$2.5x10^6$	$2.5x10^6$

Table B.2. Tuning Parameters for 1 Second Data Interval/ 1 G Profile

Transverse Acceleration Response:	3 data points
Intrack Acceleration Response:	3 data points
Maximum Longitude Error:	4.8652E-08 degrees
Maximum Latitude Error:	3.5565E-08 degrees
Maximum Heading Error:	5.9060E-02 degrees
Maximum Velocity Error:	12.606E-00 mph
Maximum Intrack Acceleration Error:	1.0000E-00 Gs
Maximum Transverse Acceleration Error:	1.0002E-00 Gs
Average Longitude Error:	9.3226E-10 degrees
Average Latitude Error:	6.7225E-10 degrees
Average Heading Error:	1.4351E-02 degrees
Average Velocity Error:	2.9281E-00 mph
Average Intrack Acceleration Error:	6.3583E-03 Gs
Average Transverse Acceleration Error:	6.4304E-03 Gs

Table B.3. Tuning Parameters for 1 Second Data Interval/ 8 G Profile

Transverse Acceleration Response:	3 data points
Intrack Acceleration Response:	3 data points
Maximum Longitude Error:	9.4847E-07 degrees
Maximum Latitude Error:	3.1304E-07 degrees
Maximum Heading Error:	0.1721E-00 degrees
Maximum Velocity Error:	122.46E-00 mph
Maximum Intrack Acceleration Error:	8.0016E-00 Gs
Maximum Transverse Acceleration Error:	8.0069E-00 Gs
Average Longitude Error:	8.4379E-09 degrees
Average Latitude Error:	3.9488E-09 degrees
Average Heading Error:	4.3402E-02 degrees
Average Velocity Error:	23.553E-00 mph
Average Intrack Acceleration Error:	5.2539E-02 Gs
Average Transverse Acceleration Error:	5.3162E-02 Gs

Table B.4. Tuning Parameters for 5 Second Data Interval/ 1 G Profile

Transverse Acceleration Response:	3 data points
Intrack Acceleration Response:	3 data points
Maximum Longitude Error:	6.2785E-07 degrees
Maximum Latitude Error:	4.6424E-07 degrees
Maximum Heading Error:	0.2721E-00 degrees
Maximum Velocity Error:	58.266E-00 mph
Maximum Intrack Acceleration Error:	1.0003E-00 Gs
Maximum Transverse Acceleration Error:	1.0011E-00 Gs
Average Longitude Error:	4.6313E-08 degrees
Average Latitude Error:	3.8776E-08 degrees
Average Heading Error:	7.1894E-02 degrees
Average Velocity Error:	14.770E-00 mph
Average Intrack Acceleration Error:	3.2101E-02 Gs
Average Transverse Acceleration Error:	3.2316E-02 Gs

Table B.5. Tuning Parameters for 5 Second Data Interval/ 8 G Profile

Transverse Acceleration Response:	3 data points
Intrack Acceleration Response:	3 data points
Maximum Longitude Error:	1.2968E-05 degrees
Maximum Latitude Error:	^.1694E-06 degrees
Maximum Heading Error:	0.7991E-00 degrees
Maximum Velocity Error:	465.07E-00 mph
Maximum Intrack Acceleration Error:	8.0074E-00 Gs
Maximum Transverse Acceleration Error:	8.0317E-00 Gs
Average Longitude Error:	5.5798E-07 degrees
Average Latitude Error:	2.7917E-07 degrees
Average Heading Error:	0.2180E-00 degrees
Average Velocity Error:	119.34E-00 mph
Average Intrack Acceleration Error:	2.6643E-01 Gs
Average Transverse Acceleration Error:	2.6437E-01 Gs

Table B.6. Tuning Parameters for 10 Second Data Interval/ 1 G Profile

Transverse Acceleration Response:	3 data points
Intrack Acceleration Response:	3 data points
Maximum Longitude Error:	8.0031E-06 degrees
Maximum Latitude Error:	6.2315E-06 degrees
Maximum Heading Error:	0.5704E-00 degrees
Maximum Velocity Error:	124.76E-00 mph
Maximum Intrack Acceleration Error:	1.0039E-00 Gs
Maximum Transverse Acceleration Error:	1.0018E-00 Gs
Average Longitude Error:	1.0665E-06 degrees
Average Latitude Error:	9.6199E-07 degrees
Average Heading Error:	0.1441E-00 degrees
Average Velocity Error:	31.040E-00 mph
Average Intrack Acceleration Error:	6.8328E-02 Gs
Average Transverse Acceleration Error:	6.1714E-02 Gs

Table B.7. Tuning Parameters for 10 Second Data Interval/ 8 G Profile

Transverse Acceleration Response:	3 data points
Intrack Acceleration Response:	3 data points
Maximum Longitude Error:	1.4035E-04 degrees
Maximum Latitude Error:	5.0741E-05 degrees
Maximum Heading Error:	1.7785E-00 degrees
Maximum Velocity Error:	995.74E-00 mph
Maximum Intrack Acceleration Error:	8.0141E-00 Gs
Maximum Transverse Acceleration Error:	8.0263E-00 Gs
Average Longitude Error:	1.4039E-05 degrees
Average Latitude Error:	8.0500E-06 degrees
Average Heading Error:	0.4299E-00 degrees
Average Velocity Error:	261.70E-00 mph
Average Intrack Acceleration Error:	5.9445E-01 Gs
Average Transverse Acceleration Error:	5.1069E-01 Gs

Appendix C: Four State Kalman Filter Flowchart

This appendix details the flowchart for the four state Kalman filter algorithm used to process incoming sensor data. It includes the preprocessing of data angles to latitude and longitude.

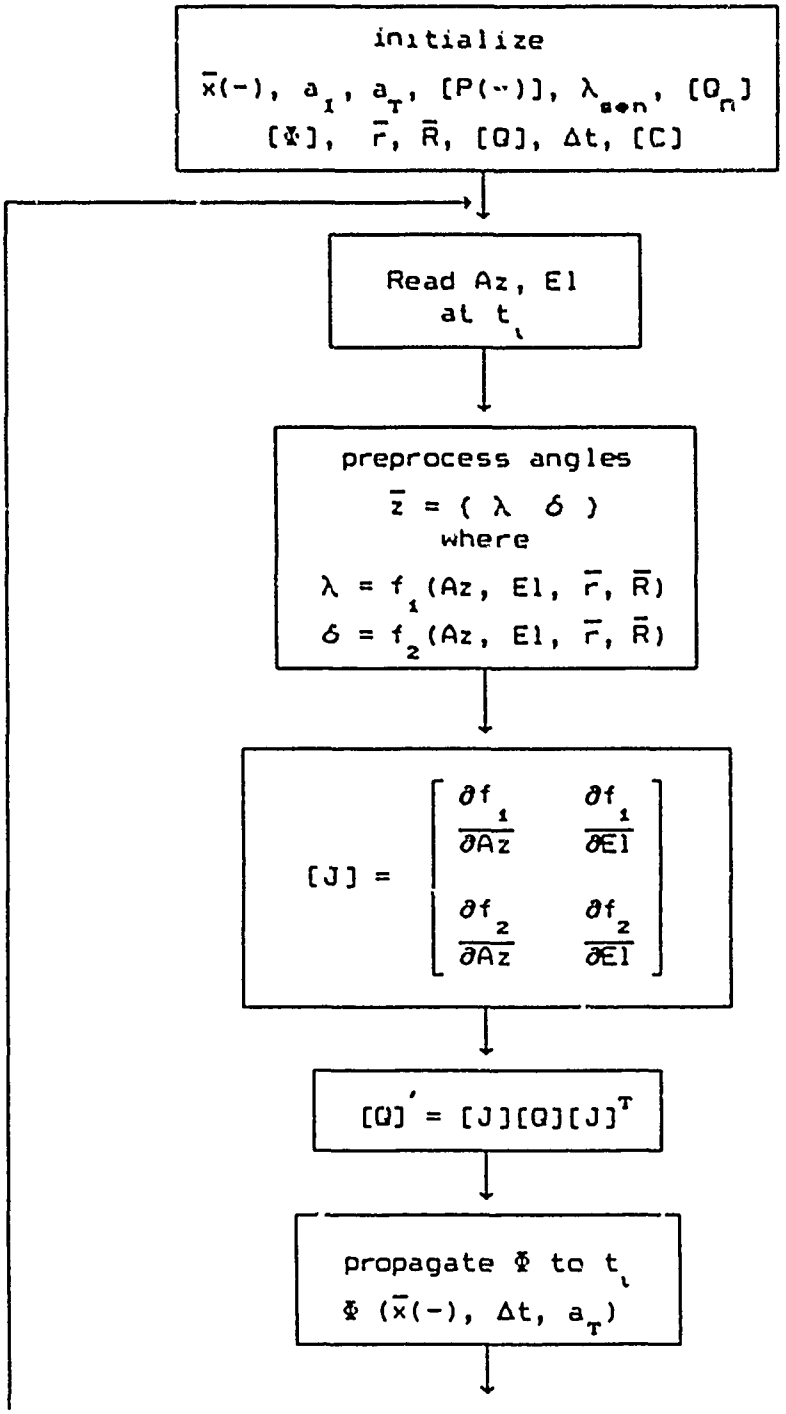

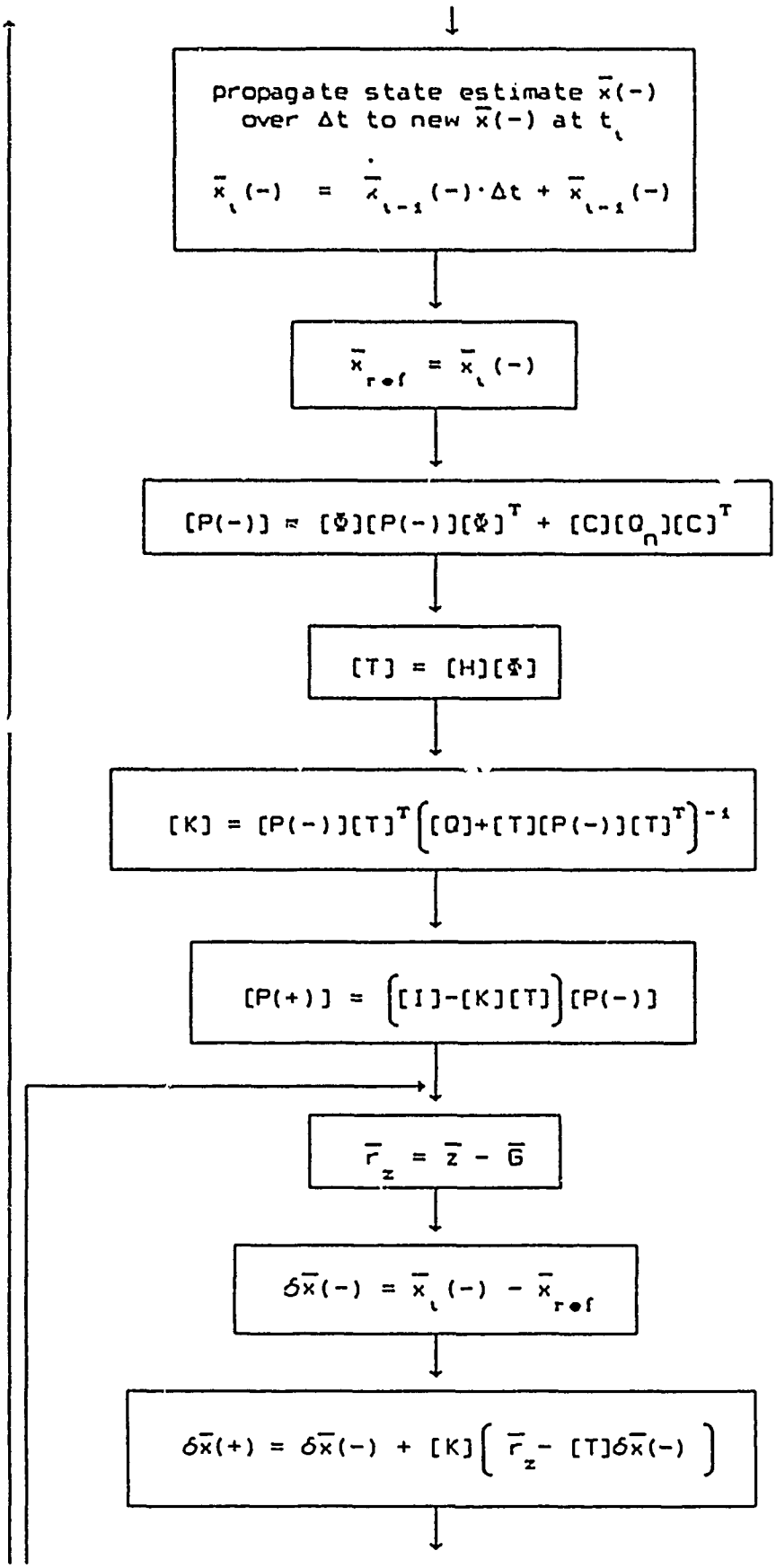
propagate state estimate $\bar{x}(-)$ over Δt to new $\bar{x}(-)$ at t_i
$\bar{x}_i(-) = \dot{\bar{x}}_{i-1}(-)\cdot\Delta t + \bar{x}_{i-1}(-)$
$\bar{x}_{ref} = \bar{x}_i(-)$
$[P(-)] \approx [\Phi][P(-)][\Phi]^T + [C][Q_n][C]^T$
$[T] = [H][\Phi]$
$[K] = [P(-)][T]^T\left([Q]+[T][P(-)][T]^T\right)^{-1}$
$[P(+)] = \left([I]-[K][T]\right)[P(-)]$
$\bar{r}_z = \bar{z} - \bar{G}$
$\delta\bar{x}(-) = \bar{x}_i(-) - \bar{x}_{ref}$
$\delta\bar{x}(+) = \delta\bar{x}(-) + [K]\left(\bar{r}_z - [T]\delta\bar{x}(-)\right)$

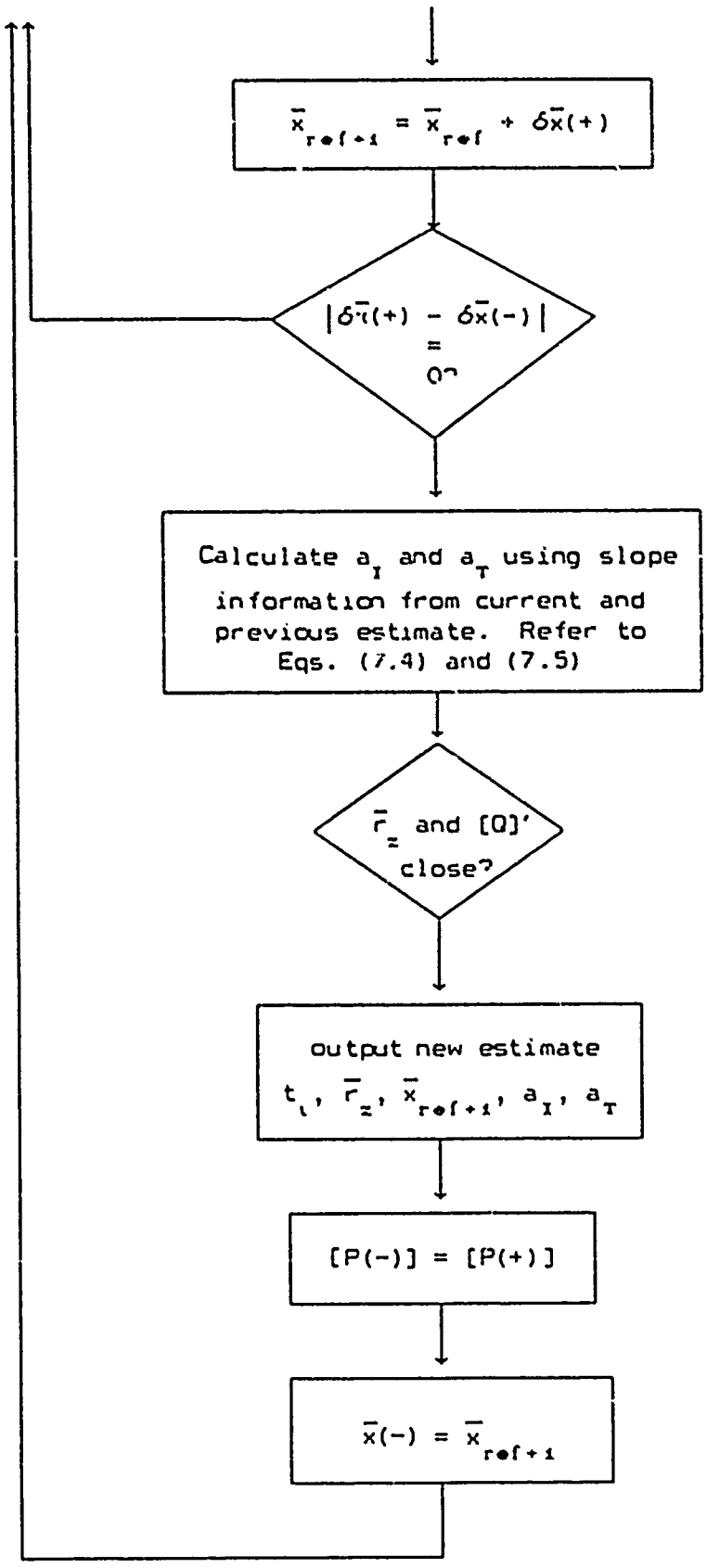
$\bar{x}_{ref+1} = \bar{x}_{ref} + \delta\bar{x}(+)$
$|\delta\bar{z}(+) - \delta\bar{x}(-)| = 0$?
Calculate a_I and a_T using slope information from current and previous estimate. Refer to Eqs. (7.4) and (7.5)
$\bar{r}_z$ and $[Q]'$ close?
output new estimate t_i, $\bar{r}_z$, $\bar{x}_{ref+1}$, a_I, a_T
$[P(-)] = [P(+)]$
$\bar{x}(-) = \bar{x}_{ref+1}$

Bibliography

1. Bate, R.R. et al. Fundamentals of Astrodynamics. New York: Dover Publications, Inc., 1971.

2. Maybeck, Peter S. Stochastic Models, Estimation, and Control (Volume 1). New York: Academic Press, Inc., 1979

3. Osedacz, Capt Richard M. Orbit Determination of Sunlight Illuminated Objects Detected by Overhead Platforms. MS Thesis, AFIT/GA/ENY/89J-3. School of Engineering, Air Force Institute of Technology (AU), Wright-Patterson AFB OH, June 1989

4. Wiesel, William E. Lecture Notes for MC 7.31, Modern Methods of Orbit Determination. School of Engineering, Air Force Institute of Technology (AU), Wright-Patterson AFB OH, 1989.

Vita

Captain David W. Ziegler was born on [redacted] in [redacted] In 1978, he graduated from high school in Torrance, California and attended the United States Air Force Academy. Graduating in June 1982, with a Bachelor of Science in Astronautical Engineering, he soon was assigned to the Air Force Satellite Control Facility in Sunnyvale, California. There he served, until 1984, as an Operations Requirement Officer for transitioning the new Consolidated Space Operations Center in Colorado to operations. He subsequently was assigned as Deputy Mission Director in the Special Programs Division where he advanced Air Force operations in the Strategic Defense Initiative and Space Test Program arenas until 1988. In May 1988, he entered the School of Engineering, Air Force Institute of Technology.

Permanent address: [redacted]

UNCLASSIFIED
SECURITY CLASSIFICATION OF THIS PAGE

REPORT DOCUMENTATION PAGE

Form Approved
OMB No. 0704-0188

1a. REPORT SECURITY CLASSIFICATION UNCLASSIFIED	1b. RESTRICTIVE MARKINGS
2a. SECURITY CLASSIFICATION AUTHORITY	3. DISTRIBUTION/AVAILABILITY OF REPORT Approved for public release; distribution unlimited
2b. DECLASSIFICATION/DOWNGRADING SCHEDULE	
4. PERFORMING ORGANIZATION REPORT NUMBER(S) AFIT/GA/ENY/89D-7	5. MONITORING ORGANIZATION REPORT NUMBER(S)
6a. NAME OF PERFORMING ORGANIZATION School of Engineering 6b. OFFICE SYMBOL (If applicable) AFIT/ENY	7a. NAME OF MONITORING ORGANIZATION
6c. ADDRESS (City, State, and ZIP Code) Air Force Institute of Technology (AU) Wright-Patterson AFB OH 45433-6583	7b. ADDRESS (City, State, and ZIP Code)
8a. NAME OF FUNDING/SPONSORING ORGANIZATION 8b. OFFICE SYMBOL (If applicable)	9 PROCUREMENT INSTRUMENT IDENTIFICATION NUMBER
8c. ADDRESS (City, State, and ZIP Code)	10. SOURCE OF FUNDING NUMBERS PROGRAM ELEMENT NO. / PROJECT NO. / TASK NO / WORK UNIT ACCESSION NO.

11. TITLE (Include Security Classification)
TRACKING A HYPERSONIC AIRCRAFT FROM A SPACE PLATFORM

12. PERSONAL AUTHOR(S)
David W. Ziegler, B.S., Captain, USAF

13a. TYPE OF REPORT	13b. TIME COVERED	14. DATE OF REPORT (Year, Month, Day)	15. PAGE COUNT
MS Thesis	FROM _____ TO _____	1989 December	118

16. SUPPLEMENTARY NOTATION

17. COSATI CODES			18. SUBJECT TERMS (Continue on reverse if necessary and identify by block number)
FIELD	GROUP	SUB-GROUP	
17	11		Kalman Filtering; Infrared Tracking; Hypersonic Vehicles; Tracking

19. ABSTRACT (Continue on reverse if necessary and identify by block number)

Thesis Advisor: William E. Wiesel, Jr.
Professor of Astronautics
Department of Aeronautics and Astronautics

20. DISTRIBUTION/AVAILABILITY OF ABSTRA ☒ UNCLASSIFIED/UNLIMITED ☐ SAME AS RPT ☐ DTIC USERS	21. ABSTRACT SECURITY CLASSIFICATION UNCLASSIFIED
22a. NAME OF RESPONSIBLE INDIVIDUAL William E. Wiesel, Professor	22b TELEPHONE (Include Area Code) (513) 255-2362 22c OFFICE SYMBOL AFIT/ENY

DD Form 1473, JUN 86 *Previous editions are obsolete.* SECURITY CLASSIFICATION OF THIS PAGE

UNCLASSIFIED

This study developed a data processing algorithm for a space-based platform engaged in tracking a hypersonic transatmospheric vehicle. The geosynchronous platform was assumed to possess passive sensors measuring target position from data angles. The hypersonic vehicle was assumed to be operating in the outer fringes of the atmosphere.

Four element and six element state Kalman filters were developed, coded, and tested against typical transatmospheric flight profiles. Accuracy of the filters in estimating position, velocity, heading, and acceleration was determined for 1, 5, and 10 second data intervals.

From this test data, it was concluded that the six element state Kalman filter posed a viable option for tracking and estimating performance of hypersonic aircraft.